NATIONAL TECHNICAL UNIVERSITY OF ATHENS

SCHOOL OF APPLIED MATHEMATICAL AND PHYSICAL SCIENCES - INTERDISCIPLINARY PROGRAM OF POSTADUATE STUDIES “APPLIED MECHANICS”

MASTER THESIS

CRASHWORTHINESS RESPONSE OF THIN-WALLED STEEL CIRCULAR TUBES UNDER OBLIQUE LOADING

KONSTANTINA D. KARANTZA

Supervisor Professor: D. MANOLAKOS

Athens
February 2022

In memory of my beloved late father

who inspired me throughout my life to this day

Abstract

The aim of current master thesis is to investigate the behavior of thin-walled circular steel tubes subjected to both axial and oblique crushing in order to evaluate their crashworthiness efficiency. In order to assess the energy absorption capability and the occurred collapse mechanism both experimental tests and numerical finite element simulations are carried out providing the load-displacement curve and the main crashworthiness response parameters, while further different collapse states are captured during plastic deformation. Regarding the examined oblique crushing conditions, various loading angles lying from 3° to 11° are studied aiming to estimate their effect on the absorbed energy and the failure mode occurred during plastic collapse.

At first, experimental compression tests are conducted in quasi-static conditions under a constant loading rate of 10 mm/min by adjusting properly the loading angle representing off-axis oblique crushing conditions. For each examined specimen, two compression tests are carried out in order to secure the reliability of experimental results. At next, numerical simulation are carried out in LS-Dyna software by developing the finite element models of the examined cases. The developed models are simulated in dynamic conditions by adjusting a crushing speed of 1 m/s. Tubular specimens are modelled via 4-node shell elements, while at each examined configuration by both experiments and simulations the bottom tube end was considered as fixedly supported. The experimental and the numerical results were firstly compared between each other to validate the created finite element models, while also both were taken into account in order to evaluate the crashworthiness efficiency of the examined structures and assess the loading angle effect on their response.

Both experiments and simulations showed a sufficient agreement in both occurred collapse mechanism and crashworthiness response parameters. The highest crashworthiness efficiency revealed by the axially collapsed specimen, while oblique loading conditions reacted to lower energy absorption capacity for the examined tubes. In fact, as the loading angle gets higher, additional bending loads are introduced capable of causing local bending to the crushed structure decreasing significantly its energy absorption capacity. In subsequence, as the loading angle increases, both plastic collapse load and absorbed energy revealed a decrease which showed a significantly sharper drop for loading angles beyond 6° highlighting the last one as a critical oblique loading angle compared to the examined ones.

Acknowledgements

I would like to deeply thank my thesis supervisor professor D. Manolakos for entrusting me with such an interesting subject, as well as for his valuable guidance, advice and constant encouragement throughout my master thesis study.

Also, I want to express my grateful thanks to the technical staff of the Manufacturing Technology Lab of NTUA for their useful help on specimens productions and experimental tests conduction.

Finally, I would like to specially thank my mother for her support during my studies and my life.

Contents

List of Figures

List of Tables

1. Introduction

1.1 Introduction to crashworthiness

The desire of designers and engineers to increase occupant safety in vehicle structures has brought the need of improving the crashworthiness characteristics of structures. Crashworthiness is a design philosophy applied in every vehicle structure of the current transportation field, from automobiles and trains to aircrafts and helicopters. The overall objective of designing for crashworthiness is to reduce the impact of crash on the passengers resulting in increased structure safety levels. The reduction of crash impact aims to eliminate injuries and fatalities in the case of mild impacts, and minimize them in severe collisions. Also, modern crashworthy vehicles are designed to control the extent of crash impact damage by dissipating large amounts of crushing energy, while an adequate space for the passengers has to be maintained in addition. Thus, the design of crashworthy structures targets in absorbing the greater possible amount of energy produced during the crash. However, the energy absorption is preferable to be accomplished with controllable collapse in the event of a collision, and within certain constraints, such as limits on force transmission, permissible deformations and failure.

More specifically, if only small deformations are permitted regarding to occupant space, then large amounts of momentum transfer and force levels will be occurred, which may be unacceptable to be experienced from the passengers. On the other hand, a limit in permanent deformations must be enforced to retain a minimum volume for survival. So, in order to achieve an optimal combination of permitted frame deformation and transmitted forces to passengers, specific energy absorbing devices, strategically placed in the appropriate frame positions, are applied to vehicle structures to improve their crashworthiness behavior. Energy absorbers are mainly constructed by metals (steel, aluminum etc.), polymers, composite or bi-metallic materials. The two latter materials are widely used in current technology, as they provide light structures capable of absorbing large amounts of impact energy under axial crushing, bending and/or combined loading conditions. Further, research studies and experiments propose that thin-walled structures are more beneficial for use as energy absorbers, as they provide devices with high energy absorption capability and reduced total weight. The greater energy absorption capacity of a thin-walled structure is based on the fact that a thin-walled structure requires lower crushing loads to behave plastically and dissipate amounts of energy. In contrast, compact structures require greater loads to receive plastic deformations, which may keep them behaving completely elastic without dissipating any energy, or deform them in low strain levels, reducing the energy absorption capability in every case. As a result, the energy absorbers are preferable to be thin-walled structures.

In general, crashworthiness behavior and survivability can be improved by modifying the structural geometry or by introducing specifically designed energy absorbing devices. Both research directions have been investigated from the designers to produce crashworthy structures which dissipate the kinetic energy of crash in the most effective way. Figure 1 illustrates typical frame positions in which energy absorbers are usually placed for both automobile and aircraft's fuselage cases. As shown, energy absorbers are used in modern structures as collapsible tubular rails in the front end of automobiles, or in the case of aircrafts, as collapsible floor stanchions and beams.

The new design philosophy of crashworthiness has replaced more traditional design approaches, which considered strong, massive and stiff structures as the better ones. Such approaches have been rejected by current design trends as they fail to dissipate energy during impact, conveying it to the occupants and the cargo. In contrast, crashworthy structures are designed to provide a progressive controllable collapse, during of which they ensure a safe dissipation of adequate amounts of kinetic energy.

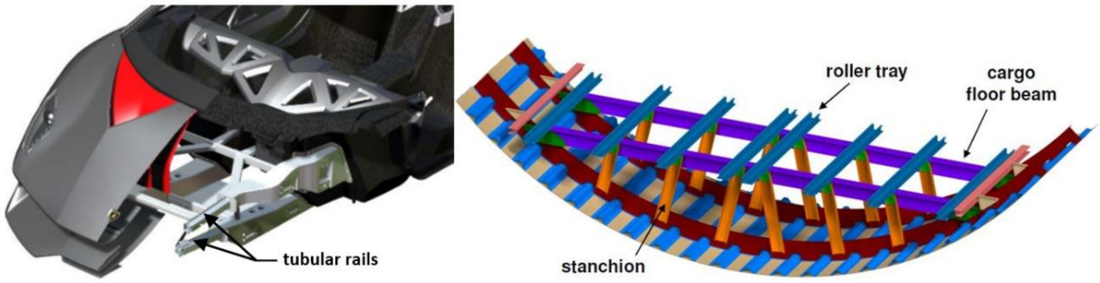

Figure 1 Energy absorbers positions in automobile and aircraft's fuselage structures, [1]

A structure designed to satisfy the main crashworthiness requirements must ensure five conditions for survival which are:

- Maintaining sufficient and survivable occupant space
- Providing adequate occupant restraint
- Limiting acceleration and loads experienced from the occupants by employing energy absorbing devices
- Providing protection from the release of items of mass
- Allowing for a safe post-crash egress from the vehicle

Regarding to aircraft structures, crashworthiness regulations have been set in Advisory Circular (AC) of Federal Aviation Administration (FAA) as suggested in [2]. The regulations were introduced based on experiences gained during actual aircraft operations. In order to set the appropriate regulations, FAA considered the impact response characteristics of the fuselage to examine the crashworthiness efficiency of aircrafts. On the other hand, regarding to automobiles, the crashworthiness regulations are set based on either past experience from incidents and accidents or according to safety rules.

The need of designing for crashworthiness has turned the research interest into investigating how structures response in crushing conditions. The complexity of understanding how factors, such as structure materials, geometry, failure mechanisms and crushing modes, affect the energy absorption capability of the structures, has led the engineering community to carry out several research works. As a result, many studies on crashworthiness behavior and energy absorption capability of structures have been carried out by conducting experimental crash tests and by using finite element analysis (FEA) numerical simulations.

1.2 Aim of this thesis

The aim of current master thesis is to investigate the crashworthiness response of thin-walled steel circular tubes under both axial and oblique compressive loading by conducting experimental tests and numerical simulations. The first ones are carried out in quasi-static conditions with constant loading rate in order to observe the occurred collapse mechanism and estimate the response characteristics for assessing the crashworthiness behavior of the examined specimens. Furthermore, finite element numerical simulations are also carried out utilizing ANSYS LS-Dyna software as the modelling and simulating tool of this work. The created finite element models are initially validated against the experimental results of the conducted tests in order to assess their accuracy level, while the provided numerical results are also taken into consideration for estimating the crashworthiness behavior of the examined tubes. Finally, the analysis of this study is focused on both failure mechanism occurred during collapse and crashworthiness metrics provided by the load-displacement curve for each specimen, in order to evaluate the energy absorption capability and the collapse stability for each examined configuration.

1.3 Scope

Current part of this master thesis introduces shortly the basic meanings of crashworthiness designing philosophy in a preliminary and theoretical level. The main reasons considered as most responsible for designing crashworthy structures are pointed out, describing in parallel the advantages which can be brought from this design trend. So, the aim of current chapter is to highlight the need and importance of implementing the crashworthiness philosophy in the design of every transportational structure such as vehicles, aircrafts, ships, trains etc. For this reason, some main regulations and requirements which a crashworthy structure must satisfy are described in order to define some metrics which are taken into account for evaluating the crashworthiness behavior of such structures. Finally, this initial part ends with the presentation of the aim of this master thesis.

Chapter 2 presents the main characteristics of crashworthiness behavior of structures in more detail and from a more technical point of view. Also, the way many factors affect the energy absorption capability is described, followed by a detailed description of the failure mechanisms and crushing modes which can be observed under crushing conditions. At next, the two main types of experimental crush tests which can be conducted for crashworthiness analysis are described by presenting the benefits and the drawbacks of each one. Finally, chapter 2 summarizes and reviews a number of research studies on crashworthiness response in both axial and oblique loading conditions, presenting also a theoretical analysis to calculate the mean crushing load which is considered one of the most significant metrics for evaluating crashworthiness efficiency and energy absorbing capability.

Chapter 3 presents the experimental tests carried out for assessing the crashworthiness behavior of examined thin-walled steel circular tubes and providing the necessary data for the validating procedure of the created finite element models. The experimental results contain both stage-by-stage observations of the collapse in order to obtain the occurred failure mechanism, and the estimating of critical crashworthiness response characteristics provided by the experimental data for evaluating the energy absorption capacity of each specimen.

Chapter 4 presents the modelling approach followed to simulate each test case. Initially, a short description of LS-DYNA software is presented, followed by the FEA models development for the purpose of current work. After that, the numerical results are presented and assessed by both calculating the main crashworthiness metrics and observing the predicted collapse mechanism for each examined specimen.

Chapter 5 consists of the respective comparisons between the experimental and the numerical results with the relative errors to evaluate their level of agreement. The comparison offers the opportunity to provide useful conclusions for the crashworthiness behavior of the examined thin-walled tubes and to examine the accuracy and validity of the numerical simulations. After the comparison between experimental and numerical simulation results in terms of crashworthiness response characteristics, the occurred collapse mechanism for each specimen is also observed and coupled to the revealed results regarding the collapse stability and energy dissipation capability offered. Finally, the effect of crushing angle is also discussed and compared against axial crushing focusing on failure mode change that affects the crushing efficiency of tubes.

Finally, chapter 6 contains a short summary of the aim of this thesis, the utilized modelling tool and the conducted experiments and numerical simulations followed by the provided results. Critical conclusions are next extracted for both crashworthiness response characteristics and collapse mechanisms, while finally some recommendations about future work are made.

2. Crashworthiness

2.1 Principles of crashworthiness design

The main goal of crashsworthiness design philosophy regarding every transportational or structural construction can be summarized in converting the greater possible amounts of crushing kinetic energy to plastic deformation ones. This specific capability of structures must be achieved under a stable and safe mode, maintaining a sufficient and survivable structural volume and limiting the inertial forces experienced from the passengers/occupants. Therefore, some of the most significant objectives of a crashworthy structure can be described by the main below aims:

a) Irreversible energy conversion

In order to achieve the greater possible absorption of crushing kinetic energy, a structure must be capable of deforming plastically for dissipation significant amounts by converting them into plastic strain energy. Therefore, the structure must be designed regarding its geometry and material properties in a way that the crushing load should be sufficient enough to overcome its yield stress and deform it plastically, otherwise the provided elastic strains could not be capable of absorbing any crushing energy amounts as they would result in a “spring back” effect on the structure which would rebound to its initial shape and geometry without dissipating any amounts of crushing kinetic energy.

b) Constant and stable crushing force

For minimizing the inertial forces transported to passengers/occupants during collision, a well crashworthy behaving structure should be capable of absorbing amounts of crushing energy by deforming plastically under a constant and stable sustained load, which ideally should be close enough to the peak crushing force applied initially, but also below a threshold amount, resulting that way in the minimum possible injuries caused by sudden decelerations. Thus, an energy absorbing device of high crashworthiness efficiency should possess a rectangular load-displacement characteristic, deforming that way stable under a constant and sustained load during its collapse.

c) Long stroke

Increasing the useful crushing distance by compressing the structure under long strokes, results in dissipating greater amounts of crushing kinetic energy, as the more the structure deforms the greater amounts of plastic strain energy requires. Thus, longer deformation levels allow generally higher energy absorption capacity to the designed structures. However, the maximum stroke is often constrained to limits regarding a sufficient and survivable structure volume.

d) Light weight with high energy absorption capacity

Structures weight is commonly treated as one of the most significant design parameters for both transportational and structural constructions. Therefore, designing under low weights is always considered as a significant feature, turning that way the crashworthiness design trend into thin-walled structures. In addition, thin-walled structures facilitate the plastic deformation initiation, resulting in greater amounts of absorbed crushing energy under low weight in fact. Thus, thin-walled structures are widely preferred in crashworthiness design as they provide high specific energy absorption levels.

2.2 Energy absorption characteristics

The main aim of designing crashworthy structures is to improve their capability in absorbing the amount of energy produced during a crush event. A typical response of a crushed structure in terms of applied force versus shortening (or stroke) of the structure is depicted in Figure 2. Some basic terms referring to crashworthiness behavior are pointed-out below.

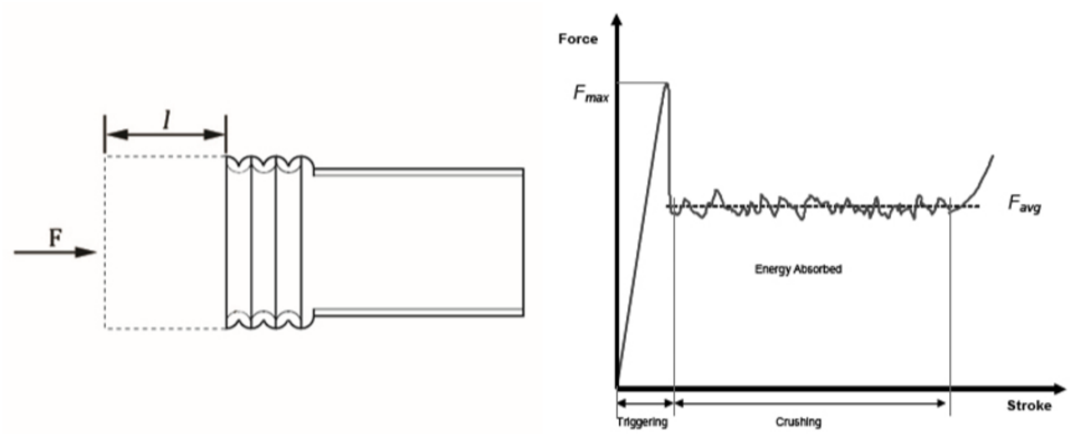

Figure 2 Load-displacement curve of a crushed structure, [3]

- Stroke, or displacement, is the structure length being compressed (shortened) during the crush.
- Peak force (F_{max}), or Peak Crush Force (PCF), is the maximum load observed in the force-stroke (or force-displacement) diagram.
- Average crushing force (F_{avg}), or sustained load, is the displacement-averaged or time-averaged value of crush force.

$$F_{avg} = \frac{1}{s} \cdot \int_0^s F \cdot ds \tag{1}$$

1. Crush initiator, or trigger mechanism, is a design feature that causes the start of a progressive collapse of the structure, avoiding the tendency of an unpredictable and unstable collapse which sometimes is possible to be occurred.

2. Crushing Force Efficiency (CFE), or Load uniformity (LU), is the ratio of mean sustained load to the peak load. CFE represents the uniformity of applied load considering the displacement.

$$CFE = \frac{F_{avg}}{F_{max}} \tag{2}$$

3. Energy Absorption (EA) is the amount of crush kinetic energy dissipated from the structure. It is equal to the total area under the load-stroke curve (Figure 3).

$$EA = \int_0^s F \cdot ds = F_{avg} \cdot s \tag{3}$$

4. Specific Energy Absorption (SEA) is the absorbed energy per unit mass of crushed structure expressed in J/g.

$$SEA = \frac{\int_0^s F \cdot ds}{m} = \frac{EA}{\rho \cdot A \cdot l} \tag{4}$$

5. Stroke Efficiency (SE) is the ratio of final structure length (l_s) after the crush to the initial one (l_0) before the crush.

$$SE = \frac{l_s}{l_0} \tag{5}$$

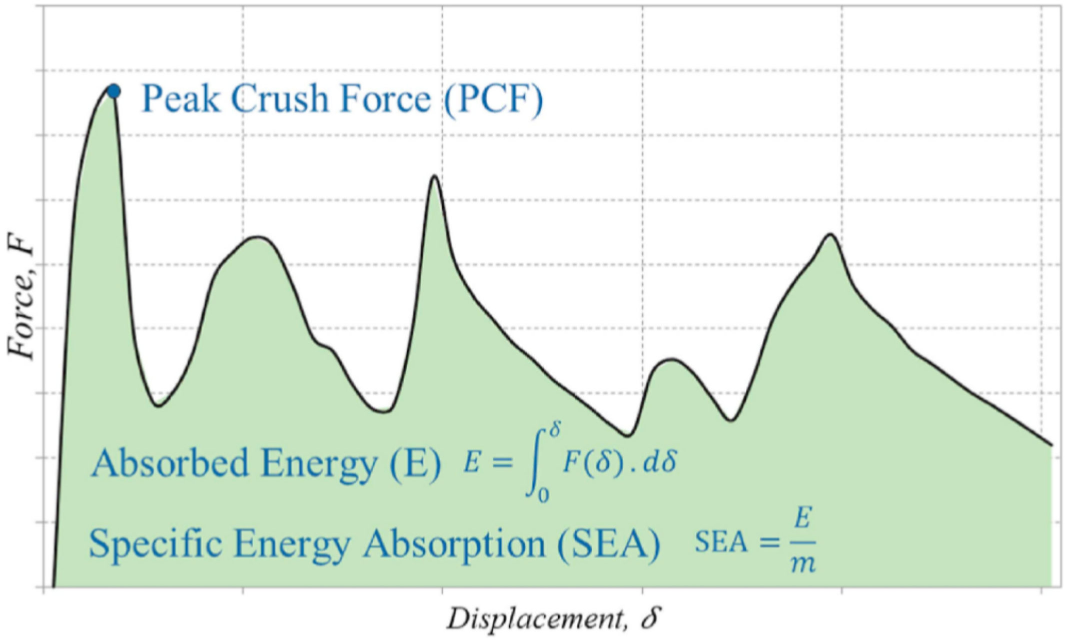

Figure 3 Energy absorption basic terms referring to load-stroke diagram, [4]

Structures of high energy absorption capability can be described as efficient ones in terms of crashworthiness. However, the specific energy absorption (SEA) is the main parameter for the evaluation of material efficiency. As a result, the comparison of two structures in terms of energy absorption capability is made comparing their SEA values. Obviously, the structure with greater SEA is the more efficient one. Additionally, a parameter of high importance is the peak crush force (PCF or F_{max}). PCF must be a reasonable value because if peak load is too great, the crush load may not reach the required force level, which is the F_{max}, to deform the structure plastically, meaning that the structure will retain behaving completely elastic without absorbing any energy. PCF is a function of geometric (thickness in case of thin-walled structures) and material characteristics of the structure.

Further, the crushing force efficiency (CFE) is an important factor representing the decelerating force which is applied to the passengers as the structure is loaded from maximum load to sustained one. A CFE of 100% is an ideal value as it provides a completely uniform applied load of high energy absorption. Finally, stroke efficiency (SE) is preferred to be as great as possible, resulting in high plastic deformations which increase the energy absorption capability of the structure and make the use of the material efficient in terms of crashworthiness behavior. A representative example of the effect of SE on energy absorption capacity is the comparison between brittle and ductile materials. As shows, ductile materials are characterized by greater SE as they can be deformed plastically without failing, resulting in greater energy absorption capacity compared to brittle.

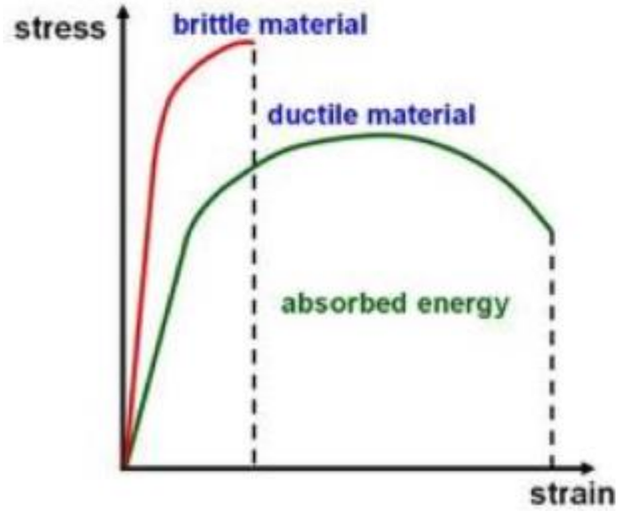

Figure 4 Energy absorption for brittle and ductile materials, [5]

Summarizing, an ideal energy absorber is characterized by high specific energy absorption (SEA), a reasonable peak load, a crushing force efficiency (CFE) of 100% and a stroke efficiency (SE) as closer to 100% as possible. The following figures depict typical energy absorbing devices for frontal longitudinal crushes in case of automobiles.

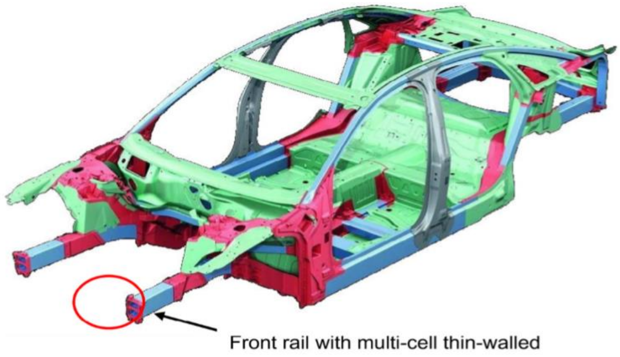

Figure 5 Frontal longitudinal energy absorbers of typical automobile, [6]

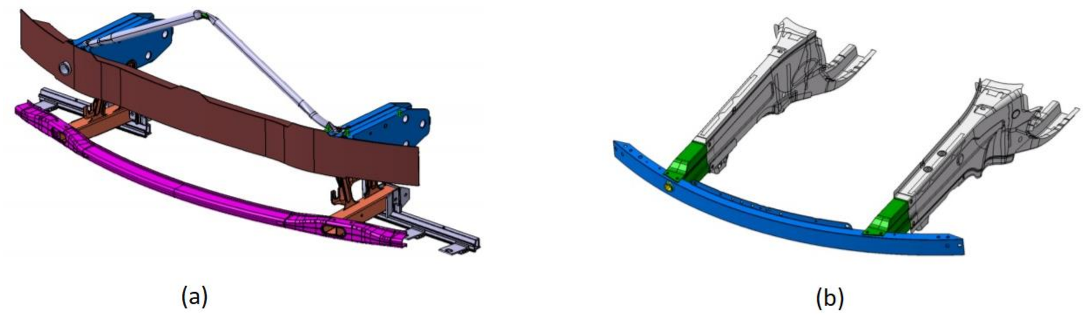

Figure 6 Energy absorbing system of front end of automobiles, (a) BMW 3 series model and (b) Mercedes C Class, [7]

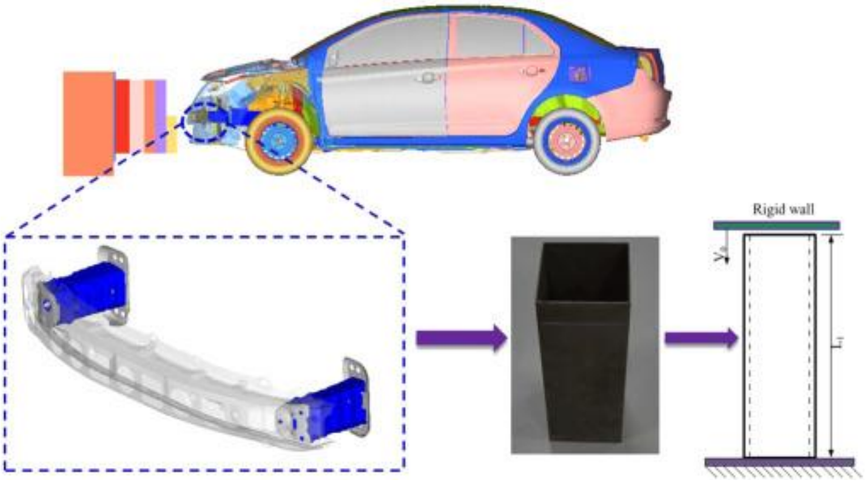

Figure 7 Energy absorbing system of front end of automobiles, [7]

The two next figures show the crashworthiness design of the fuselage of aircrafts, in which energy absorbing devices (beams and stanchions) are located in order to dissipate the necessary amounts of energy under loading, during vertical crushing conditions of the fuselage.

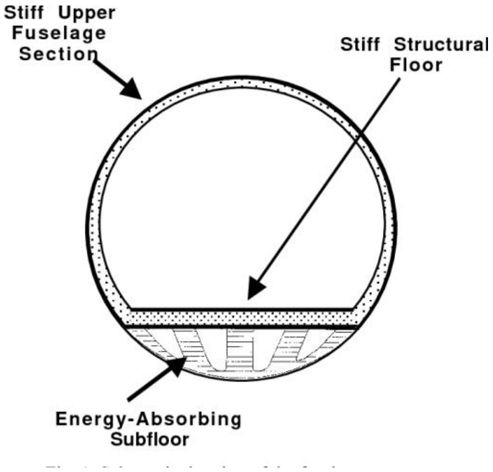

Figure 8 Crashworthiness design of aircraft's fuselage, [8]

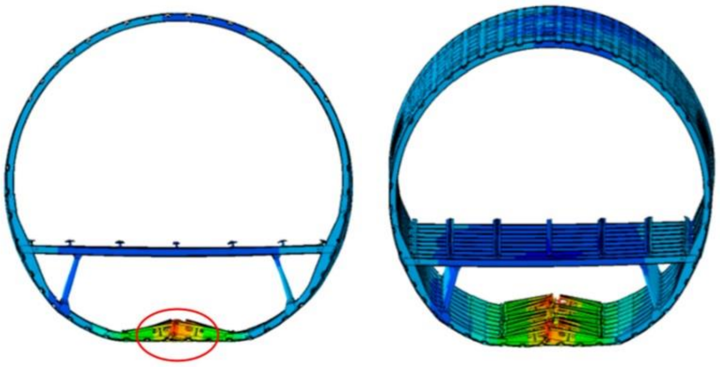

Figure 9 Aircraft's fuselage crushing behavior, [8]

2.3 Energy absorption and failure mechanisms

The specific energy absorption, which is the main parameter characterizing the energy absorption capability of a structure, strongly depends on the mode the structure fails. In fact, two different crushing modes can occur; the catastrophic failure mode and the progressive failure mode.

The catastrophic failure mode occurs when unstable interlaminar crack growth occurs and it is characterized by a sudden increase in load until the peak load, followed by a low post-failure load. This type of failure mode is also described as uncontrollable.

In contrast, the progressive failure mode is controllable and progresses through the material at the loading speed. In this case, a triggering mechanism is provided at the one of the structure ends, as a stress concentrator, and causes the failure initiation. A reduction of peak load is observed down to a lower, almost constant, sustained load, under of which a stable collapse is provided. The advantages of a progressive failure mode are that the energy absorption is larger in a progressive crush compared to a catastrophic failure, while structures designed to response to loads by progressively failing have proved to be lighter than the ones which are designed to react to loads by catastrophically failing. Thus, the progressive failure mode is more beneficial compared to the catastrophic one because it provides lighter structures of higher energy absorption capability, or on other words structures of higher SEA.

According to Farley and Jones [9], the crushing mode is an indicator of how efficiently the structure is being crushed. The prediction of crushing response includes the understanding of how the energy absorption is affected by both material mechanical properties and specimen structure (geometry). Farley and Jones suggest that the crushing speed affects the energy absorption capability of a structure in the same way the strain rate affects the mechanical response of a material (Figure 10). As a result, the amount of absorbed energy depends on the crushing speed in a proportional way.

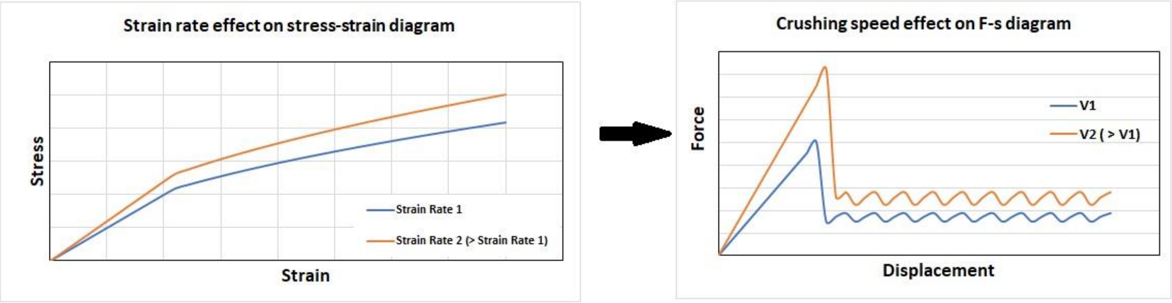

Figure 10 Effect on crushing speed on energy absorption according to [9]

Referring to the studies of Farley and Jones (1989), four different crushing modes have been identified considering composite materials. These four proposed crushing modes are presented below. All of them are exhibited by brittle composite materials, but the last crushing mode is the only one which can be also exhibited by ductile materials.

1. Transverse shearing and fragmentation mode

It is characterized by laminate cross-section with short interlaminar and longitudinal cracks that form partial lamina bundles (Figure 11). The main energy absorption mechanism is the fracturing of lamina bundles; when the fragmentation occurs, the length of interlaminar and longitudinal cracks is lower than that of the lamina. The mechanism is observed when the crushed material length is short. The mechanism that controls the crushing process is the transverse lamina bending strength, which is a function of fiber stiffness and strength in case of composite materials. As Farley and Jones suggested, if the fiber mechanical response depends on the strain rate, then the energy absorption depends on crushing speed in a similar way.

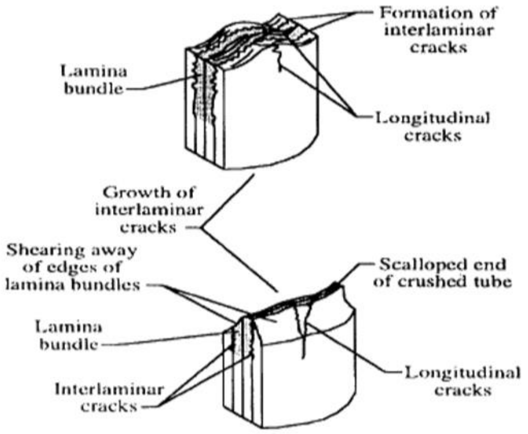

Figure 11 Transverse shearing and fragmentation crushing mode, [3]

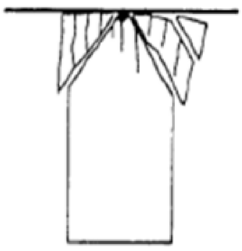

Figure 12 Fragmentation crushing mode, [1]

2. Brittle fracturing

The brittle fracturing crushing mode exhibits the same energy absorption mechanism like the fragmentation mode, which is the failure of lamina bundles. However, the length of interlaminar cracks in brittle fracturing lies from one to ten times the lamina thickness. The longer the fractured lamina bundle is, the less efficient the crushing mode is. Lamina bundles in brittle fracturing mode often exhibit some bending and usually fracture near the base. When the first lamina bundles fracture, the load is redistributed resulting in cracks growth and further lamina bundles fracturing. The controlling mechanisms in brittle fracturing mode, for composite materials, are the matrix stiffness and the lamina bundle tensile strength. The first controls the interlaminar and parallel-to-fiber crack growth, while the second controls the fracture of lamina bundle.

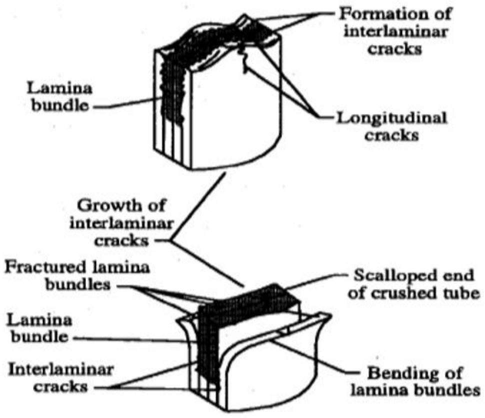

Figure 13 Brittle fracturing crushing mode, [3]

3. Lamina bending or splaying mode

Splaying mode is characterized by very long interlaminar and parallel-to-fiber cracks, but the lamina bundle does not fracture. The energy absorption mechanism here is crack growth. The respective cracks length is greater than ten times the lamina thickness. In splaying crushing mode, the lamina bundles exhibit significant bending deformation but do not fracture. The not fractured long lamina bundles result in an inefficient crushing mode. The matrix strength is the controlling mechanism of the splaying mode, as it controls the cracks growth. Once again, the way the strain rate affects the mechanical response of a material, is the same to the way the crushing speed affects the lamina bending and in consequence the energy absorption.

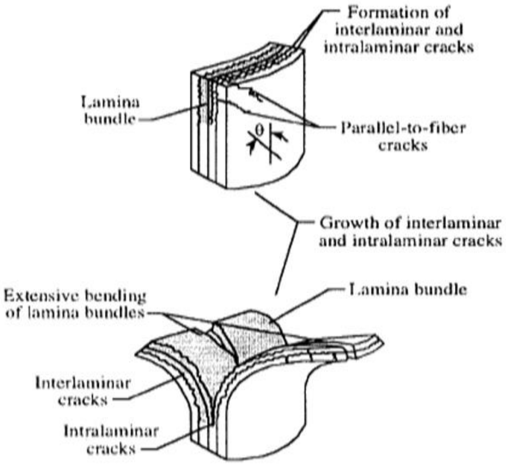

Figure 14 Splaying mode, [3]

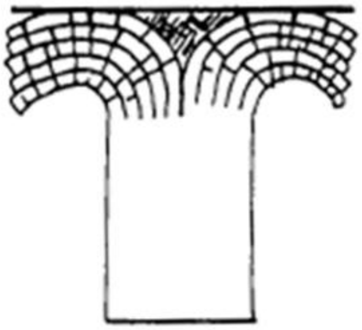

Figure 15 Splaying mode, [3]

4. Local buckling or progressive folding

The progressive folding crushing mode is characterized by the formation of local buckles, or folds, by means of plastic material deformation. This mode is exhibited by both brittle and ductile materials. The ductile fiber-reinforced composites remain intact after the crush due to the fiber and matrix plasticity and fiber splitting. In the case of brittle composite materials, the structure collapses in folding mode when matrix has higher failure stress than the one of the fibers. The mechanisms that control the progressive folding crushing mode is the plastic yielding of the fiber and/or the matrix. More specifically, the matrix non-linear stress-strain response controls the local buckling progress in case of brittle materials, while the matrix or fiber stiffness controls the progress of local buckling in case of ductile materials.

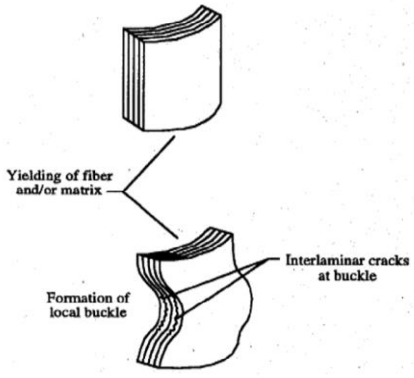

Figure 16 Local buckling or progressive folding mode, [3]

Further crushing modes referring to specific materials and geometries can be found in many studies of open literature, which have examined certain structures. A typical example is the study carried out by Bisagni [10] who observed the failure modes occurred in crushed circular carbon fiber tubes.

The energy absorption capability of a structure is a function of both geometry and material properties. In addition, energy absorption capacity of a structure depends strongly on the failure mechanism (crushing mode) which is observed during the collapse. So, regarding to composite materials, progressive crushing with microfragmentation is associated with the larger amount of absorbed crush energy according to Mamalis et al. [11]. However, when the fragmentation is quite intense providing large debris which have the tendency to concentrate in the interior of the tube, the fragmented and compacted debris limit the available stroke, resulting in lower stroke efficiency and in consequence lower levels of energy absorption capability. Furthermore, structures which collapse according to the crushing mode of progressive folding and hinging, are characterized by medium energy absorption capacity, while brittle fracturing mode results in very little levels of energy absorption providing a catastrophic failure. Finally, in every failure mode, environmental factors react in the same way on crashworthiness behavior. An important factor is the ambient temperature which reduces the amount of energy absorption according to Ptak et al. [12], as the force levels decrease in higher temperatures, moving the force-displacement curve downwards, reacting on lower energy absorption. The same paper underlined also the effect of crushing speed concluding that increased crushing speeds increase in turn the energy absorption as Figure 10 shows.

More emphasis will be given to local buckling and progressive folding crushing mode, as different types of folding modes can be occurred in the case of an axial crushed structure. The progressive folding and hinging is an oftenly observed failure mode. The four main types of progressive folding crushing mode are:

1. Concertina mode or ring mode
2. Diamond mode (3 lobes, 4 lobes etc.)
3. Mixed mode
4. Euler-type buckling mode

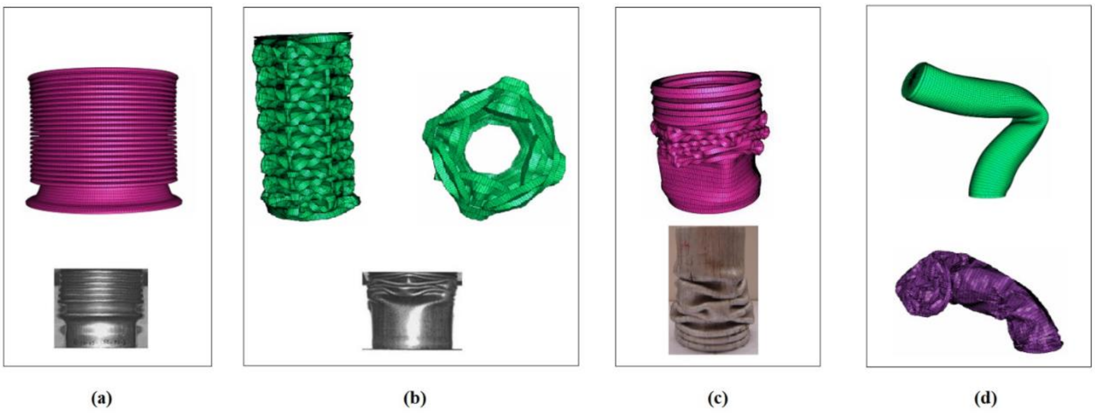

Figure 17 Progressive folding crushing mode, (a) concertina mode, (b) diamond mode, (c) mixed mode and (d) Euler-type buckling mode

The type of folding crush mode in which a structure is expected to collapse strongly depends on geometric characteristics. Specifically, a thin-walled tube will collapse under axial crushing load either axisymmetrically or non-asymmetrically, depending on the ratio of diameter to thickness (D/t) and the ratio of the length to the diameter (L/D). The axisymmetric mode is often called as concertina mode (or ring mode), while the non-symmetric one as diamond mode. For a certain D/t ratio, a tube may start collapsing in concertina mode and switch to diamond mode, exhibiting in that way a mixed crushing mode. Finally, a tube can also collapse in Euler-type buckling mode, which is a catastrophic and uncontrollable collapse provided by large bending of the tube resulting in significant loss in energy absorption capacity.

As mentioned before, the energy absorption capability strongly depends of failure mode. In case of folding and hinging crushing mode, research studies and experimental works have shown that concertina mode seems to be the best folding mode providing the highest energy absorption levels. A little lower energy absorption capability is provided by diamond mode, while the Euler-type buckling mode is characterized by very low energy absorption levels due to its catastrophic and unstable collapse progress.

Regarding to geometric characteristics which have a strong influence on expected type of folding, Florent et al. [13] examined aluminium tubes, suggesting that thick and short tubes are expected to collapse in concertina mode. As the tube thickness reduces and the length of the tube increases, a mixed mode is more expected to be observed, while even thinner and longer tubes may collapse in diamond mode. However, for extremely thin and long tubes, Euler-type buckling mode may be occurred. So, the length of the crushed structure or specimen must be very carefully selected in order to avoid the uncontrollable and catastrophic collapse of Euler-type buckling mode. For this reason, extremely long tubes must be avoided. Figure 18 illustrates the expected type of folding for aluminium tubes according to [13].

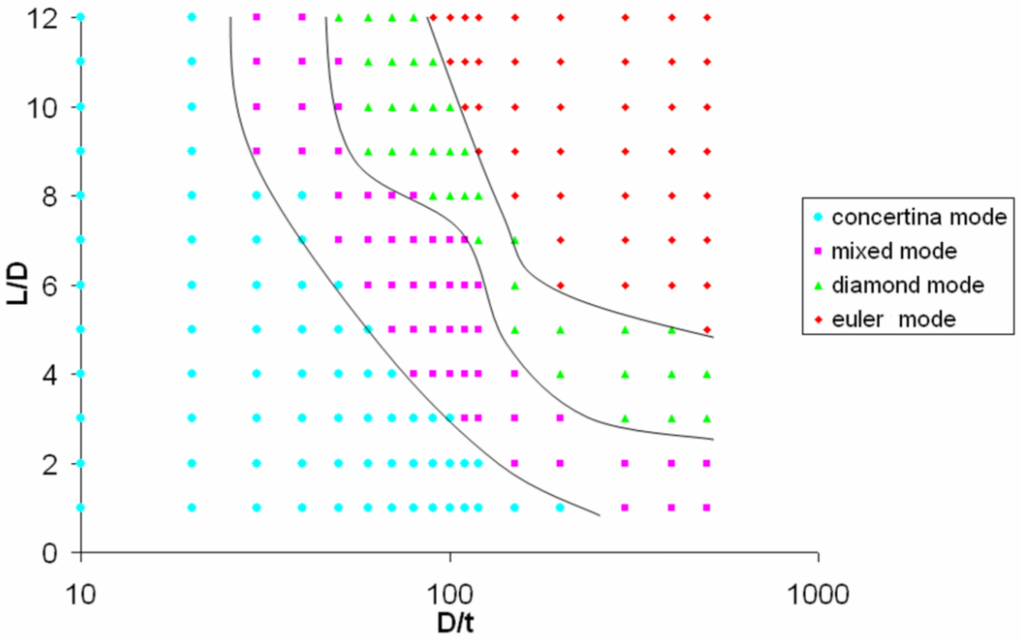

Figure 18 Folding mode classification for aluminium tubes, [13]

In addition, an important parameter in designing energy absorbers is their cross-section. Recent studies have examined single cross-sectioned tubes, concluding that circular tubes provide the highest energy absorption capability. A little lower levels of energy absorption capability are provided by square cross-section, and even lower by rectangular ones. In general, for cross-sections with corners (square, hexagonal, octagonal etc.), the energy absorption levels increase as the number of corners is getting higher. For example, the energy absorption capability of a circular tube is higher than an octagonal, which in turn is higher than a hexagonal one, which in turn is higher than a square one etc.

Finally, Florent et al. [13] investigated the effect of the type of support applied at structure ends. Specifically, the examined support types were tie constraint, roller and fixed, while four different boundary conditions were examined; (1) tie constraint-roller, (2) fixed-fixed, (3) fixed-roller and (4) roller-roller. The first support type refers to the bottom of the tube, while the second one refers to the top of the tube. For an examined specimen which was expected to collapse in concertina folding mode, the four types of support which were examined affected the folds formation as the next figure shows. A key-factor is that at symmetric supports, (2) and (4), the folds formation was also symmetric, as folds appeared at both ends of the specimen (aluminium tube).

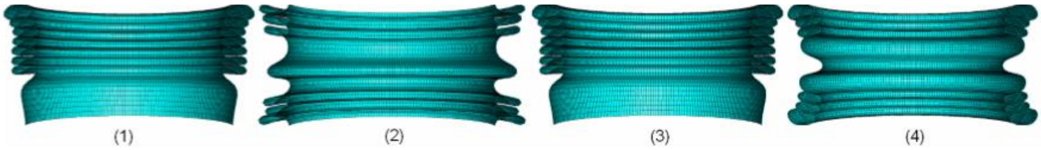

Figure 19 Effect of support types on specimen expected to collapse in concertina mode, (1) tie constraint-roller, (2) fixed-fixed, (3) fixed-roller and (4) roller-roller, [13]

Following, an examined specimen in [13], expected to collapse in mixed folding mode, in fact collapsed in concertina mode for fixed-roller supports as shown in next figure, suggesting that when the one of two tube ends is fixed, the concertina folding mode is occurred.

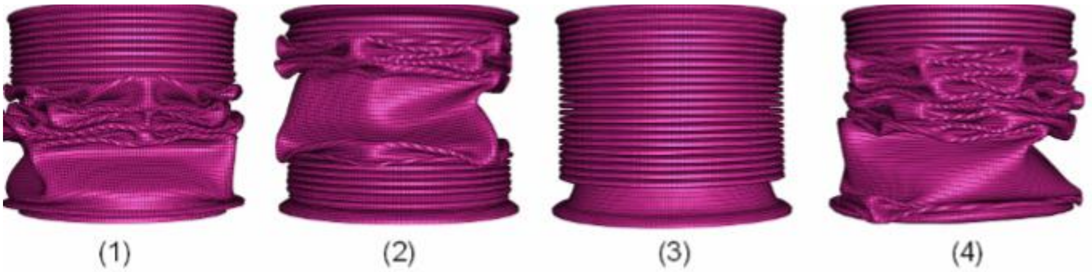

Figure 20 Effect of support types on specimen expected to collapse in mixed mode, (1) tie constraint-roller, (2) fixed-fixed, (3) fixed-roller and (4) roller-roller, [13]

Finally, the same study, [13], examined a specimen expected to collapse in Euler-type buckling mode. It was concluded that the end of specimen which was fixed or tied to the plate, was remained in contact to the plates after the collapse, while the end in which a roller boundary conditions was applied, was losing its contact to the plate by sliding over it.

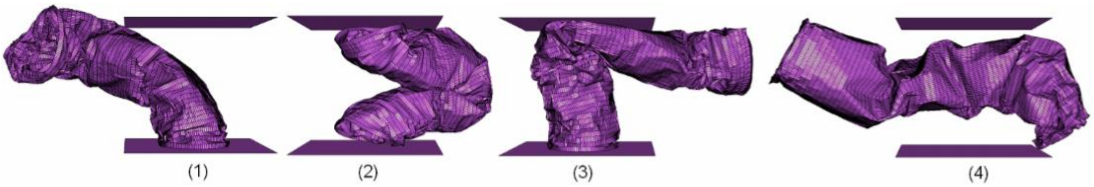

Figure 21 Effect of support types on specimen expected to collapse in Euler-type buckling mode, (1) tie constraint-roller, (2) fixed-fixed, (3) fixed-roller and (4) roller-roller, [13]

Summarizing on the effect of support types on folding collapse mode, when at least one end is fixed, more axisymmetric folds are created, providing so the best supported structure in terms of energy absorption capability which is at the higher levels. In contrast, when both ends are free, the energy absorption is significant low.

2.4 Crush tests

The crashworthiness behavior of a structure and its main characteristics can be studied through numerical simulations or experimental tests. The experimental tests often provide more accurate results in every aspect; prediction of energy absorption capability, maximum load, maximum specimen shortening, force-displacement curve, failure mode etc. The experiment tests, oftenly called as crush tests, can be conducted in two different ways: quasi-static and impact conditions.

Figure 22 Impact crush test of aircraft's fuselage, [8]

In quasi-static conditions, the specimen is crushed at constant speed. However, quasi-static conditions do not represent a true simulation of crush conditions, because in real crush conditions the structure is subjected to a decrease in crushing speed, from the initial impact to rest. Given that many materials are strain rate sensitive and the energy absorption capability depends on crushing speed according to Farley and Jones [9], the quasi-static tests may not lead to an accurate prediction of the amount of absorbed energy. Although, the advantages of quasi-static tests are that they are simple and easy to control without requiring expensive equipment to record the crush events.

On the other hand, the impact tests represent a true simulation of real crushing conditions, as the crushing speed decreases from the initial impact velocity to rest because of the energy absorption by the specimen. The benefit of impact tests is their accuracy in predicting the collapse mode and the main crashworthiness characteristics (energy absorption capability, maximum load, maximum specimen shortening, force-displacement curve, failure mode etc.). Their major disadvantage though is that they require expensive equipment, such as high-speed cameras, data recorders of very high frequency etc., as the crushing process takes place in a fraction of second.

2.5 Previous research studies

A plenty of research studies on crashworthiness have been carried out through the recent years utilizing numerical simulations with finite element analysis software or experimental crush tests. The main emphasis has been paid on investigating different materials (aluminium, composite materials etc.), cross-section designs, support types, the effect of triggering mechanisms for crush initiation or finally the loading conditions such as the crushing angle in case of axial or oblique impact loading. The metrics used by the majority of the studies to evaluate the crashworthiness efficiency are parameters such as specific energy absorption (SEA), mean crushing force (MCF), peak crushing force (PCF) and crushing force efficiency (CFE). Further, the observation of the occurred failure mechanism is always of significant importance affecting the collapse stability and in subsequence the energy dissipation capability.

Florent et al. [13] (2007) examined the impact of support types and foam filling on the crashworthiness behavior of aluminium thin-walled tubes, and more specifically on exhibited crushing modes. The study utilized as modelling tool the LS-DYNA software. The examined support types were tie-constraint end of tube, fixed end and roller in the tube end. The boundary conditions (support types combination for the two tube ends) have been referred to previous subsection of this chapter (2.2). It was concluded that for a specimen expected to collapse in concertina failure mode, both shell elements model and solid elements model predicted correctly the failure mode. However, given that a certain initial tube length can be formed in a standard number of folds, the shell elements model predicted more accurately the number of folds compared to the solid elements model (Figure 23). Additionally, the impact of boundary conditions in terms of support type of each tube end was examined providing the conclusions referred to subsection 2.2 of this chapter. Finally, the aluminium foam filled tubes showed higher energy absorption levels. However, the aluminium foam filling resulted in shortening the folding length (Figure 24), while a change in collapse failure mode from diamond mode to concertina or Euler-type was occurred. The last observation is considered to be disadvantageous as it may cause unstable collapse (Euler-type buckling mode).

Figure 23 Bare tube folds prediction (shell elements model, experimental specimen, solid elements model), [13]

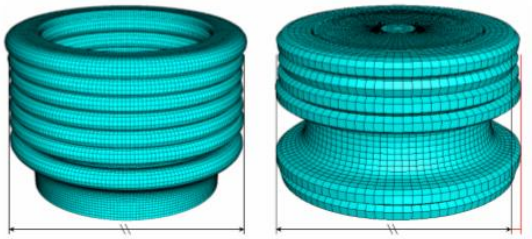

Figure 24 Effect of aluminium foam filling on exhibited number of folds, [13]

Mamalis et al. [11] (2009) studied square tubes of vinyl-ester and fiberglass composite material, internally reinforced with aluminium or polyurethane foam. Both experimental tests and numerical simulation in LS-DYNA software were conducted to observe and analyze the collapse mechanisms. The numerical simulations in LS-DYNA predicted correctly the failure mode, while mean deviations in predicted F-s curve of 20% and 15% were observed in the case of bare tube and tube reinforced with foam (both aluminium and polyurethane cases), respectively. It was concluded that the energy absorption was higher for the foam filled tubes compared to the bare ones. In fact, the aluminium foam filled tube was the one of higher SEA. Also, filling with aluminium foam provided better stabilization of the collapsed specimen and the crush energy was absorbed in completely plastic way in form of heat energy. In contrast, polyurethane foam filling provided an elastoplastic behavior during energy absorption, retransferring the amount of absorbed energy back to the crushing system.

Suzhen et al. [6] (2016) examined the effect of multi-cell cross-section designs on the crashworthiness characteristics of aluminium square tubes. The finite element analysis models which were developed for the needs of the study were initially validated by both quasi-static experimental tests. A typical representation of the study results is shown in the next two figures, where the collapsed specimens are depicted in the first figure, and the influence of multi-cell cross-section on energy absorption is depicted in the second figure. As Figure 26 shows, all SEA, PCF and MCF parameters increase as the number of cells increases too.

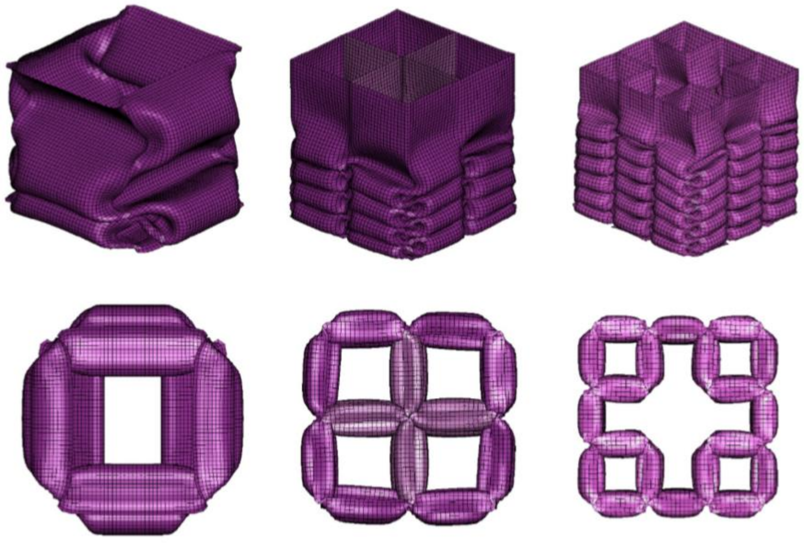

Figure 25 Collapsed specimens (single-cell, four-cell and five-cell cross-sectioned square tubes), [6]

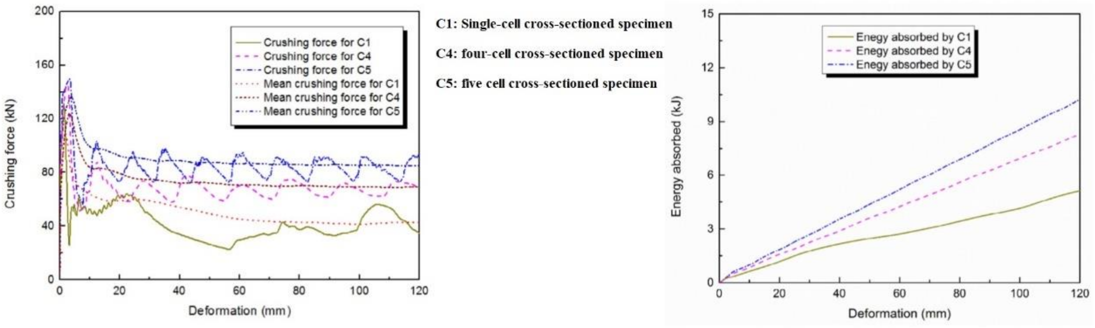

Figure 26 Effect of multi-cell cross-sections on energy absorption, [6]

Nikkhah et al. [4] (2019) studied the crashworthiness behavior of thin-walled windowed tubes made of aluminium. Different multi-cell cross-section designs were also considered in this research work too. It was concluded that the windowed thin-walled tubes were characterized by lower peak crush force (PCF) and lower specific energy absorption (SEA). The first consequence is positive, considering that PCF must be a reasonable value in order to the specimen be able of being deformed plastically absorbing energy. However, low SEA means in turn reduced energy absorption capability.

Acar et al. [14] (2019) examined different designs of multi-cell cross-sectioned thin-walled aluminium tubes, too. An optimization of crashworthiness response considering the CFE and SEA parameters was performed. The finite element models which were developed for the needs of the study were initially validated with experimental results. For the optimization, the same weighting factors were considered in the objective function for both CFE and SEA, paying in that way the same importance on maximizing both parameters. It was concluded that designs of thinner and larger in diameter tubes were provided for CFE maximization compared to the ones provided for SEA maximization.

Although most research works have been performed on crashworthiness analysis of simple composite structures such as tubes, Mamalis et al. [15] (1991) studied the effect of specimen geometry of thin-walled conical shells on energy absorption capability. Specifically, geometry characteristics like thickness, shell length and apical angle were investigated both experimentally and analytically. A standard crushing speed of 10mm/min was applied at all test cases until a deformation of 63mm being reached. The examined specimens were fiber-reinforced thin-walled composite conical shells with the semi-apical angle lying in the region of 5^o to 30^o. The failure mode of collapse and the effect of geometry characteristics (shell length, thickness of thin-walled shell, apical angle, diameter) on energy absorption capability were obtained. In general, thin-walled shells revealed a more efficient crashworthy behavior compared to thin-walled tubes. The experimental data provided that the specific energy absorption is a linear function of diameter to thickness ratio, or SEA (kJ/kg) = $1469.4 \cdot t/D - 6.8$. For axial compression of thin-walled composite shells, it was concluded that catastrophic brittle fracture and elastic instability must be prevented in order to achieve stable collapse during crushing conditions. In case of conical shells, stable collapse may be developed with absence of external trigger mechanism, as conical shells develop self-triggering mechanism with fracture initiating at regions of highest stress. The transition from stable to unstable collapse mode regarding to semi-apical angle was found to be in the region of 15^o to 20^o. Finally, the results showed that specific energy absorption decreases as semi-apical angle of shell increases, as thickness increases or as diameter decreases. In fact, though, large diameter shells may collapse under catastrophic failure.

Regarding oblique impact conditions, Shivdayal et al. [16] (2019) examined circular polymer tubes under both axial and oblique impact loading aiming to investigate the effect of various design variables on crushing response of road vehicle structures. Carbon and glass fiber reinforced plastic (CFRP / GFRP) composite tubes were evaluated respectively through their crashworthiness behavior examining homogeneous and heterogeneous ply orientation of 0^o, $\pm 45^o$ and 90^o for the laminated tubes. Non-linear crushing analysis was carried out by implementing finite element modelling in ABAQUS software for assessing peak crushing force (PCF), deformation length and energy absorption capability through the revealed failure mode. A Continuum Damage Mechanics (CDM) approach was taken into account introducing an effective damage tensor for estimating material plastic response during collapse according to Hashin damage criteria. The above approach offered the capability of estimating the damage propagation and possible delamination of composited tubes, allowing that way to predict their effect on the revealed crashworthiness. More, the upper edge of examined tubes was 45^o beveled behaving as a triggering mechanism which facilitates the initiation of a progressive failure. The created finite element models were initially validated against experimental data provided from 10^o oblique loading tests of CFRP tubes, while the numerical simulations carried out concerned about both axial and oblique loading in various angles with uniform or non-uniform contact between tube and impactor.

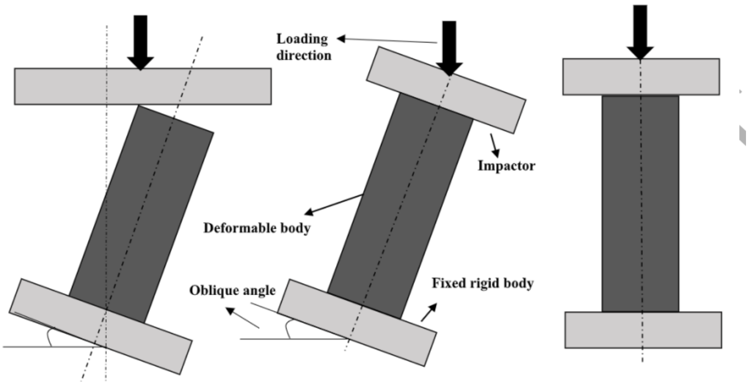

Figure 27 Axial and oblique loading conditions of uniform and non-uniform contact, [16]

The simulation results showed that CRFP tubes revealed greater energy absorption capability, while the heterogeneous ply orientation structures proved to be more efficient structures. Finally, axial loading provided higher energy dissipation levels for the collapsed tubes compared to oblique one, in which higher loading angles resulted in lower energy absorption levels as the failure mechanism proved to be less progressive, which was amplified more in oblique loading with non-uniform contact.

Zarei [17] (2019) examined hybrid composite aluminum tubes under both dynamic and oblique impact loadings. The examined specimens consisted of 6060 aluminum alloy tubes with external composite layers varying in number from one to three in total, consisted of E-glass fiber and epoxy resin. The crashworthiness behavior was evaluated through experimental tests under dynamic conditions and also finite element analysis carried out in LS-Dyna software. The thin-walled tubes were modelled utilizing shell elements, while Chang-Chang failure model was accounting for material plastic response. In every case, the specific energy absorption was considered as the main metric for the assessment of crashworthiness efficiency for each structure. The results revealed a decrease in maximum and mean crushing forces as loading angle gets higher, while the greater energy absorption capacity revealed by the hybrid aluminum tube of one composite external layer, as in that case the structure collapsed maintaining the adhesion between the tube and the external layer which was not observed in the case of two or three external composite layers.

Further, Fauzan et al. (2016) [18] investigated a design optimization of foam-filled circular 6060 T4 aluminum tubes regarding their crashworthiness response under both axial and oblique impact loading. The examined structures contained of an empty double tube, an internally foam-filled double tube and a fully foam-filled double tube. The finite element models were developed in ABAQUS software and were validated via experimental data. Single 4-node shell elements were utilized for tubes modelling, and 8-node solid elements for aluminium foams. In each examined configuration, the bottom tube end was considered fixed, while oblique loading angles were adjusted to the range of 0^o to 40^o. Fully foam-filled double tubes proved as the more crashworthy structures revealing the greatest energy absorbing levels since they could withstand an oblique impact load as effectively as an axial compression and bending mode.

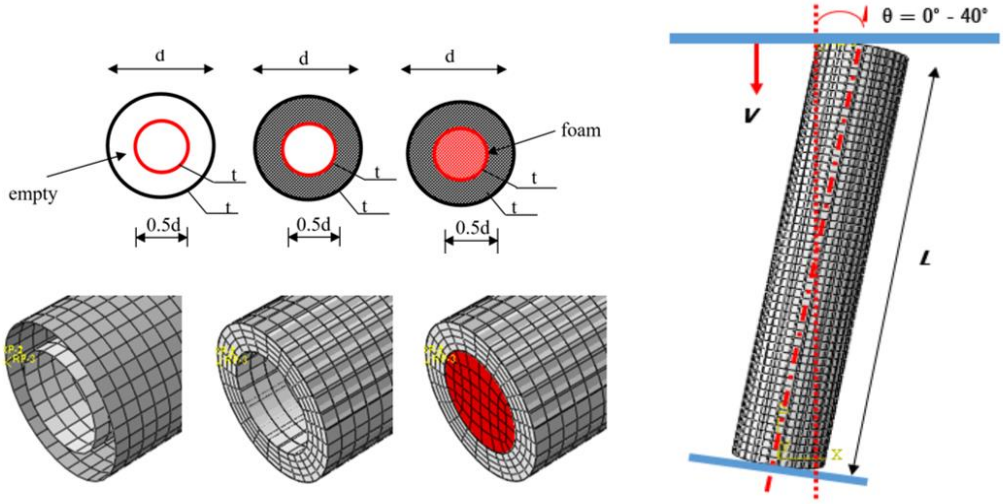

Figure 28 Foam-filled examined double tubes under oblique collapse, [18]

Kim and Wierzbicki [19] identified two different cases of oblique impact loading; angled loading and off-axis loading. In the first case, the tube is supported to the impactor and moving with its velocity towards the crushing surface which is positioned in an oblique angle. In the second case, the tube is supported in a bottom holder, both positioned in an oblique angle compared to the impactor which moves vertically crushing the tube. For this purpose, square and rectangular section beams were examined through non-linear finite element analysis in PAM-CRASH software. Their work highlighted the different loading conditions which the examined tube faces in the above two oblique loading cases, calculating a critical angle which defined the more preferable loading case. Finally, their research concluded further that the loading angle revealed a significant effect on collapse mode, as below a critical angle of bending moment with respect to axis-symmetry of section, the initial fold would formulate in the weaker side of the tube section revealing lower energy absorption capacity.

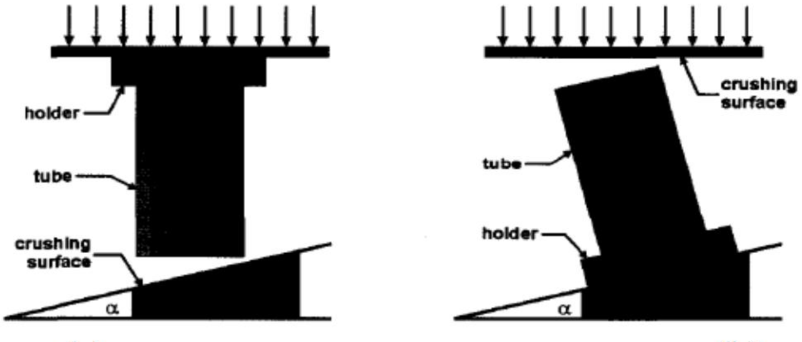

(a) (b)

Figure 29 types of oblique crushing: (a) angled loading, (b) off-axis loading, [19]

Moreover, Han and Park [20] (1999) used the angled loading type, depicted above, in their numerical analysis of oblique loading of mild steel square columns. The examined columns were simulated assuming frictionless conditions under a crushing velocity of 30 mph to an inclined wall. The results revealed that above a critical loading angle, a transition of axial collapse to Euler-type buckling mode takes place decreasing significantly the energy dissipation levels of the impacted structure. Finally, their work utilized normalized numerical results from multiple simulations cases in order to derive an approximate expression for mean crushing force and critical angle for the modelled steel tubes.

Reyes et al. [21] (2002) studied the crashworthiness behavior of AA6060 aluminum extruded thin-walled square columns under subjected to off-axis oblique loading. Both experimental tests under quasi-static conditions and numerical analyses via finite element models in LS-Dyna were conducted in order to assess the effect of wall thickness, initial length, loading angle and impact velocity, while all examined structures were clamped to their bottom end. All columns revealed an unstable bending collapse mode with significant decrease in mean crushing force for loading angles greater than 5^o. The energy absorbing levels seemed to flatten out in the range of 15^o to 30^o loading angle, while the wall thickness and initial length proved additionally to be the dominant parameters in structure response.

Crutzen et al. [22] (1996) indicated a possible solution through numerical analysis results for avoiding the unstable Euler-type bending mode during oblique impact, by redistributing the specimen mass along its length properly causing a more stable and progressive collapse. In that direction, columns of variable thickness or cross-section were proposed instead of straight columns, dissipating greater amounts of crushing energy due to their progressive failure.

Finally, more novel tubular configurations have been investigated under oblique impact loading conditions, such as multi-cell tubes and windowed tubes. In specific, Qi et al. [23] (2012) examined the crashworthiness behavior of tapered square tubes under oblique impact loading by studying numerically several geometrical configurations such as single-cell and multi-cell tubes, concluding that multi-cell tapered tubes revealed more efficient crashworthy structures. Additionally, Song [24] (2013) studied the crushing response of obliquely loaded square windowed tubes by conducting numerical finite element analysis. The examined parameters contained of the loading angle, tube windows dimensions and impact velocity. The results of his work highlighted that windowed tubes revealed lower energy absorbing levels under oblique impact compared to conventional tubes, while a novel design of windowed tubes was then proposed by varying windows dimensions along the tube in order to increase the critical angle achieving a more stable collapse mode, maintaining however the absorbed energy high enough, proving that way this design more efficient in terms of crashworthiness response.

2.6 Analytical expressions of mean crushing load for axial collapse

Efforts during the past have been made in order to calculate an analytical and theoretical expression for the mean crushing load of structures axially collapsed by formulating convolutions. One of the first works was carried out by Alexander [25] made in 1960. That research work was conducted considering thin-walled cylindrical shells which were expected to collapse in concertina mode under axial loading, formulated that way straight-sided convolutions consisted of 3 stationary plastic hinges. The mean collapse load is calculated by equating the internal deformation work to the external loading one. In specific, as required work considered the one which would deform the metal in one straight-sided convolution causing bending at circular joints and stretching the metal between them, as depicted following. From that study, Alexander suggested the following expression for mean collapse load.

$$\bar{P} = M_0 \cdot (20{,}73 \cdot \sqrt{2R_0/h_0} + 6{,}283) \tag{6}$$

In the above equation, let M_0 be the fully plastic bending moment, h_0 the initial wall thickness and R_0 the tube mean radius.

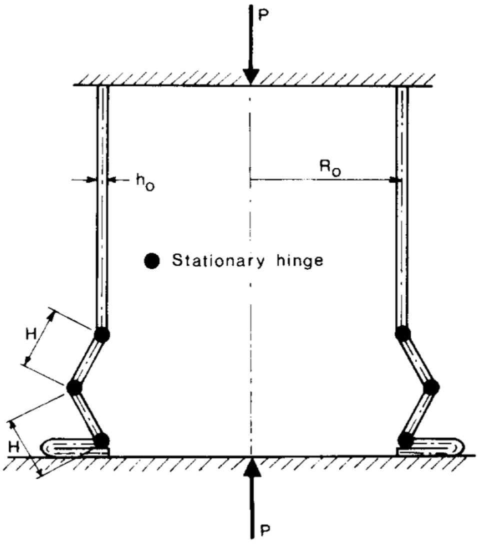

Figure 30 Alexander's model for axisymmetric axial crushing of circular tube, [25]

Further, Abramowicz and Jones [26] improved afterwards the Alexander solution by introducing a correction for the effective crushing distance. The internal energy dissipation was computed according to Alexander's approach, utilizing a rigid-perfectly plastic material idealization with stationary plastic hinges. However, in the improved approach the work of external forces was estimated based on a linear strain-hardening material behavior. Thus, Abramowicz and Jones' proposed theory predicts more accurately the magnitude of mean crushing force over a wide range of wall thickness to width ratio, allowing for an estimation for both symmetric and non-symmetric collapse modes as cited below by equations (7) and (8) for concertina and diamond mode respectively.

$$\bar{P} = M_0 \cdot \frac{20{,}79 \cdot \sqrt{2R/h} + 11{,}9}{0{,}86 - 0{,}568\sqrt{h/2R}} \tag{7}$$

$$\bar{P} = M_0 \cdot 86{,}14 \cdot \sqrt[3]{2R/h} \tag{8}$$

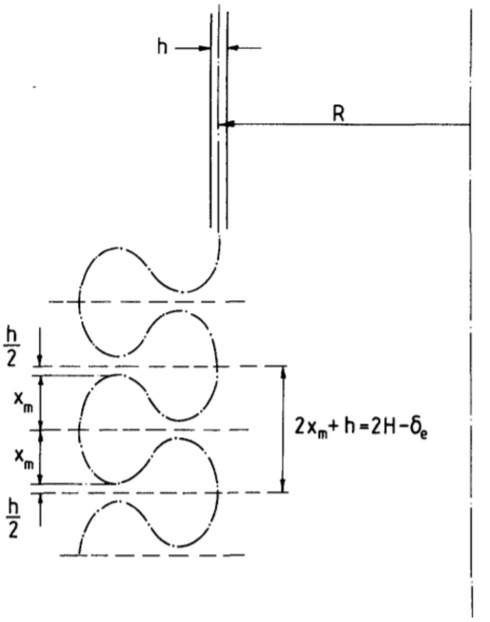

Figure 31 Effective crushing distance δ_e (Abramowicz and Jones), [26]

More, Wierzbicki et al. [27] proposed additional improvements replacing the stationary plastic hinges of Alexander's theory with moving hinges representing that way a more realistic shape of deformed convolutions formulated during collapse. According to this treatment, two folding waves are being created in an active crush zone considering two different cases. In the first one, a model with two straight elements constrained by stationary hinges was analyzed, while in the second case two S-shaped superfolding elements were taken into account revealing a more realistic prediction for the mean crushing load, capable also of predicting the existence of intermediate peaks in load-displacement response. Each treatment revealed the following expressions for the two straight elements consideration constrained by stationary hinges and for the S-shaped superfolding elements respectively:

$$\bar{P} = M_0 \cdot 22{,}27 \cdot \sqrt{{}^{2R}/_{h}} \tag{9}$$

$$\bar{P} = M_0 \cdot 31{,}74 \cdot \sqrt{{}^{2R}/_{h}} \tag{10}$$

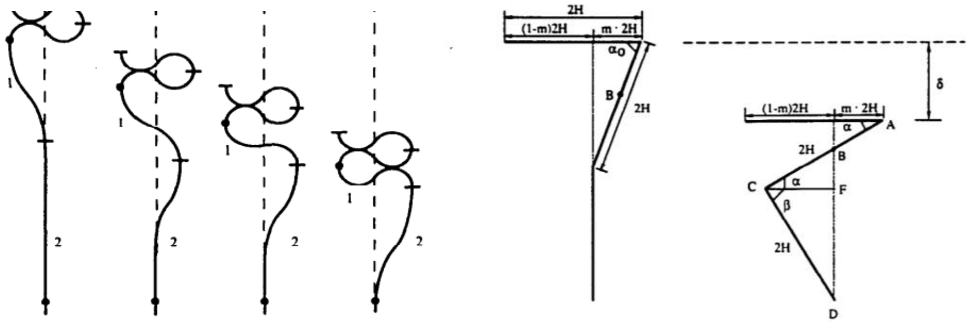

Figure 32 Superfolding elements assumption (Wierzbicki), [27]

Furthermore, Wierzbicki and Abramowicz expanded the initial theory into two specific types of superfolding elements; type I and type II. Both types are capable of predicting accurately the idealized collapse behavior of square tubes, as the combination between them offers sufficient estimations for both symmetric and non-symmetric modes. So, for symmetrically formulated convolutions the mean crushing load can be estimated as:

$$\bar{P} = M_0 \cdot 52{,}22 \cdot \sqrt[3]{{}^{c}/_{h}} \tag{11}$$

while for non-symmetrically formulated convolutions:

$$\bar{P} = M_0 \cdot (42{,}92 \cdot \sqrt[3]{{}^{c}/_{h}} + 3{,}17 \cdot \sqrt[3]{({}^{c}/_{h})^2} + 2{,}04) \tag{12}$$

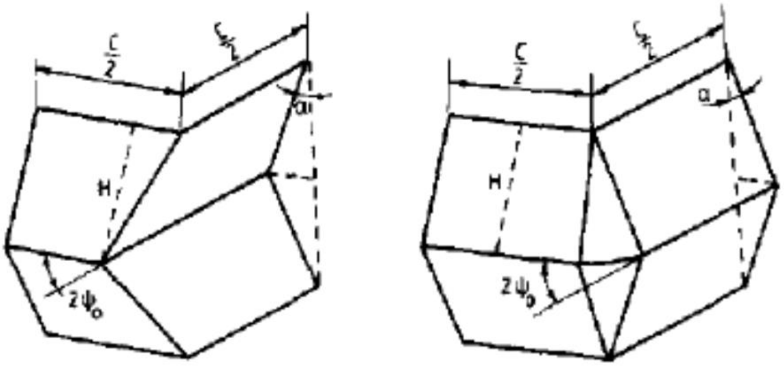

Figure 33 Superfolding elements; type I (left) and type II (right), [27]

Additionally, more studies have been carried out aiming to estimate the mean crushing load of an axially collapsed tubular structure. Specifically, Johnson et al. [28] studied the inextensional collapse modes of thin-walled tubes under axial loading. Tubes deformation assumed to take place under folding about fixed hinge lines formulating a number of flat triangular plates. The proposed failure mechanism accounts for a progressive collapse starting from the one tube end and following then a passage of a travelling hinge, resulting in the formulation of horizontal stationary hinges as depicted below.

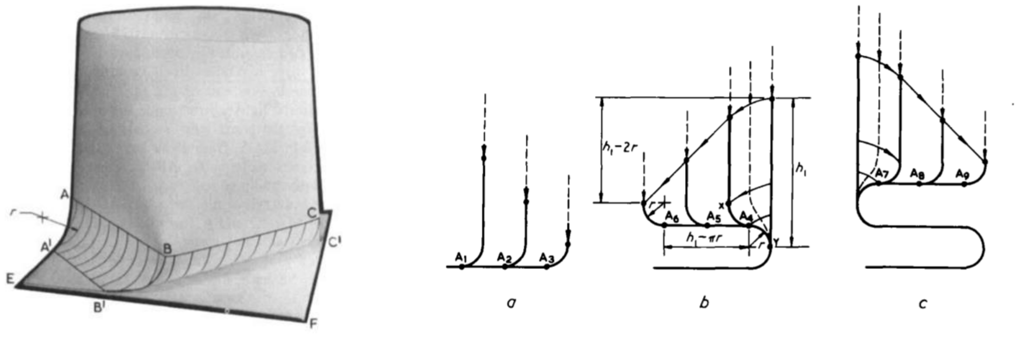

Figure 34 Horizontal stationary hinges formulation from travelling hinge assumption, [28]

The above model considers also the number of circumferential lobes n (n=2 for 2D-diamond mode, n=3 for 3-D diamond mode etc.) and the number of axial lobes m, proposing the following expression for the mean crushing force:

$$\bar{P} = 2\pi M_0 \cdot \left(1 + n \cdot cosec\frac{\pi}{2n} + \frac{m-1}{m} \cdot n \cdot cot\frac{\pi}{2n}\right) \qquad (13)$$

Also, Mamalis et al. [29] studied the crushing response of thin-walled bi-material tubes under extensible collapse, providing an analytical expression for the mean crushing force by equating the internal deformation work to the one of the external forces required to formulate a convolution. Considering thus, common material properties for the internal and external shells, the revealed analytical expression can be summarized following considering Y as the material yield stress, t the tube wall thickness and D its external diameter:

$$\bar{P} = 5{,}6Y \cdot t \cdot \sqrt{D \cdot t} \tag{14}$$

The above expression revealed sufficient agreement with Alexander's theory, while both took into account Tresca' yield criterion for the plasticity initiation during collapse. Finally, regarding the Euler-type buckling failure mode, the crushing load resulting in this mechanism has not been yet computed with similar accuracy due to its unstable behavior which leads to significantly lower energy absorbing levels. However, semi-empirical criteria have been developed based on experimental data considering the effect of geometrical parameters such as tube length, diameter and wall thickness. Although, Kecman [30] proposed bending collapse mode is usually localized at plastic hinges while the other tube sections behave as rotating rigid bodies. Kecman studied prismatic tubes collapsed under Euler-type buckling, observing that this mechanism takes place in four phases; a) a bulge is initially forming without any apparent rolling deformation, b) rolling deformations starts then to occur, c) the rolling deformations are jammed creating new bending line and d) two buckled halves coming in contact followed by the total jamming of the original hinge causing the initiation of an adjacent secondary hinge, as depicted in the following figure.

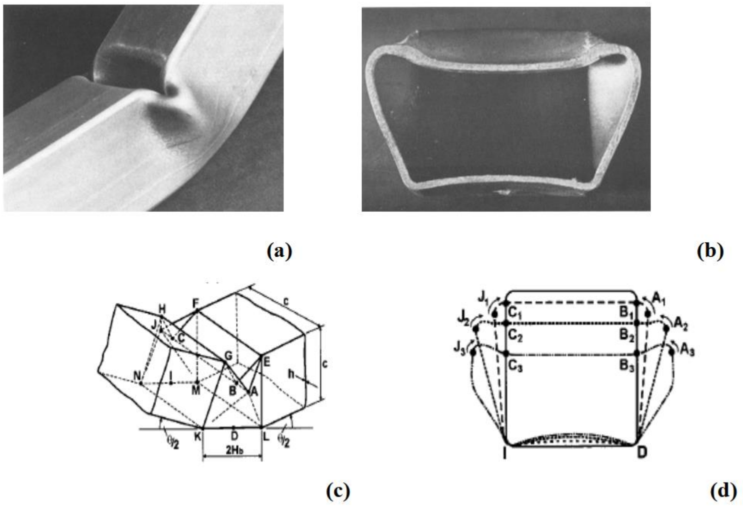

Figure 35 Euler-type buckling model by Kecman, [30]

The theory developed by Kecman was emphasized in the second stage of bending collapse, proposing that the absorbed energy can be estimated through its dependence to hinges rotation angle (15), as shown in Figure 33 (c). Finally, the bending zone width was also estimated based on rectangular tube width and wall thickness (16).

$$EA = \sum_{i=1}^{8} EA(\theta_i) \tag{15}$$

$$H_b = 1{,}276 \cdot c^{2/3} \cdot h^{1/3} \tag{16}$$

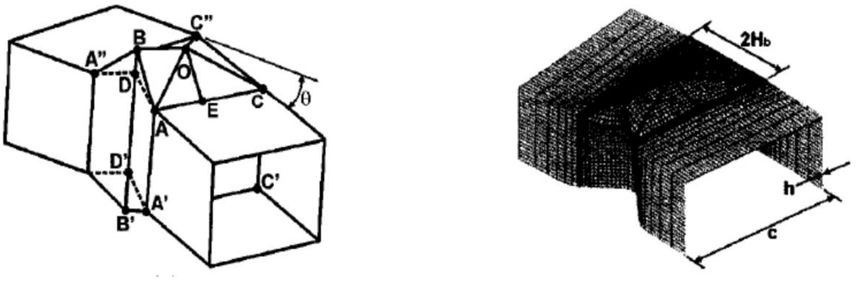

Figure 36 Bending zone width, [30]

3. Experimental investigation of crashworthiness behavior

3.1 Introduction

Current chapter contains the experimental investigation of crashsworthiness response under axial and oblique compressive loading for the examined thin-walled tubes. The conducted tests carried out in quasi-static conditions for a range of oblique angles lied from 0° to 11°, aiming to assess the loading angle effect on the response characteristics. In each test case, the main response metrics were estimated via the load-displacement curve provided from the experimental data, while the occurred collapse mechanism was also captured. Finally, the experimental results are analyzed for the evaluation of the crashworthiness efficiency regarding the examined configurations.

3.2 Experimental tests

This study carries out both experimental tests and numerical simulations in order to assess the response of thin-walled steel tubular structures under both axial and oblique crushing loads. The main goal of each analysis is to obtain the main response characteristics of a crashworthy structure and observe the crushing mode occurred during the collapse. Peak crushing load, mean sustained load, load uniformity factor, specific energy absorption and the amount of absorbed energy are some critical key parameters. These parameters together with the appeared collapse mechanism are considered as the appropriate metrics for comparisons between the provided experimental and numerical results. The conducted experimental tests can be used for two main reasons; the first one is to observe the crashworthiness behavior of the structure during the collapse and extract critical conclusions for key response characteristics, while in addition, the results from experimental tests can be utilized as validation source to assess the accuracy of developed numerical models. The last ones are widely used as they provide useful results in predicting the collapse mode and response characteristics of a crushed structure when they have been validated and their accuracy has been proved by sufficient matching against experimental data. The important advantage of carrying out numerical simulations is that they require less cost than conducting experimental tests where the necessary equipment (machine, high-frequency data recorders and high-speed cameras) is oftenly of high cost.

As reported previously in subsection 2.3, the experimental tests which can be conducted are either quasi-static or dynamic tests. The first ones require less expensive equipment but they provide less accurate results, as they are conducted at lower loading speeds than the appeared conditions in real crushes. In contrast, the dynamic crush tests represent more real crushing conditions and provide more accurate results as they are conducted at high loading speeds. However, the cost of such tests is quite higher and they are rarely preferred due to that.

For the purposes of current thesis study, the examined tubular specimens are tested to assess their crashworthy behavior under both axial and oblique loading conditions. The experimental tests are conducted in quasi-static conditions by compressing each specimen in a pressing machine with a loading rate of 10 mm/min. For each one of the tested specimens, different states are captured during their collapse, while stress and strain measurements are recorded providing the experimental load-displacement curve. From the provided experimental curves, parameters which characterize the structure response in crashworthiness - such as peak crushing force (PCF), mean sustained load (F_{avg}), amount of absorbed energy (EA) and specific energy absorption (SEA) - can be computed.

3.3 Examined test cases

The examined structures consist of thin-walled circular mild steel tubes with external diameter of 32.75±0.25 mm and wall thickness of 1.56 mm as depicted in Figure 37. Each examined configuration contained the tested tubular specimen, a bottom ringed base offering a fixed support zone to the tube bottom end and an upper plate moving downwards vertically in order to apply the compressive loads (Figure 38).

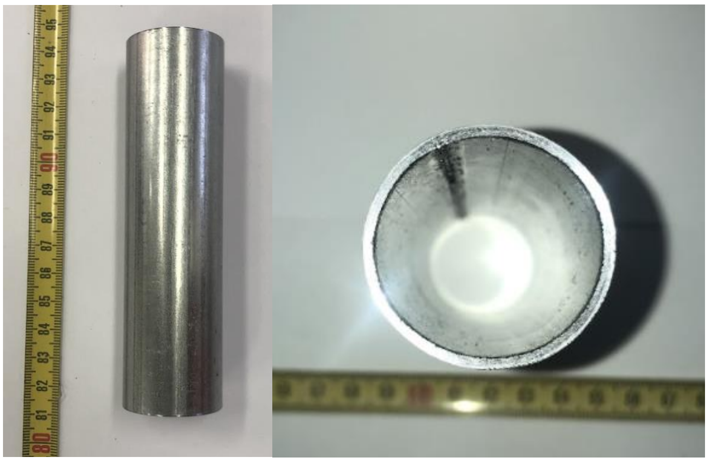

Figure 37 Initial specimen aspects

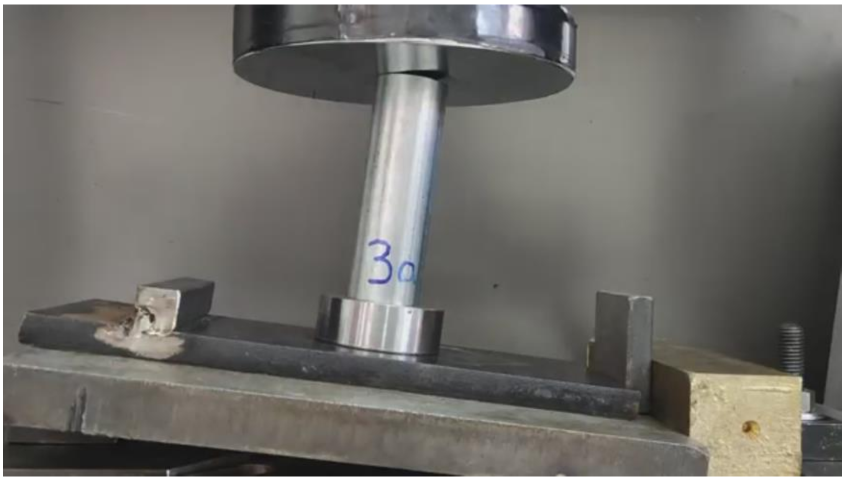

Figure 38 Examined configuration

The conducted tests carried out in INSTRON pressing machine with which the MTL of NTUA is equipped. Each experimental compression test carried out in quasi-static conditions under a constant loading rate of 10 mm/min, while the specimens are subjected to both axial and oblique compressive loads by examining various loading angles lying from 0^o to 11^o regarding the last case in order to assess its effect on crashworthiness response and energy absorption capability of the crushed structures. The loading angle was adjusted properly by rotating bottom ringed base together with the tube representing in that way off-axis oblique loading conditions. Each test case is conducted twice for the same specimen and loading condition aiming to provide more reliable results avoiding any possible deviations due to material defects, data recording errors, varied environmental testing conditions etc. The specimens subjected to axial loading was about 119 mm long, while the ones compressed obliquely were about 88 mm long and were crushed until the upper plate marginally approach the bottom base. Thus, the examined test cases can be summarized to the following table regarding the tested specimen, its initial dimensions and mass and the loading angle. In particular, the specimens are specifically grouped regarding mainly the loading angle in which was subjected to, where specimens 1a-1b are axially compressed, while specimens 2a-2b to 5a-5b are obliquely compressed under 3^o to 11^o crushing angle.

Specimen	Loading angle (deg)	Initial length (mm)	Specimen Mass (gr)
1a	0	119.0	152.3
1b	0	119.4	154.0
2a	3	88.1	113.6
2b	3	88.3	112.9
3a	6	88.4	115.0
3b	6	88.0	113.1
4a	9	88.5	114.7
4b	9	88.1	114.3
5a	11	88.5	114.5
5b	11	88.7	115.2

Table 1 Examined test cases

Finally, the provided experimental results are offered for both crashworthiness evaluation of the examined conditions regarding their effect on structures energy absorption capacity, and numerical models validating procedure. In every case, the results analysis consists of estimating the main crashworthiness response characteristic parameters from the revealed load-displacement curve and the observing the occurred collapse mechanism the mode of which affects significantly the energy absorption capability of the crushed structure.

3.3.1 Test Case of Specimens 1a – 1b

For the first test case of this study, the tubular specimens 1a and 1b are subjected to axial compressive loading until maximum shortening of about 76 mm. Both specimens are about 119 mm long, however their effective initial length is considered almost 109 mm, as the ringed base configuration offers a fixed support about 20 mm in height for the tube bottom end. The recorded experimental data during the test revealed the load-displacement curves for the examined specimens, depicted in Figure 39, regarding the which a summary of previous studies on crashworthiness behavior of thin-walled structures suggest that each local peak of the curve refers to the formulation of an external fold, while each locally minimum curve point refers to the formulation of an internal fold. Table 2 presents the critical response parameters for each test case as the experimental data processing revealed for specimens 1a-1b. Finally, Figure 40 depicts the states of the axial collapse for the two specimens, while Figures 44 and 45 show different aspects of the final crushed structures.

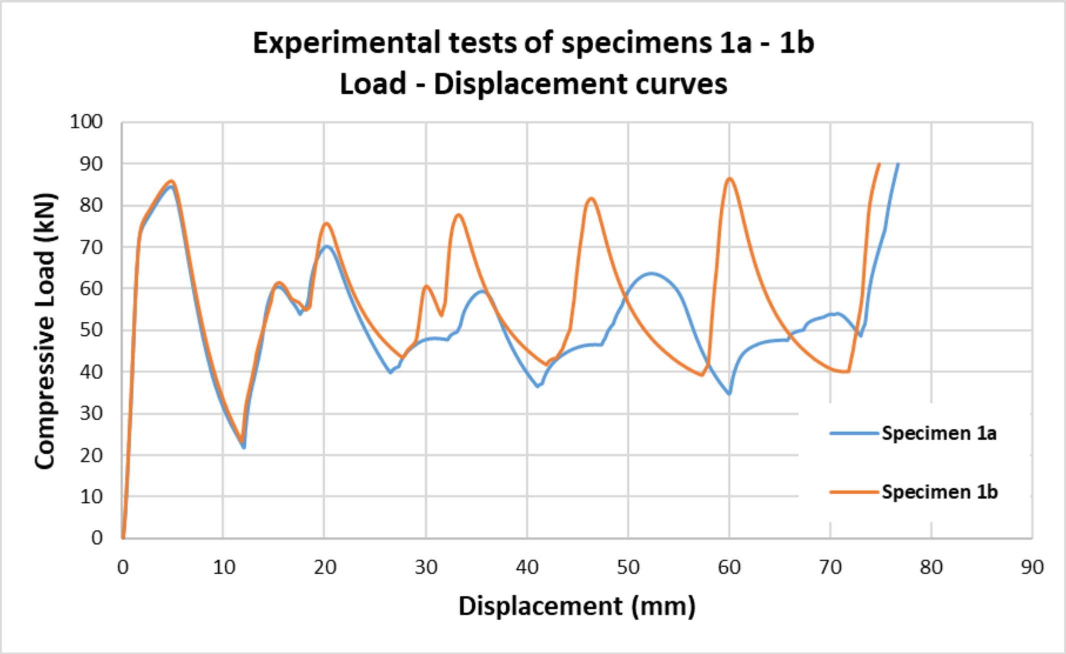

Figure 39 Experimental load-displacement curves of specimens 1a-1b

	Specimen 1a	Specimen 1b	Deviation (%)
Peak Load (kN)	90.01	90.04	0.03
Mean Load (kN)	52.11	56.03	6.99
Absorbed Energy (kJ)	4.00	4.19	4.65
SEA (kJ/kg)	26.25	27.23	3.58
Load Uniformity (-)	0.58	0.62	6.96

Table 2 Critical response metrics for specimens 1a-1b

Experimental results revealed a sufficient agreement between the two compression tests with specimen 1b providing a greater energy absorption capability as the sustained load in post-buckling range proved to be almost 7% higher than the one of specimen 1a. In addition, although the crushing force for the collapse initiation was about 85 kN for both specimens, the peak load for both ones lied around 90 kN due to the fact that at the final stages of the tests, the crushed specimen mass was concentrated around ringed base configuration resulting in higher resistance against further shortening.

Moreover, as depicted by the following figures, both specimens responded in axial loading by collapsing in a progressive and stable mode, making them capable of dissipating significant amounts of the crushing energy. Both specimens formulated the same number of convolutions during their plastic collapse as the load-displacement curves and the following figures confirm, starting from the top tube end where the crushing loads were applied, while bottom tube end remained undeformed due to its fixed constraint by the ringed base. More specifically, specimen 1a deformed subjected to a mixed collapse mechanism (Figure 41) formulating initially axisymmetric folds and then 2D-diamond folds. In contrast, specimen 1b collapsed formulating all its folds axisymmetrically revealing a concertina mode (Figure 42) which brought slightly higher energy absorbing levels as the concertina collapse mode offers the greater energy dissipation capacity among the other collapse mechanisms.

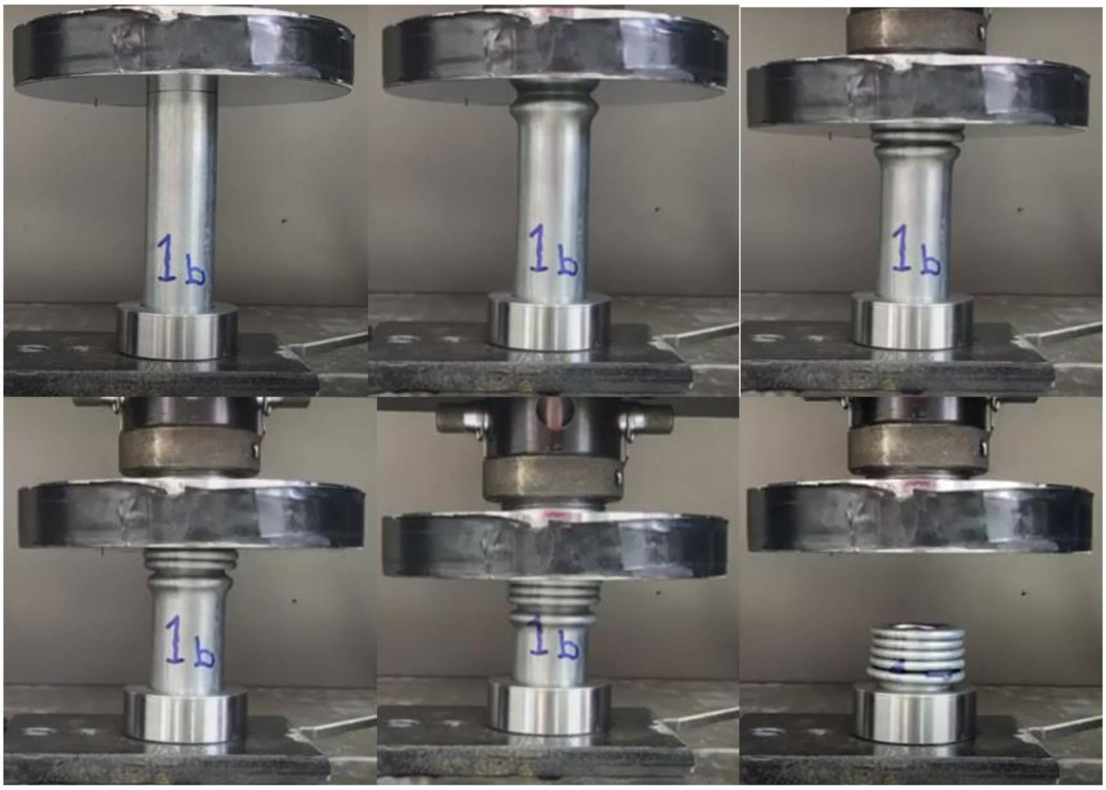

Figure 40 States of specimen 1b axial collapse

Figure 41 Crushed structure of specimen 1a

Figure 42 Crushed structure of specimen 1b

3.3.2 Test Case of Specimens 2a – 2b

The tubular specimens 2a and 2b are tested in oblique compression against 3^{o} loading angle until maximum shortening of about 54 mm. Both specimens are about 88 mm in length, however their effective initial length is considered almost 68 mm, as the bottom tube zone of 20 mm is fixedly supported by the ringed base. The experimental recorded data revealed the load-displacement curves for the examined specimens, depicted in Figure 43. The critical crashworthiness response metrics for each test case are presented in Table 3 as the experimental data analysis revealed for specimens 2a-2b.

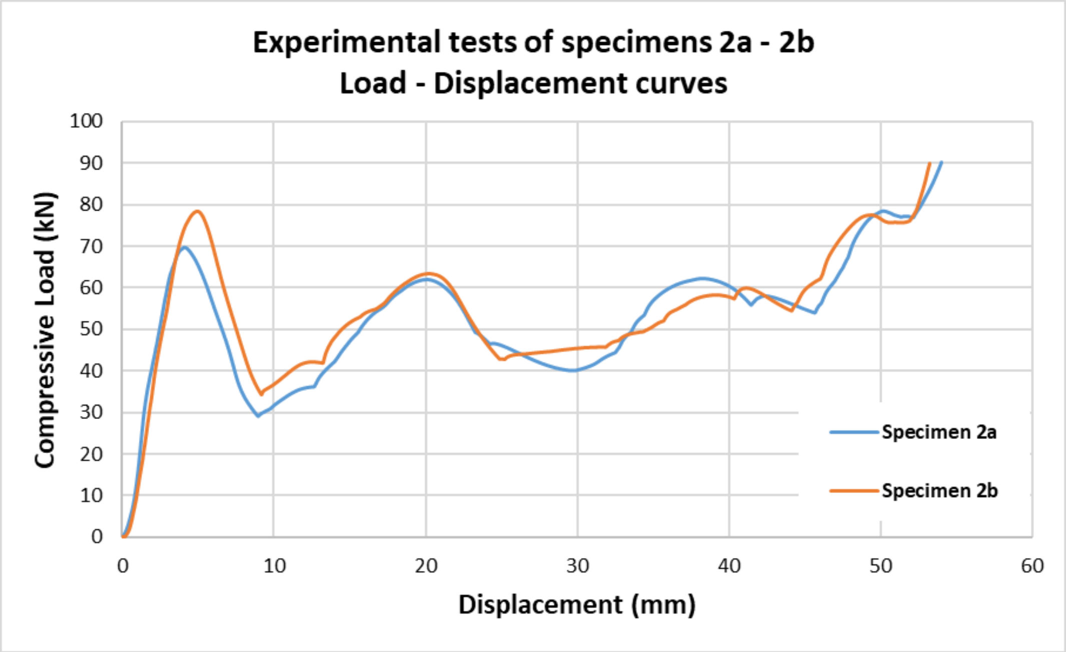

Figure 43 Experimental load-displacement curves of specimens 2a-2b

	Specimen 2a	Specimen 2b	Deviation (%)
Peak Load (kN)	90.06	90.04	0.03
Mean Load (kN)	52.81	54.29	2.73
Absorbed Energy (kJ)	2.85	2.89	1.30
SEA (kJ/kg)	25.12	25.61	1.91
Load Uniformity (-)	0.59	0.60	2.76

Table 3 Critical response metrics for specimens 2a-2b

The provided results from the experimental data analysis revealed a sufficient agreement between the two conducted tests with specimen 2b providing a greater specific energy absorption level around 1.9% compared to specimen 2a mainly due to its higher collapse initiation load. More specifically, both specimens revealed a maximum crushing load at 90 kN, however the required load for the plastic collapse initiation seemed slightly lower about 80 kN and 70 kN for specimens 2b and 2a respectively. During the post-buckling region of the tested tubes, the load distribution tends to increase with peaks and lows due to folds formulation, while the concentrated mass of each crushed structure results in increasingly higher resistance against further deformation. This tendency is considered to be introduced due to loading angle effect as the deformed structure collapses subjected to combined compressive and bending loads which increase as the failure mechanism progresses.

Following figures depict the captured states during the collapse of specimen 2b and the final views of the crushed structures. Both specimens subjected to 3^o oblique compression responded by collapsing in a progressive and stable mode formulating 2D-diamond convolutions. The loading angle proved to be not enough to result in an unstable bending collapse mode, however the occurred diamond mode revealed lower energy absorbing levels compared to previous specimens 1a and 1b which collapsed axially. The lower mean crushing force levels observed in current test case can be attributed to the combined compressive and bending loadings of oblique crushing conditions which resulted in lower structure resistance against the initiation and progression of the plastic collapse.

Figure 44 States of specimen 2b oblique collapse

Figure 45 Crushed structure of specimen 2a

Figure 46 Crushed structure of specimen 2b

3.3.3 Test Case of Specimens 3a – 3b

For current third test case, specimens 3a and 3b are tested against oblique compression under 6^{o} loading angle. Both specimens are of 88 mm initial length, however their effective initial length is considered 20 mm lower due to their fixedly supported bottom zone which is constrained from the ringed base. The specimens are shortened about 60 mm during the compression tests until the upper plate approaches marginally the bottom base. The experimental data analysis revealed the load-displacement curves for the examined specimens and the critical crashworthiness response parameters presented following respectively.

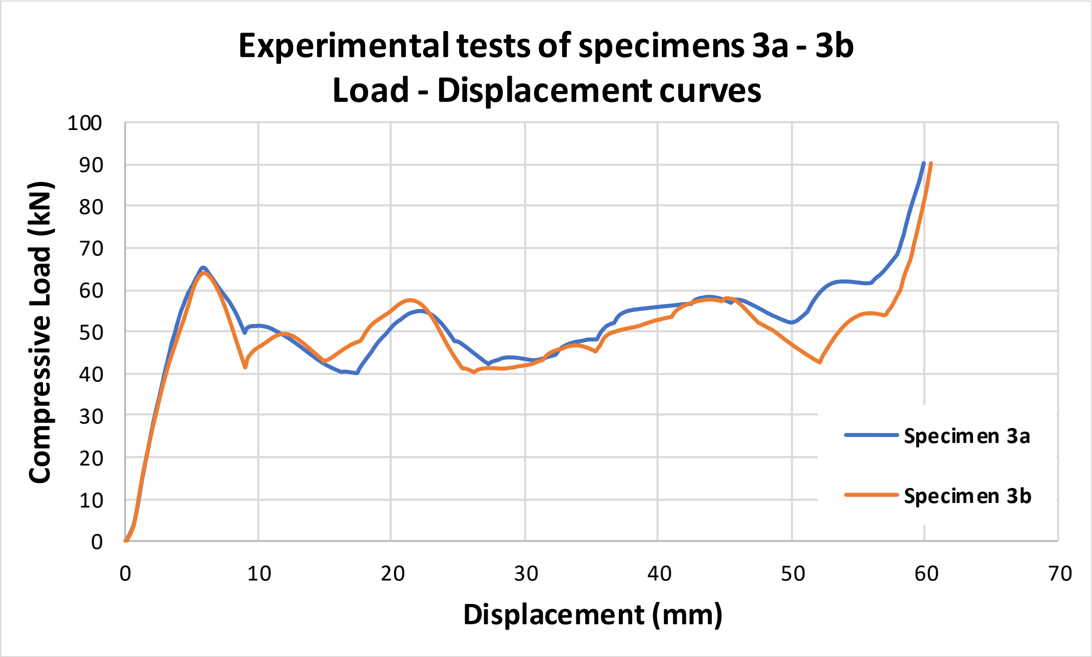

Figure 47 Experimental load-displacement curves of specimens 3a-3b

	Specimen 3a	Specimen 3b	Deviation (%)
Peak Load (kN)	90.22	90.19	0.03
Mean Load (kN)	51.42	49.19	4.53
Absorbed Energy (kJ)	3.08	2.97	3.58
SEA (kJ/kg)	26.79	26.30	1.87
Load Uniformity (-)	0.57	0.55	4.50

Table 4 Critical response metrics for specimens 3a-3b

The two experimental tests appeared a sufficient agreement in the main crashworthiness response metrics as the load-displacement curves depict above. The two specimens revealed a maximum crushing force around 90 kN, while the initial peak load for plastic collapse initiation lied about 66 kN. In both test curves depicted in Figure 47, the applied forces tend to increase dramatically at the final stages of the collapse due to the concentrated mass of crushed structure around the ringed bottom base. Further, the specimens of current test case revealed lower amounts of dissipated energy compared to the ones subjected to axial loading as expected because the oblique loading angle of 6^o resulted in further bending loads except the axially compressive ones. Additionally, compared to the examined specimens of 2nd test case under 3^o oblique angle, the specific energy absorption is also expected to lie to lower levels considering a relative correction for provided results of specimens 2a and 2b accounting for an equal final shortening which would result in greater amounts of absorbed energy. In particular, considering an equivalent shortening of 60 mm for specimens 2a and 2b, the absorbed energy should increase around 3.21 kJ resulting in greater crashworthiness efficiency as expected due to the loading angle impact which is also confirmed by major previous relative studies of open literature regarding the axial and oblique crashworthiness response.

The collapse captured states of specimens 3a and 3b showed a progressive and stable collapse as depicted in Figure 48 and Figure 49. Both specimens subjected to 6^o oblique compression responded formulating 2D-diamond folds, while the crushed mass observed to be concentrated around the ringed configuration of bottom base as the final views depict. Finally, the loading angle once again proved to be not enough to result in an unstable bending collapse mode, while the crushed mass around the fixed support ring increased the contact area with the upper plate resulting in significantly higher applied loads at the final stages of the tests.

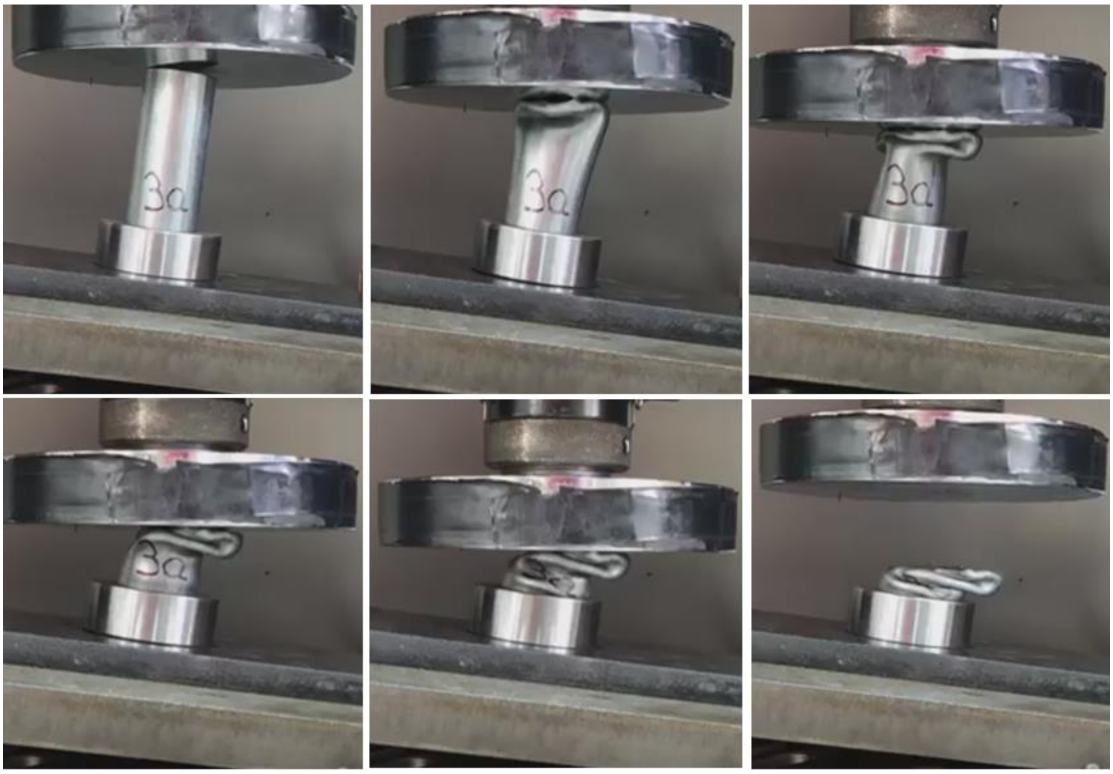

Figure 48 States of specimen 3a oblique collapse

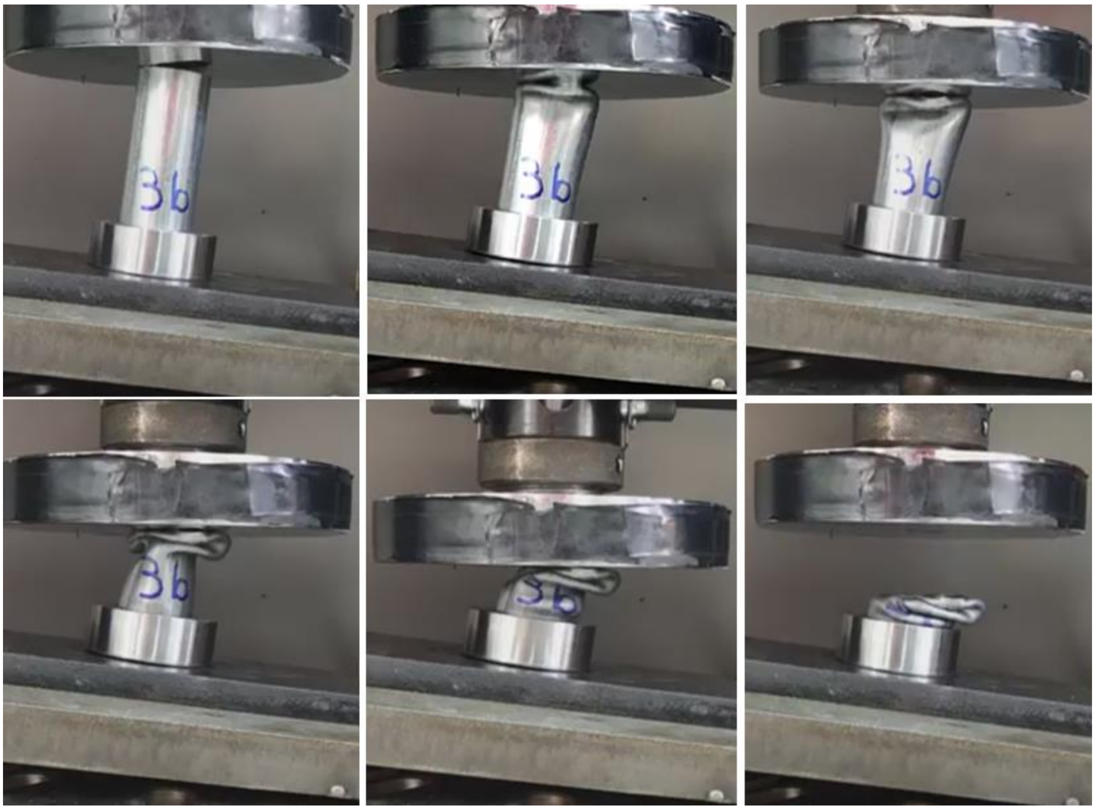

Figure 49 States of specimen 3b oblique collapse

Figure 50 Crushed structure of specimen 3a

Figure 51 Crushed structure of specimen 3b

3.3.4 Test Case of Specimens 4a – 4b

In the presented 4th test case, specimens 4a and 4b are tested against oblique compression under 9° loading angle. Both specimens are of 88 mm initial length, however their effective initial length is considered 20 mm lower due to their fixedly supported bottom zone which is constrained from the ringed base. The specimens are shortened about 64 mm during the compression tests until the upper plate approaches marginally the bottom base. The experimental data analysis revealed the load-displacement curves for the examined specimens and the critical crashworthiness response parameters presented following respectively.

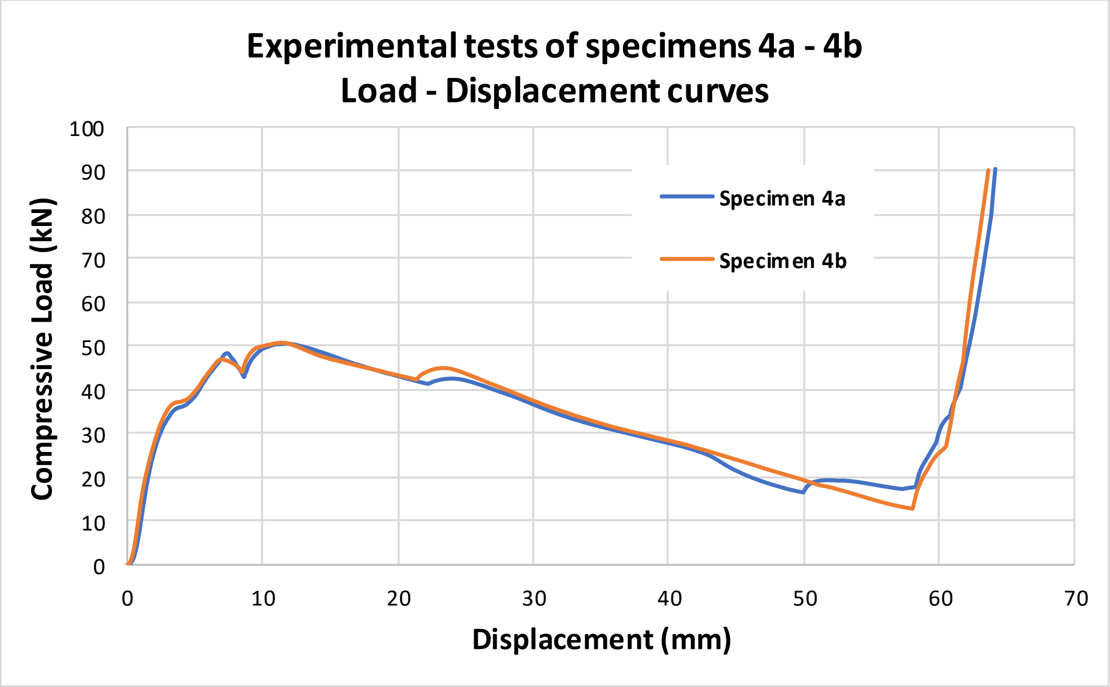

Figure 52 Experimental load-displacement curves of specimens 4a-4b

	Specimen 4a	Specimen 4b	Deviation (%)
Peak Load (kN)	90.43	90.14	0.32
Mean Load (kN)	33.99	34.27	0.83
Absorbed Energy (kJ)	2.18	2.18	0.02
SEA (kJ/kg)	19.01	19.08	0.37
Load Uniformity (-)	0.38	0.38	1.14

Table 5 Critical response metrics for specimens 4a-4b

The two experimental tests appeared a sufficient agreement in the main crashworthiness response metrics as depicted by the load-displacement curves and the results reported in Table 5. The maximum crushing force was about almost 90 kN for both specimens, however the crushing load required for the plastic collapse initiation lied to lower levels about 50 kN affected by the increased loading angle and low friction levels between top tube end and upper plate crushing surface. In both experimental curves, the applied loads start to decrease after the plastic collapse initiation due to the local bending occurred at bottom tube end, resulting in significantly lower energy absorbing levels compared to the previous test cases. However, at the final stages of post-buckling region the compressive load shows a dramatic increase due to the concentrated mass of crushed structure which not only increased the contact area with the upper plate, but also maintains contact with the ringed base surface.

Further, observing the following figures, the captured states of failure mechanism depict that both specimens began to deform by formulating initially two 2D-diamond folds; one on top tube end and one on the bottom end. Following, the specimens collapsed in a bending mode around the bottom formulated fold without being capable of absorbing significant amounts of the crushing energy. Therefore, specimens 4a and 4b revealed the lowest energy absorption capacity compared to the previous test cases, as the increased loading angle of 9^o resulted in an unstable failure under bending collapse mode which is responsible for the continuous decrease of the applied forces except the last stages of the collapse where the compressive load showed a local increase as the concentrated mass of the crushed structure brought higher resistance against further specimen shortening.

Figure 53 States of specimen 4a oblique collapse

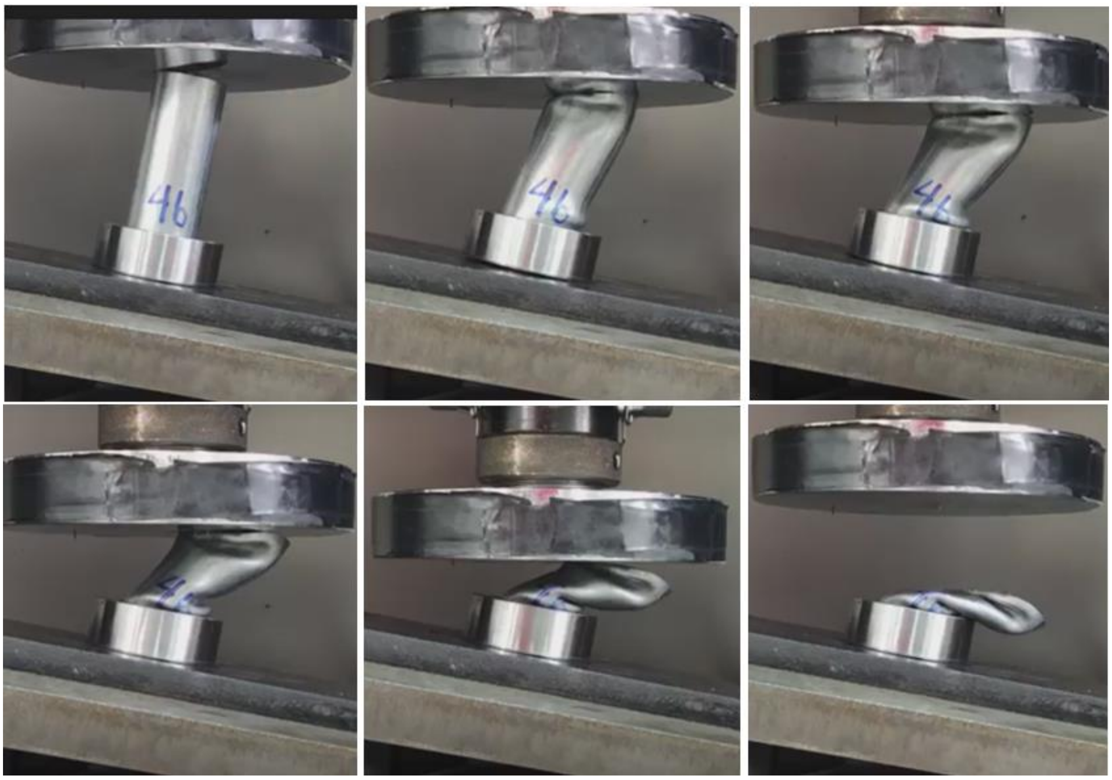

Figure 54 States of specimen 4b oblique collapse

Figure 55 Crushed structure of specimen 4a

Figure 56 Crushed structure of specimen 4b

3.3.5 Test Case of Specimens 5a – 5b

In last present test case, specimens 5a and 5b are subjected to 11° oblique compression test. Both specimens are of about 88 mm initial length with a 20 mm fixedly supported bottom end zone which results in an effective initial length around 68 mm. The specimens are compressed about maximum shortening of about 65 mm until the upper plate approaches marginally the bottom base. The experimental data analysis revealed the load-displacement curves for the examined specimens and the critical crashworthiness response parameters presented following respectively.

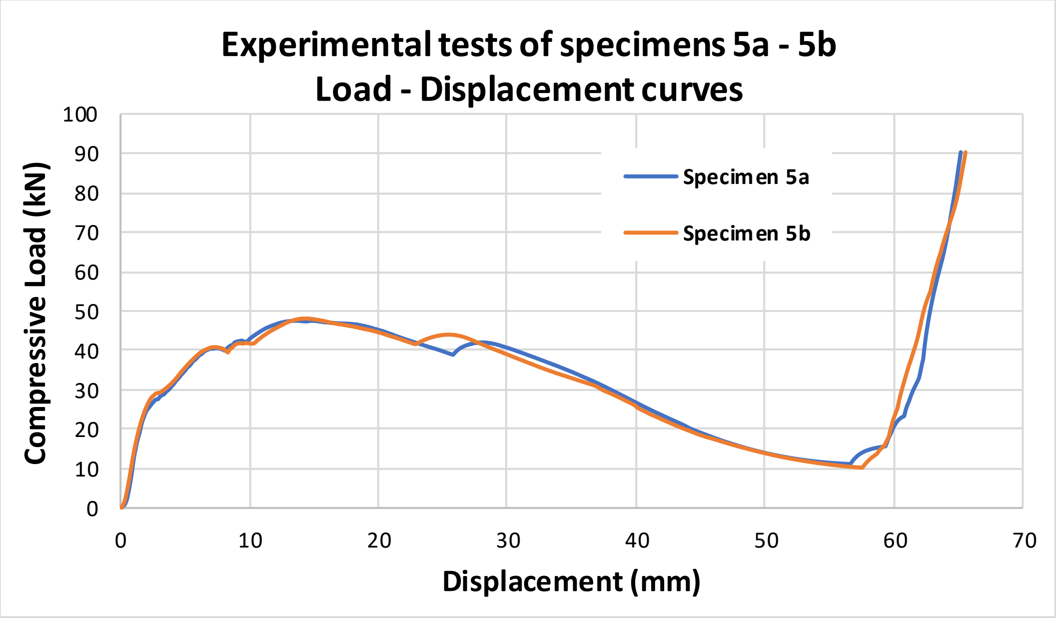

Figure 57 Experimental load-displacement curves of specimens 5a-5b

	Specimen 5a	Specimen 5b	Deviation (%)
Peak Load (kN)	90.3	90.27	0.03
Mean Load (kN)	32.40	32.81	1.24
Absorbed Energy (kJ)	2.11	2.15	1.79
SEA (kJ/kg)	19.08	18.67	1.19
Load Uniformity (-)	0.36	0.36	1.27

Table 6 Critical response metrics for specimens 5a-5b

The two experimental tests appeared a sufficient agreement in the main crashworthiness response metrics as depicted by the load-displacement curves and the provided analysis results. The maximum crushing force was about almost 90 kN for both specimens, however the required crushing load for the plastic collapse initiation restricted slightly lower than 50 kN affected by the increased loading angle of 11^{o} which resulted in sliding conditions between top tube end and upper plate crushing surface and further bending loading during collapse. In both experimental curves, the applied loads start to decrease after the plastic collapse initiation due to the local bending occurred at bottom tube end, resulting in the lowest energy absorbing levels compared to all previous test cases. However, at the final stages of post-buckling region the compressive load revealed a significant increase due to the concentrated mass of crushed structure which not only increased the contact area with the upper plate, but also maintains contact with the ringed base surface providing a stronger bottom support.

Finally, the captured states of the oblique collapse depicted in following figures confirm that both specimens started to collapse by initially formulating a 2D diamond fold on upper tube end and one on bottom tube end, while at next the structure continued to deform by being bended around the bottom fold. So, specimens 5a and 5b revealed the lowest energy absorption capacity compared to all previous test cases, as the maximum tested loading angle of 11^{o} resulted in an unstable collapse combining both compressive and bending loads which revealed their greatest magnitude as the loading angle of this case is the higher examined.

Figure 58 States of specimen 5a oblique collapse

Figure 59 States of specimen 5b oblique collapse

Figure 60 Crushed structure of specimen 5a

Figure 61 Crushed structure of specimen 5b

3.4 Conclusions

By summarizing the provided experimental results, critical conclusions can be extracted for the crashworthiness response of the examined tubular structures subjected to axial or oblique loading. The experimental data analysis carried out for each test case consisted of the provided load-displacement curve and the estimated main crashworthiness response metrics, while also the occurred collapse mechanism was further observed by capturing different states of collapse and examining the final crushed structure view. Both stages of the experimental analysis aim to assess the crashworthiness behavior of the tested specimens under the specific loading conditions in order to finally evaluate their efficiency under crushing conditions and provide the experimental results for the numerical models validation procedure. The comparison between the tested cases for the final evaluation took into consideration mainly the amount of specific absorbed energy as the most significant parameter because it offers results corrected to specimen geometry, mass or material, and therefore is treated as the most appropriate metric for the final evaluation of the crashworthiness response.

Therefore, summarizing the presented results of previous sub-sections of current chapter, regarding firstly the occurred failure mechanism, specimens 1a and 1b revealed a stable and progressive collapse under mixed and concertina modes respectively. In particular, specimen 1a collapsed by initially formulating an axisymmetric convolution and continued deforming 2D-diamond folds. In contrast, specimen 1b collapsed formulating only axisymmetric folds revealing thus the greatest energy absorption capability among the others. Further, specimens 2a-2b and 3a-3b subjected to oblique loading under 3^o and 6^o angle respectively, revealed also a stable and progressive collapse formulating 2D-dimaond folds. The oblique loading angle affected their energy dissipation levels with a progressive decrease, as bending loads are introduced except the compressive ones which took place exclusively in axial loading. Finally, specimens 4a-4b and 5a-5b collapsed by initially formulating a fold on tube top and bottom ends, while they continued deforming under a bending mode similar to Euler-type buckling one, as the compressed specimen structure was locally bended around the bottom formulated fold.

Figure 62 Final views of crushed structures (specimens 1 / 2 / 3 / 4 / 5 from left to right, a: top specimens, b: bottom specimens)

Regarding the revealed response metrics from the load-displacement curves, the maximum peak crushing force lied about 90 kN for all examined test cases, however the plastic collapse initiation load revealed a decrease as the loading angle gets higher as Figure 63 depicts. The above occurred tendency is attributed to the fact that as the loading angle increases, except the axial compressive loads, additional bending ones are introduced resulting in lower structure resistance against the initiation and progression of its plastic deformation. However, the maximum load seems almost unvaried as at the final stages of the collapse, the concentrated crushed structure mass revealed the same total resistance against further shortening, maintaining the peak load constant at 90 kN for all examined test cases.

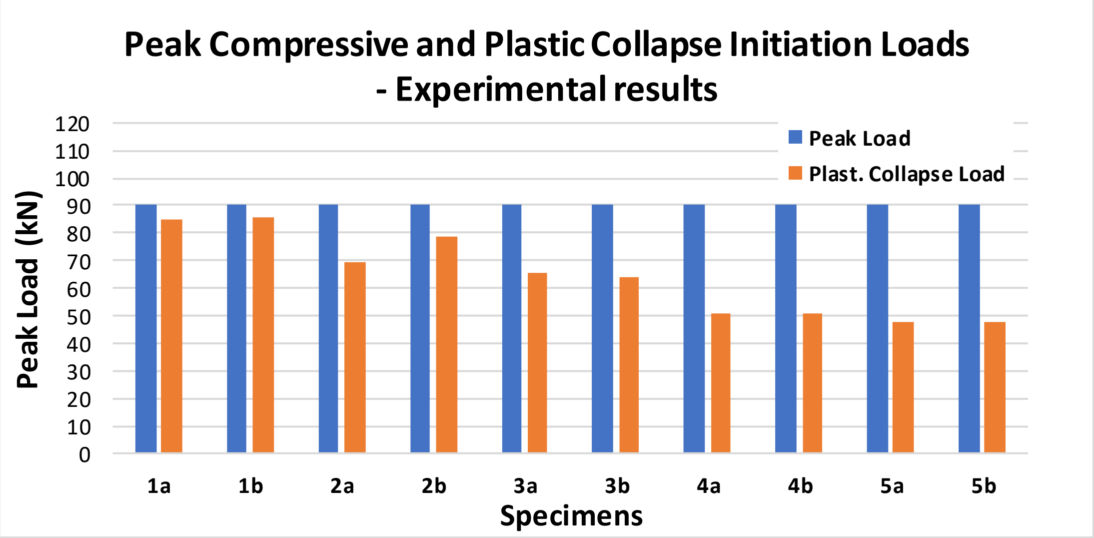

Figure 63 Experimental results for peak crushing and plastic collapse initiation loads of the examined specimens

Similarly, the mean crushing load proved to decrease as the oblique angle load becomes greater affecting in subsequence the amount of absorbed energy. In particular, specimens 4a-4b and 5a-5b revealed significantly lower levels of absorbed energy, as they were the ones where a local bending collapse mode was occurred which cause a significant drop to energy dissipation capability due to its unstable characteristics. Moreover, as depicted from the following figures, the axially compressed specimens revealed the greatest energy absorption capacity proving to be the most efficient structures in terms of crashworthiness response offering the most beneficial loading conditions.

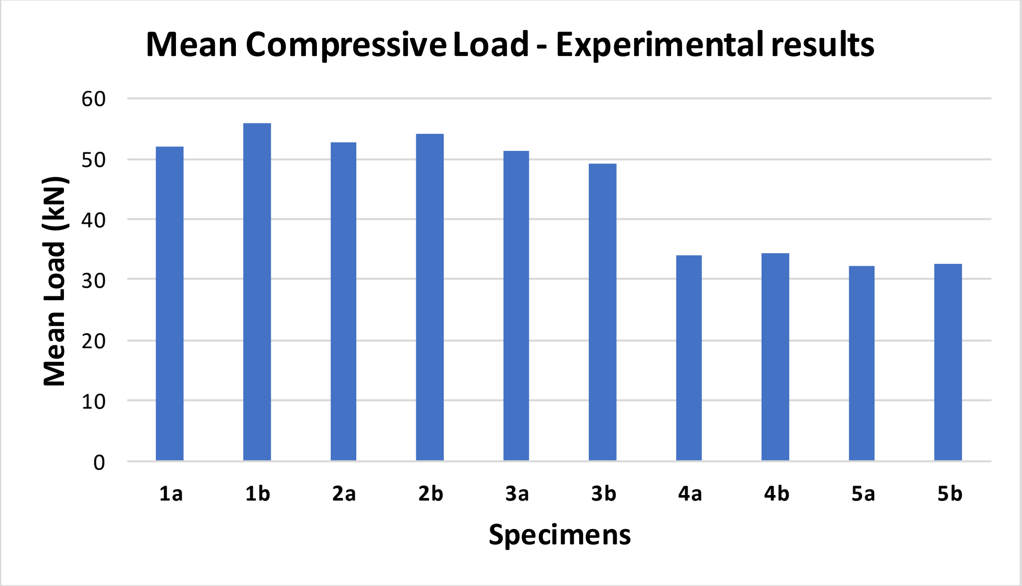

Figure 64 Experimental results for mean crushing load of the examined specimens

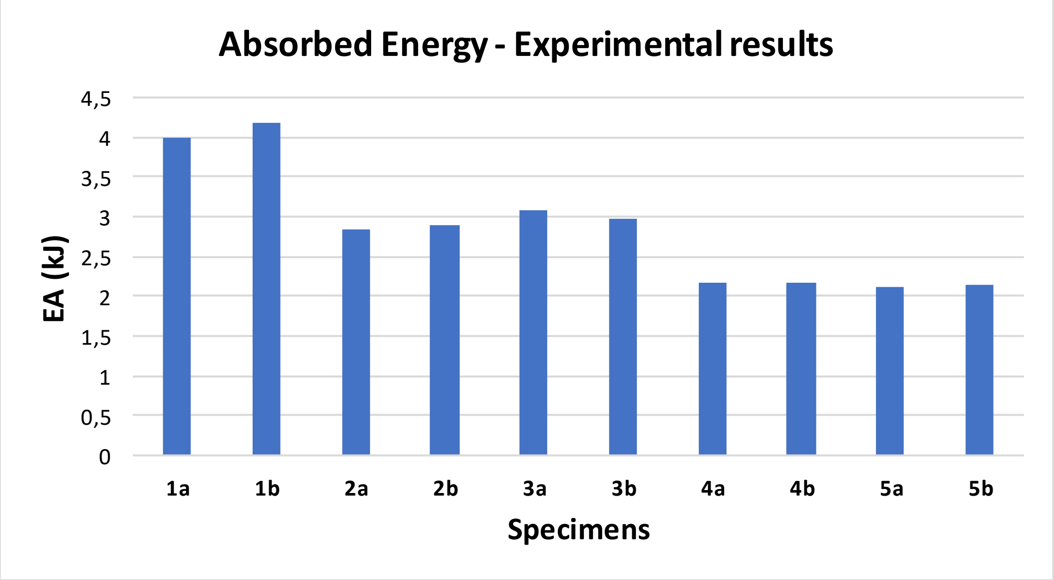

Figure 65 Experimental results for energy absorption capability of the examined specimens

In fact, Figure 66 confirms the previous conclusion, revealing that the axially compressed specimens 1a-1b are described by the highest specific energy absorption levels, which decrease as the loading angle is getting higher. The above observation could be of even more significant importance if only the post-buckling region of the load-displacement curves was taken into account without considering the final stages of collapse where the compressive loads were applied to the concentrated crushed mass the resistance of which caused a local increase of the applied forces. Further, the reported tendency is also confirmed by observing the load uniformity variation through the test cases, which also suggest specimens 1a-1b as the more crashworthy structures followed by specimens 2a-2b.

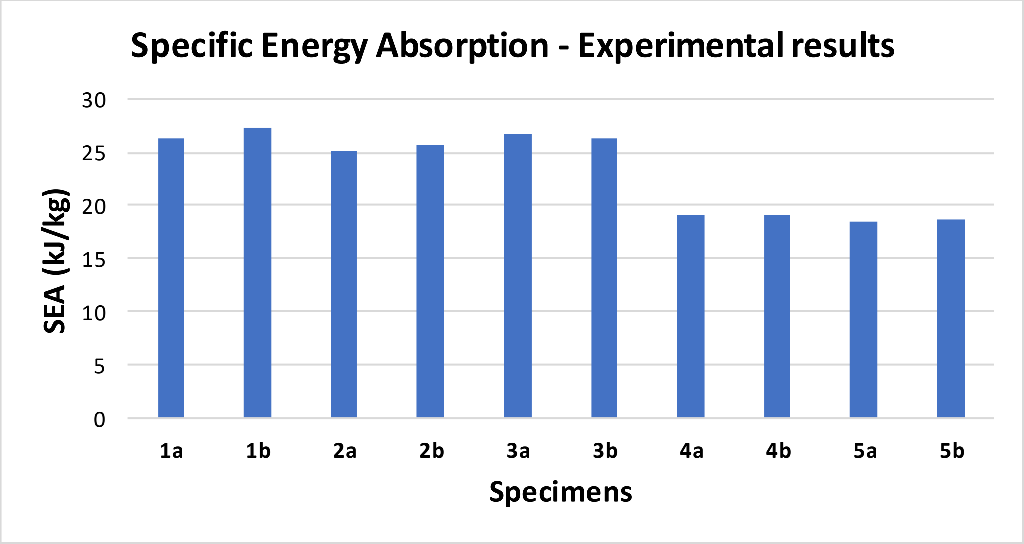

Figure 66 Experimental results for specific energy absorption of the examined specimens

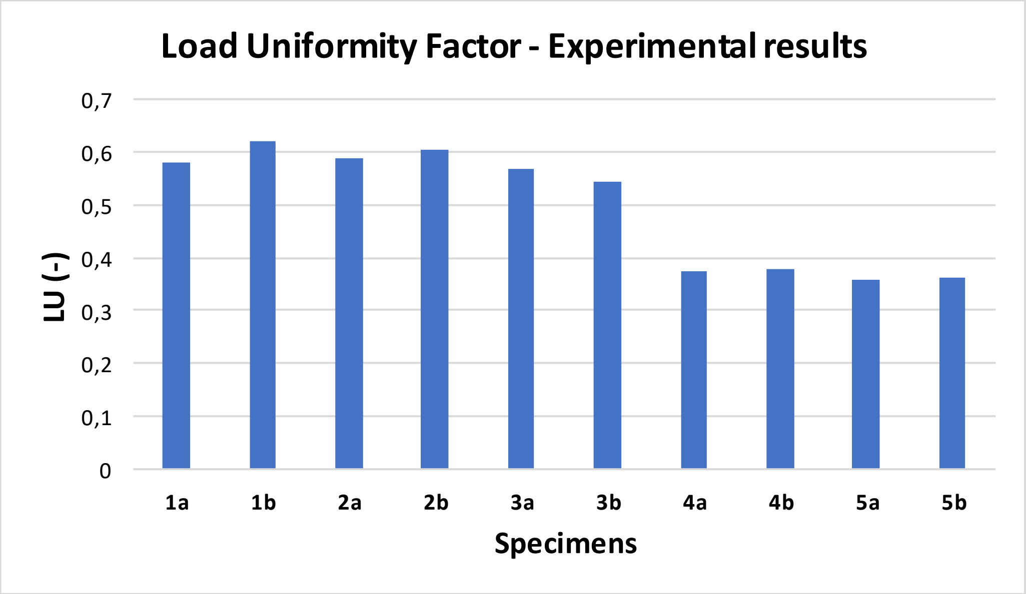

Figure 67 Experimental results for load uniformity factor of the examined specimens

Finally, the following figures depict the variation of mean and plastic collapse initiation loads with respect to the examined loading angles. As shown, the plastic collapse initiation load reveals a continuous linear decrease as the loading angle increases which can be attributed to the additional bending loads which are introduced, increasing as the oblique loading angle gets higher resulting in additionally higher bending moment facilitating the plastic collapse start. On the other hand, mean crushing load reveals a slight decrease at low loading angles due to the additional bending loads which reduce the required vertical collapse load, while the loading angle of about 6° seems to be the critical angle which affects significantly the energy absorbing levels reacting to a sharper drop due to the bending introduced mode and lower energy absorption amounts as the structure plastic deformation becomes more unstable and less progressive.

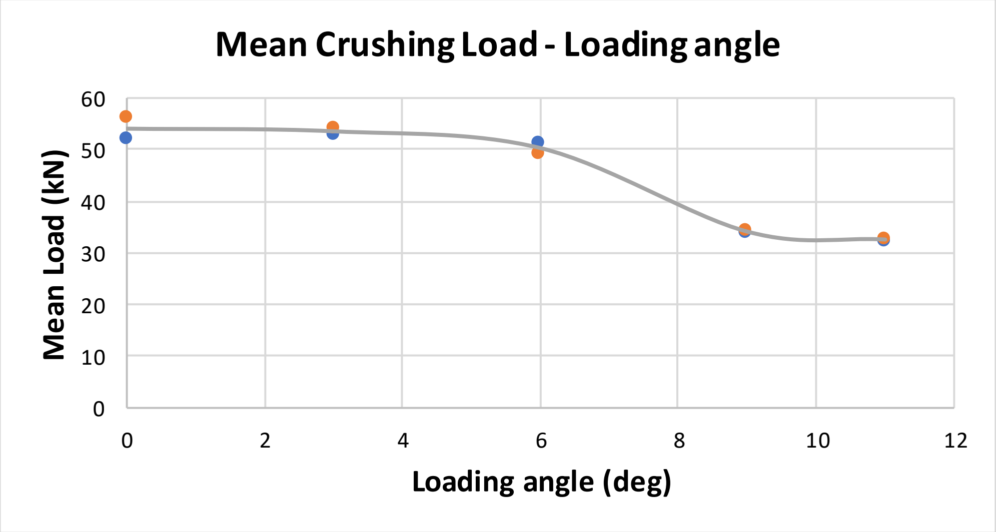

Figure 68 Mean crushing load variation with loading angle

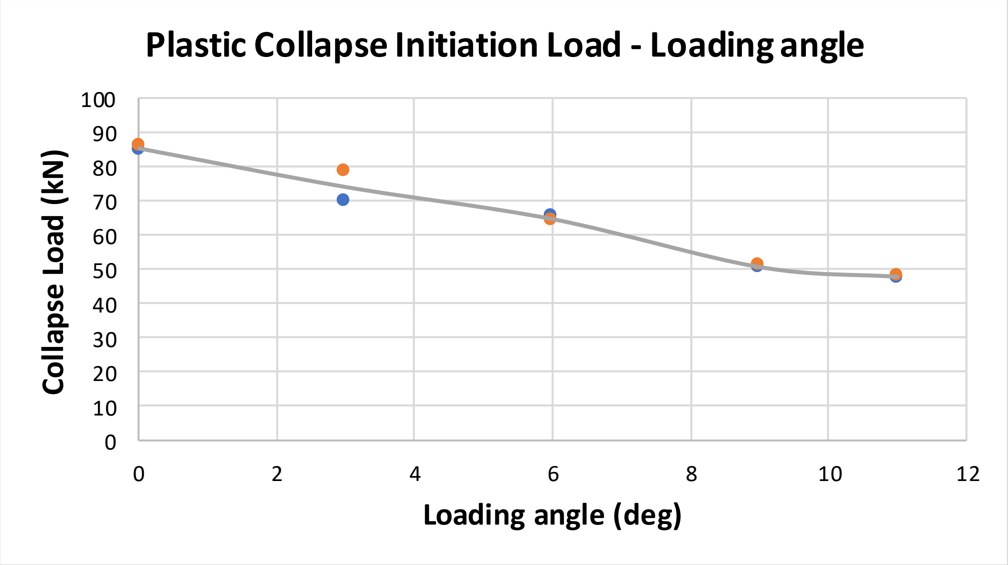

Figure 69 Collapse initiation load variation with loading angle

4. Finite element modelling approach and simulation results

4.1 Introduction

The aim of this study is to investigate crashworthiness behavior of circular thin-walled steel tubes by both conducting experimental tests and numerical simulations. The development of appropriate finite element models in software offers the capability to obtain the crashworthiness response characteristics and the failure mode without spending high costs for experimental equipment. Also, a number of simulations can be carried out to predict the effect of various parameters on crushing response of examined structures by determining both their interaction level and its magnitude. Such important and interesting to analyze parameters can be related to structure geometry, like geometrical shape and dimensions (length, diameter, thickness, cross-section geometry etc.), the kind of material, special structure configurations (edges, cross-section variation, stress concentration etc.), type of edge supports etc., or can be related to loading characteristics like crushing speed, crushing angle, temperature etc. However, an important step before carrying out any numerical simulation is the comparison of developed models with experimental data in order to assess their validity and accuracy level.

The study of current master thesis utilizes Finite Element Analysis (FEA) for the needs of model development. In particular, a finite element modelling approach is used in this work in order to create the appropriate models of the examined configurations. LS-DYNA software [31] is utilized as the modelling tool for the purposes of current study. In general, the first step of modelling procedure with FEA is the geometry determination of the structure by defining the structure geometrical shape and its appropriate dimensions. Next, mesh generation usually follows by properly distributing the finite element nodes crating that way the elements mesh. Many softwares offer the capability for an automatic mesh generation, but they allow users to select by their own the preferable mesh density and type of finite elements. Also, the material properties of the created structural model are defined too, by giving information about physical and mechanical properties, like yield stress, Young modulus, Poisson ratio, density and finally the stress-plastic strain curve. After that, the support characteristics must be enforced, while the last stage of modelling is to define the loading characteristics.

The above modelling steps are made in the pre-processor of LS-DYNA. So, by summarizing, the pre-processing procedure includes the following steps:

- ✓ Geometry determination
- ✓ Mesh generation
- ✓ Material properties
- ✓ Support characteristics
- ✓ Loading characteristics

As soon as the model is developed, LS-DYNA solver computes the response of the examined structure under the defined loading, by solving the equations provided from the implementation of FEA. Finally, when the numerical solution by the solver ends, LS-DYNA post-processor allows to observe the response of crushed structure under loading conditions. Further, post-processor provides critical data for the crushed structure like crashworthiness characteristics, observed failure mode, load-deflection diagram etc. Thus, the modelling and calculating procedure in LS-DYNA includes the following three stages as Figure 70 depicts. The first and the last stage of the illustrated procedure can be both conducted in LS Pre-Post as made in current work. LS Pre-Post includes both pre-processor and pro-processor of LS-DYNA, but not the solver which is provided by ANSYS software.

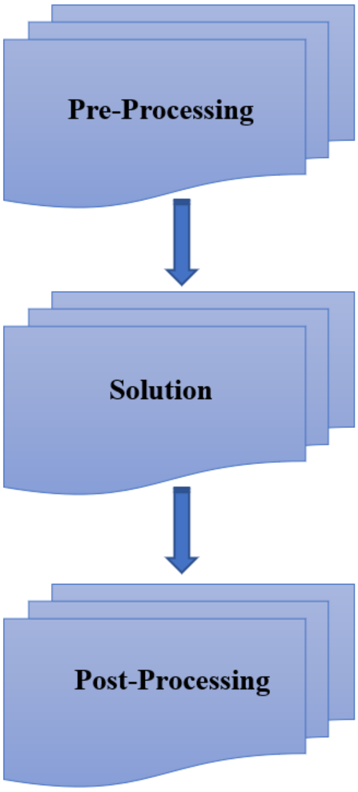

Figure 70 Modelling and calculating procedure of FEA in LS-DYNA

Finally, the unit system which LS-DYNA uses is shown in Table 7. Each produced variable is also expected to be described by the respective units, as for example the unit of N·mm = mJ for energy accounting.

Variable	Units
Mass	gr
Length	mm
Time	msec
Velocity	mm/msec
Force	N
Stress	N/mm^2
Density	gr/mm^3

Table 7 Units system in LS-DYNA software

4.2 Finite element modelling approach

The study of current work examines the crashworthiness response of thin-walled steel circular tubes under both axial and oblique loading conditions. The examined tubes are of 32.75 mm outer diameter and 1.56 mm wall thickness. The axially compressed specimen is 119 mm long, while the oblique tested specimens are 88 mm in height. Each examined configuration consists of the circular tube specimen, the bottom edge of which is supported to a stationary base with ringed configuration offering a fixed support for the tube, and an upper plate compressing the tube with constant rate as depicted in Figure 71. Both ringed base and upper plate are considered as rigid bodies, while tube deforms plastically dissipating that way amounts of crushing energy during its collapse. Further, rotating the bottom base support offers the capability to apply oblique compressive loads in the adjusted angle representing an off-axis oblique loading case. Present work examines both cases of axial and oblique crushing by adjusting 3°, 6°, 9° and 11° loading angles in the second case, aiming to assess the effect of loading angle on energy absorption capability, while a comparison between axial and oblique crushing is carried out to evaluate the collapse mode level of stability and its effect on crushing efficiency. The modelling procedure as conducted in the pre-processor of LS-DYNA (LS Pre-Post) is presented in more detail below.

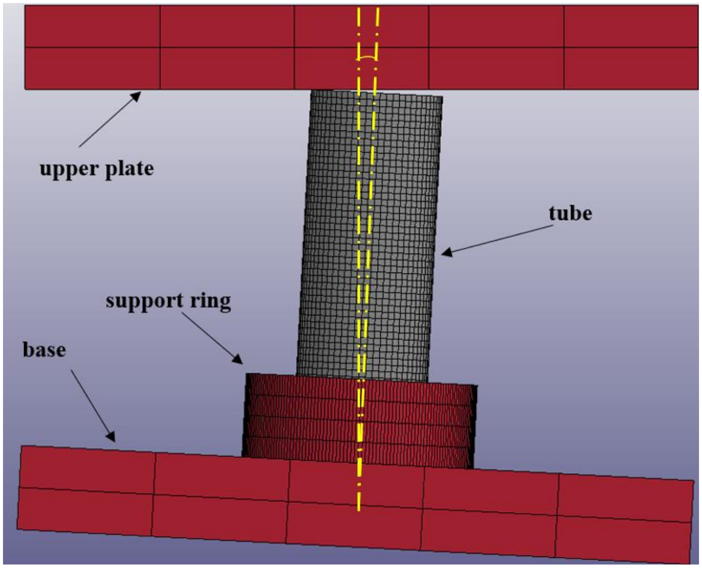

Figure 71 Examined configuration for modelling in LS-DYNA

The basic steps of modelling procedure are to initially define the desirable specimen geometry (shape and dimensions) and adjust a finite element mesh by selecting the element type and size for each body. Current work utilizes 2D shell elements for tubes and 3D solid elements for both ringed base and upper plate as they are considered as rigid bodies. Following, the material of each body is selected according to its physical and mechanical properties and the appropriate boundary conditions are defined in each interface contact. This study considers the contacts of upper plate and bottom ringed base with tube surface and also the contacts between tube folds formulated during collapse. Finally, the loading characteristics are selected by adjusting a vertical constant speed to the upper plate. In the following sections, the modelling procedure is described in more detail.

4.2.1 Geometry determination

In the first stage of modelling procedure, the specimen geometry and its dimensions are adjusted for each circular tube specimen. Because of their thin-walled structure, tube models are created using 2D plane finite elements, usually called as *shell elements*. In contrast, the upper plate and bottom ringed base which are considered compact rigid bodies, are modelled with 3D finite elements, usually called as *solid elements*. In each case, the tube models use shell elements as the size of thickness compared to the diameter or the length of the tube, is negligible. So, shell elements provide less nodes, resulting in lower computational time and cost. However, for the tube models appropriate dimensions, the use of shell elements means that each tube model is developed considering the mean tube diameter $d_m=(d_{in}+d_{out})/2=31.19$ mm. Each circular tube model is created by selecting the *Cylinder Shell* choice which is included in the *Shape Mesher* of LS Pre-Post, where the mean diameter and length dimensions are adjusted properly together with elements size. For the base and upper plate, the *Box Solid* choice of *Shape Mesher* is selected. Finally, the bottom base and the ringed configuration which offers a fixed support to tube bottom edge, are treated as common parts by selecting them and creating a common entity.

4.2.2 Mesh generation

Following, the element type and their size is selected for the bodies of the created model. In particular, the tube is modelled utilizing 4-node plane shell elements, the dimensions of which are adjusted just greater than tube wall thickness in order to make the tube model capable of predicting accurately the type and the number of the formulated folds. In fact, the elements are dimensioned such that their height is selected greater than the ratio of tube length to its wall thickness L/t, and their width similarly greater than πD/t. More specific, the tube elements are adjusted to square shape accordingly to the above assumption, while their thickness is adjusted properly within *Section Shell* option to 1.56 mm. Further, remaining in *Section Shell* option, the Belytschko-Lin-Tsay element formulation mode is selected to impose the elements deformation behavior during collapse, adjusting the ELFORM parameter equal to 2. The proposed mode of formulation is based on Reissner-Mindlin kinematic assumption, proposed also by Timoshenko, which considers the superposition of mid-surface displacements and rotations to describe plate deformation, treated in that way suitable for plane shell elements. More, Reissner-Mindlin theory assumes that cross section remains straight and unstretched like Bernoulli's theory, while shear deformations are also possible to be taken into account.

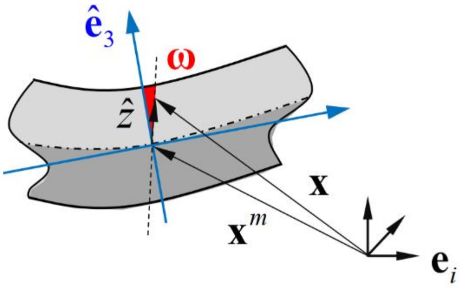

$$\mathbf{x} = \mathbf{x}^m + \hat{z}\,\hat{\mathbf{e}}_3 \times \boldsymbol{\omega}$$

Figure 72 Reissner-Mindlin bending theory

As reported, the selected tube finite elements are 4-node shell elements following Belytschko-Lin-Tsay deformation mode which provides 5 degrees of freedom (DOF) in local coordinate system for each node which are the displacements of three axis (u_x, u_y, u_z) and the two rotations (θ_x, θ_y) from bending moments, neglecting in that way only torsional rotation (θ_z). In addition, it has been proved extremely effective as it takes into account the strain rate effect and the Cauchy stresses distribution, while it enforces a bi-linear interpolation between the element nodes, but also retains the computational time in lower levels against the other available options. More, adjusting the number of through shell thickness integration points, regarding the NIP parameter in *Section Shell* option, equal to 5, the computed variables are integrated to reveal their distribution through shell thickness. Finally, a viscous and stiffness *hourglass* control for shell elements is selected for tube body with respect to Flanagan-Belytschko stiffness form setting IHQ parameter equal to 4.

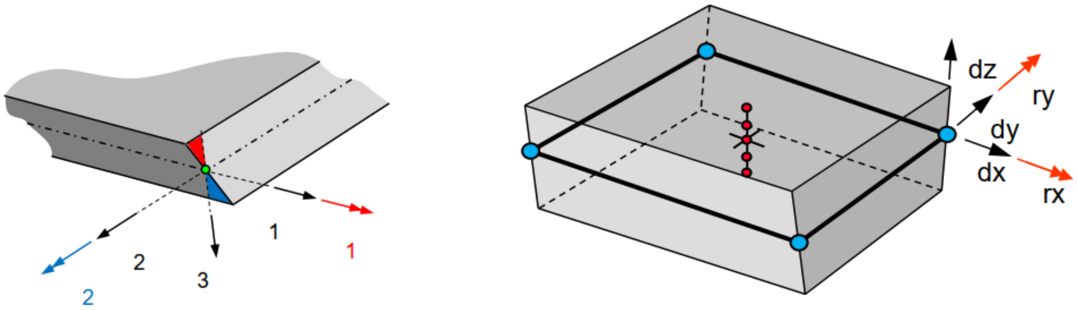

Figure 73 Belytschko-Lin-Tsay shell element with NIP = 5

For upper plate and ringed bottom base, 3D solid elements are utilized in *Solid Section*. The respective ELFORM parameter of *solid section* is kept equal to 1 as the default option, while mesh density is significantly lower as the above parts are considered as rigid bodies.

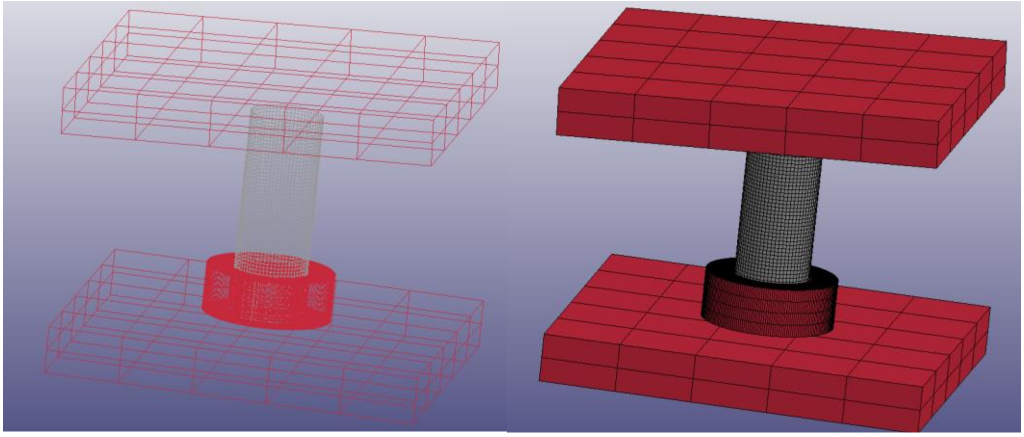

Figure 74 Mesh generation of created bodies

4.2.3 Material selection

At next, the appropriate material properties are introduced to the pre-processor. In particular, the material *MAT024_Piecewise Linear Plasticity* option is selected for tube modelling, as mild steel plastic behavior can be described by sectionally linear-hardening segments because of its ductility.

MAT024 describes the material behavior by introducing its density, Young Modulus, Poisson Ratio and yield stress, while it describes the hardening curve in plastic region with 8 points of stress and plastic strain (σ-ε_p). Specifically, density and poisson ratio of mild steel are selected according to open literature to 7.85 gr/cm^3 and 0.3 respectively. On the other hand, Young Modulus, yield stress and stress-plastic strain curve are calculated based on experimental data provided by tension test of mild steel specimen. The test was conducted in a pressing machine applying the tensile load with constant rate of 10 mm/min and recording the measured displacements and loads. The experimental tension test of mild steel specimen provided the following true stress- true strain curve as Figure 75 depicts. Table 8 presents the mechanical properties utilizing for *MAT024* description according to the experimental data provided from tension test.

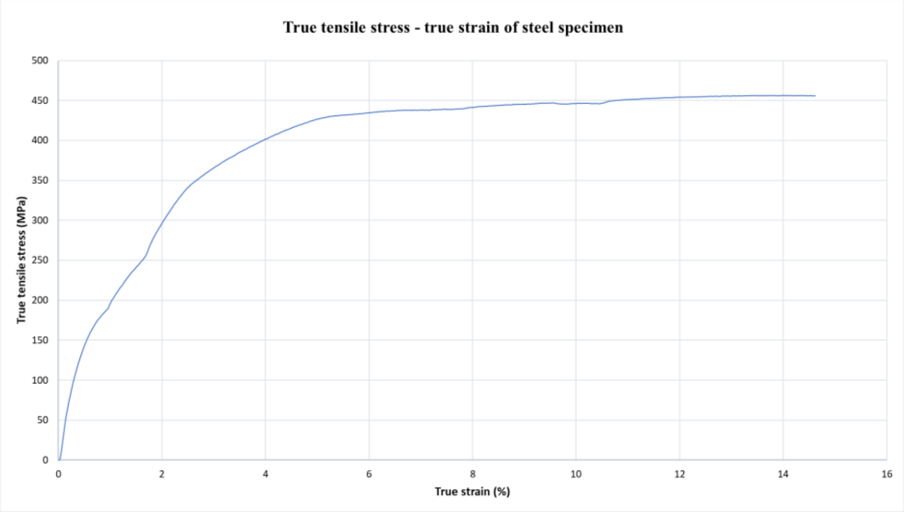

Figure 75 Stress-strain curve from experimental tension test of steel

Steel Tube		
Young Modulus (MPa)		200000
Yield Stress (MPa)		248,80
Points	*Plastic strain ε_p (-)*	*Stress σ (MPa)*
1	0	248,80
2	0,003222	308,26
3	0,007875	361,51
4	0,016826	404,88
5	0,028997	430,92
6	0,065155	444,69
7	0,089857	454,69
8	0,112053	457,27

Table 8 Test data of MAT024 tab for steel tube

In addition, material option *MAT020_Rigid* is selected to simulate upper plate and ringed bottom base bodies. Both parts are steel considered, with a typical Young Modulus of 205000 MPa, Poisson ratio of 0.3 and density of 78.5 gr/cm^3. Also, *MAT020* requires the definition of kinematic degrees of freedom (DOF) for each part. CMO parameter is set equal to 1 in order to refer to DOF constraint in global coordinate system, while an appropriate adjustment of CON1 and CON2 parameters represents the constrained displacements and rotations respectively. Thus, for the stationary ringed bottom base, CON1 and CON2 parameters are both set equal to 7 meaning that displacements and rotations are constrained in every direction. However, for the upper plate, CON1 was set equal to 4 and CON2 equal to 7 allowing the upper plate to move vertically downwards crushing the tube specimen.

4.2.4 Contacts definition

After justifying each part properties and characteristics, next step of modelling procedure is to define the type of contact between interface surfaces. For this reason, a *nodes-to-surface contact*, an *automatic surface-to-surface contact* and an *automatic single surface contact* are applied to the examined configuration to represent the no penetration boundary conditions in interface.

In particular, the *nodes-to-surface contact* does not allow the penetration of tube nodes into the surface of bottom ringed base and upper plate, and so this type of contact is applied twice to the developed model; first for upper tube edge and second for the bottom one. In each case, the tube specimen is described as the slave segment because it is considered as the deformable body in the interface, while the in-contact support is described as the master segment as rigid and non-deformable body. The master segment is stated by its part ID for upper plate case, selecting the MSTYP parameter equal to 3, while for ringed bottom base the part set ID is the definition parameter adjusting MSTYP equal to 2. The slave segment is stated by tube part ID by selecting the SSTYP parameter equal to 3. Finally, at each type of contact a static friction coefficient (FS) and a dynamic one (FD), both of 0.2 are also applied to estimate the occurred resistances from the relative motion of the two interface surfaces.

Additionally, an *automatic surface-to-surface contact* type is applied similarly as reported above, but only for the interface contact between tube folds – formulated during collapse – and ringed support surface. Further, *automatic single surface* type of contact is applied in order to avoid the penetration between the developed tube folds. In this type of contact, only slave segment is defined regarding tube part by selecting a SSTYP parameter of 3. Static and dynamic friction coefficients of 0.2 are applied in this case too.

Finally, the height of bottom tube edge which is plunged within ringed base, behaves as fixed supported end, and so after the proper node selection of tube end region, the selected nodes are constrained against displacements (DOFX = DOY = DOZ = 1) and rotations (DOFRX = DOFRY = DOFRZ = 1) in *Boundary SPC Set* option, representing in that way a fixed support for bottom tube end.

4.2.5 Loading conditions definition

The final step of modelling procedure is to define the loading curve characteristics. The crashworthiness response of the created models is simulated by adjusting a constant vertical crushing velocity of 1 mm/msec to the upper plate, which is moving down crushing tube specimen with constant rate, providing the necessary shortening regarding the conducted experimental tests.

The upper plate vertical velocity profile u(t) is properly applied in *define curve* option of keyword manager, while it is then adjusted to the upper plate in *Boundary Prescribed Motion Rigid* option, selecting a scaling factor (SF) of -1 to consider that the moving upper plate crushes the tube by moving downwards. Finally, the loading angle is adjusted by rotating both tube specimen and ringed bottom base to the proper angle about x-axis, simulating that way the examined oblique crushing conditions.

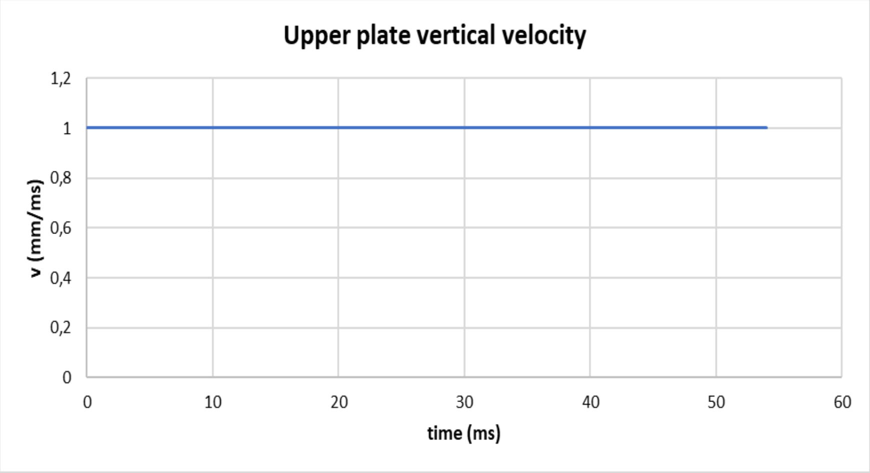

Figure 76 Loading curve

4.2.6 Database and termination

As soon as the model is developed, the database timestep is defined at 1 msec. The selected data which solver returns are the forces in the contact surfaces (*rcforc*) and the upper plate movement (*rbdout*). Thus, a load-deflection diagram is produced from the post-processor by combining the z-force (crushing load or axial compressive load) in the interface between upper plate and tube specimen, and the z-displacement of upper plate. Finally, the termination time is adjusted at proper timing for resulting in the tested specimen shortening regarding the experiments. The developed model is saved as a keyword file and after simulation termination, a *d3plot* file is created and then fed to post-processor where data processing is available, observing different stages of collapse in the same time.

4.3 Numerical simulation results

The numerical simulations of the developed finite element models are carried out in LS-Dyna software environment for the purpose of this study. The provided numerical results are presented and discussed in the following sections for each examined test case of this study. All simulations are carried out representing dynamic loading conditions by adjusting a crushing speed of 1 m/s. The analysis of numerical load-displacement curves allowed the estimation of the main crashworthiness response parameters, while also different states of collapse are recorded in order to capture the failure mechanism and assess its plastic deformation characteristics.

4.3.1 Simulation of specimen 1 case study

The finite element numerical simulation results regarding of test cases of specimens 1a-1b subjected to axial collapse under 1 m/s loading rate are presented following by Figure 77 which depicts the provided load-displacement curve and Table 9 in which the critical crashworthiness response metrics are reported.

Load-displacement curve reveals a progressive and stable collapse in post buckling region as after the plastic failure initiate to occur a sustained load of about 58 kN seems to be maintained during collapse, which varies from local peak loads indicating the external folds formulation and local minimum ones for the internal folds. Further, the plastic collapse initiation load of about 84 kN revealed to be slightly lower than the maximum one occurred around 20 mm shortening which in fact caused the formulation of third axisymmetric convolution. The stable and progressive folds formulation allowed structure 1 to develop a significant amount of absorbed energy, while also tubular structure 1 could be treated as an efficient energy absorbing device revealing a sufficiently enough load uniformity factor of 0.62 which could be also considered at 0.68 taking into account the plastic collapse initiation load instead of peak crushing load. Moreover, as Figure 78 shows, the simulation revealed a concertina collapse mode for specimen 1 formulating six axisymmetric convolutions starting for the top tube end as its bottom end is fixedly supported avoiding folding initiation in its sight according to Florent et al. [13]. The progressive deformation of concertina mode reacted in high energy dissipation levels for specimen 1 with a specific energy absorption around 27.74 kJ/kg.

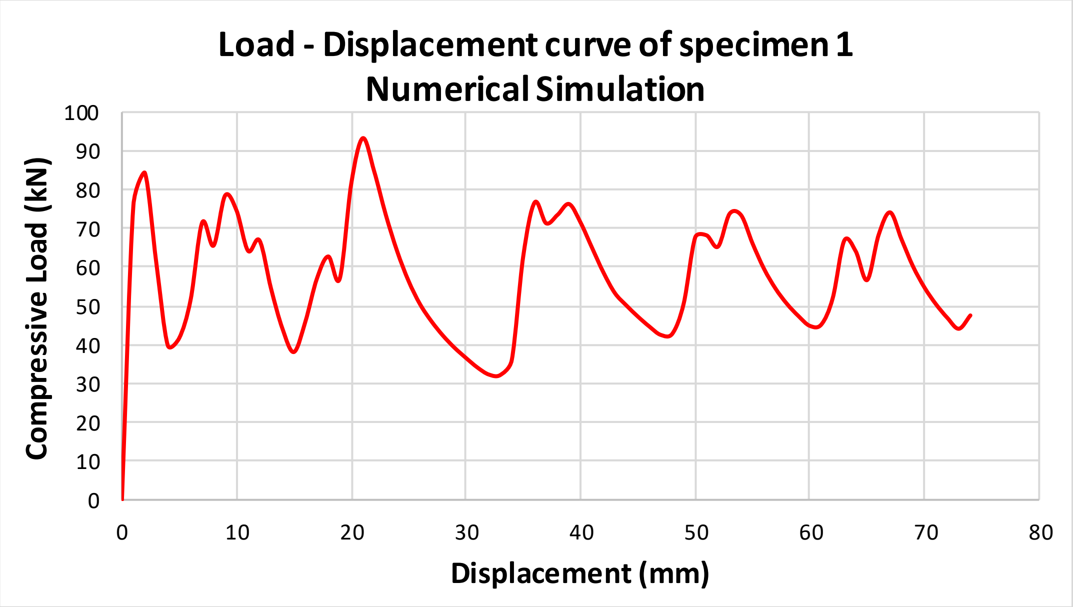

Figure 77 Numerical results for load-displacement curve of specimen 1

Numerical results – Specimen 1	
Peak Load (kN)	93.26
Mean Load (kN)	57.73
Absorbed Energy (kJ)	4.27
SEA (kJ/kg)	27.74
Load Uniformity (-)	0.62

Table 9 Numerical results for specimen 1 crashworthiness assessment

Observing more the states of axial collapse for specimen 1 in both following figures, local convolutions formulation can be attributed to some significant amounts of bending moment around the buckled folds as expected, the circumferentially uniform distribution of which is mainly responsible for the axisymmetric folds convolutions, as a non-uniform distribution of them would in contrast probably reacted to diamond folds formulation. However, opposite bending moments take place along the external and the internal fold surface, causing that way local buckling deforming conditions for the folds formulation. Figure 79 showing the local bending moments (N·mm) around the deformed structure, confirms also the peak crushing load occurring at a shortening about 20 mm where the third convolution is formulated.

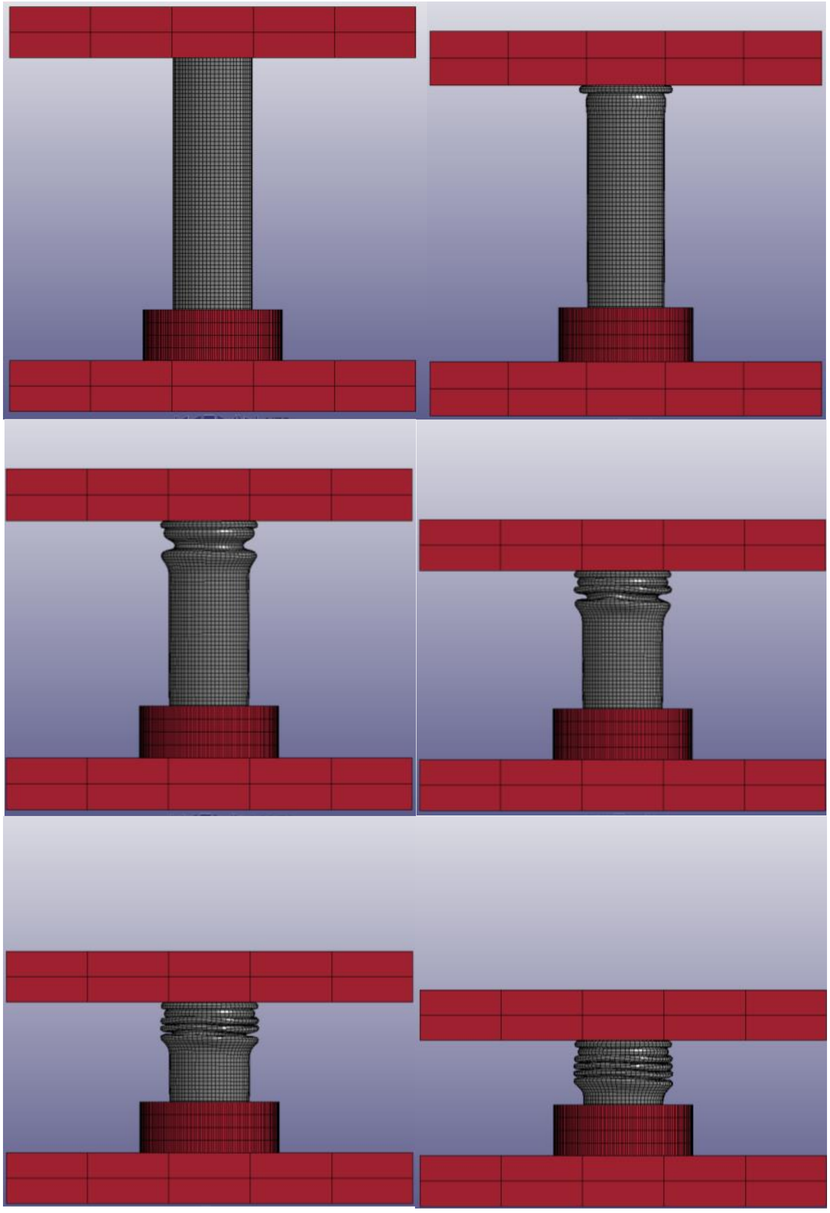

Figure 78 States of axial collapse from specimen 1 simulation

Finally, Figure 80 shows the views of the fully crushed structure of specimen 1 revealing that the fixed tube bottom end remains undeformed, while also reduced the effective initial tube length avoiding any unstable phenomena during collapse such as bending modes. Further, the concertina collapse failure mechanism is confirmed by the open literature predictions for the specific steel tube geometry taking into account its length to diameter length ratio L/D of 3 and diameter to thickness ratio D/t of 21.

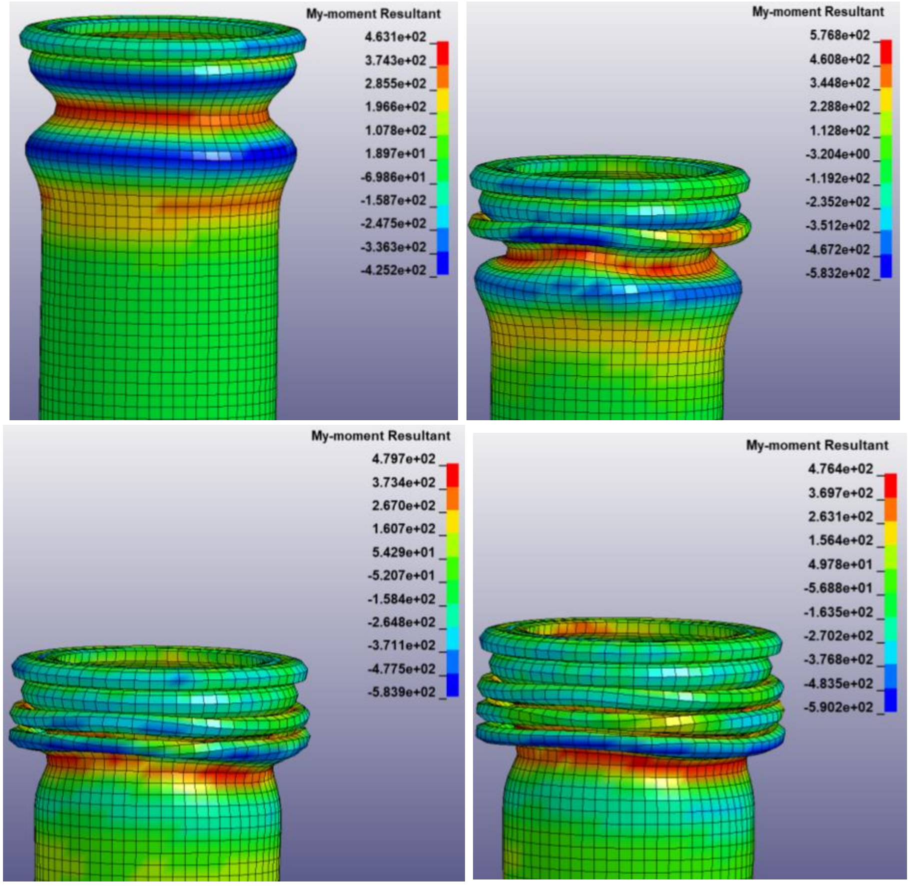

Figure 79 Local buckling and folds formulation of specimen 1

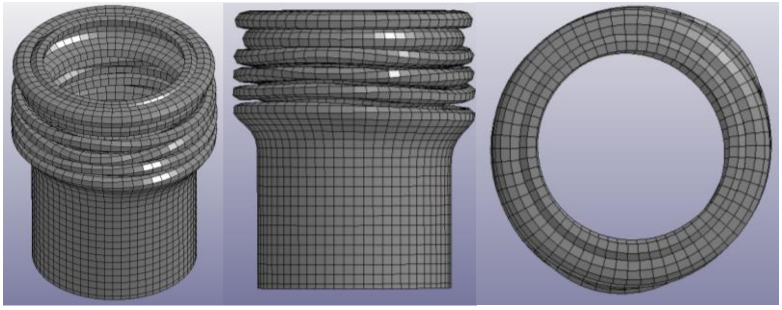

Figure 80 Fully collapsed aspect of specimen 1

4.3.2 Simulation of specimen 2 case study

The results regarding the numerical finite element simulation for specimen 2 case subjected to oblique loading of 3^{o} angle are presented following from the provided load-displacement curve and the estimated critical crashworthiness response metrics as reported in Table 10.

In particular, numerical load-displacement curve reveals a progressive and stable collapse in post buckling region of crushed structure formulating three 2D-diamond folds during its plastic deformation. The progress and stability of the collapse is also observed to the revealed load distribution, as after the plastic collapse initiation occurred about 3mm shortening at 62 kN, the vertical compressive load ranges around the mean sustained magnitude of 50.67 kN showing some local peaks and lows in the load-displacement curve due to the folds formulation. The maximum crushing force occurs at about 36 mm shortening lying to 72 kN due to the formulation of 3rd convolution. The oblique loading angle of 3° proved to be not high enough to cause any bending deformation mode which would decrease significantly the energy dissipating levels lying currently to 24.17 kJ/kg regarding the specific absorbed energy. The last one in fact is obtained around 12% compared to the one of specimen 1 according to the numerical results, as this drop is considered due to both the loading angle effect which introduces bending loads – not existed in the case of axial collapse of specimen 1– while also the 2D-diamond type of collapse is additionally responsible for the lower energy absorbing levels compared to the concertina mode occurred in specimen 1 case. Further, load uniformity revealed almost 13% greater for specimen 2 compared to specimen 1, as the loading angle of 3° caused a decrease of plastic collapse initiation load and subsequently of maximum load, without however dropping similarly enough the sustained load as the oblique collapse remained stable and progressive enough to maintain the mean load considerably high.

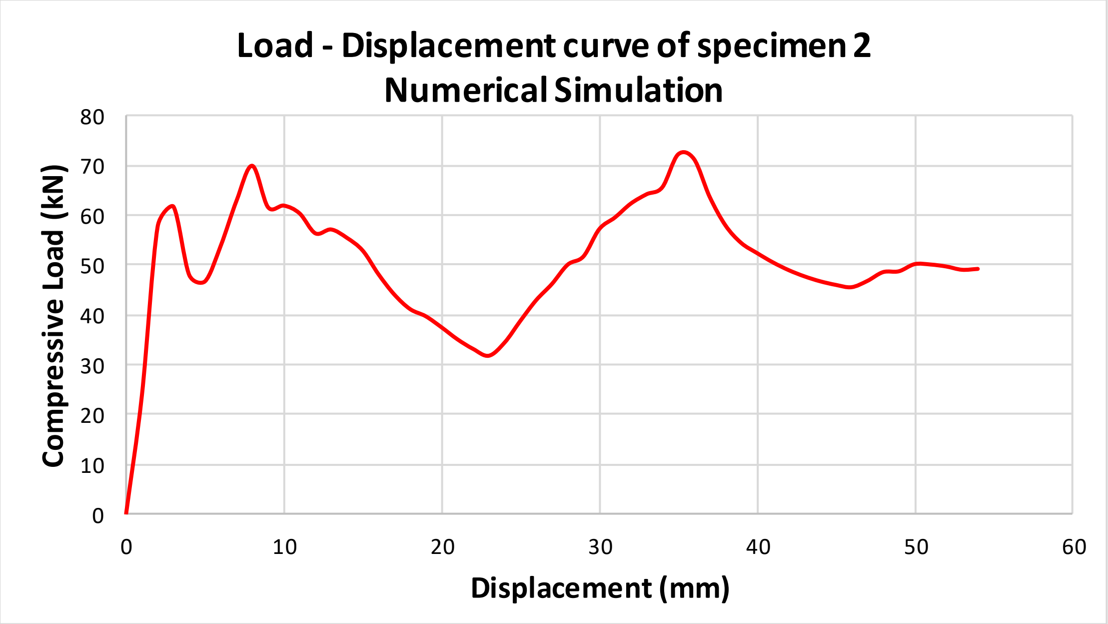

Figure 81 Numerical results for load-displacement curve of specimen 2

Numerical results – Specimen 2	
Peak Load (kN)	72.15
Mean Load (kN)	50.67
Absorbed Energy (kJ)	2.74
SEA (kJ/kg)	24.17
Load Uniformity (-)	0.70

Table 10 Numerical results for specimen 2 crashworthiness assessment

Observing more the states of collapse for specimen 2 in both following figures, specimen 2 deforms under 2D-diamond mode by formulating three elliptical convolutions. The 2D-diamond type folds are considered to be deformed mainly due to non-uniform bending moment distribution along the tube cross-section circumferential direction. Thus, as an opposite bending loading occurs through the circumference, an internal fold and an external one are formulated by opposite moments, causing a local buckling of the material in a way the cross-section transforms for circular to elliptical. As Figure 84 depicts, the tube bottom end remains undeformed as fixedly supported end, which further reduces the effective initial tube length, resulting to higher resistance against a possible bending type of collapse due to the loading angle effect which introduces additional bending loads to the compressed structure.

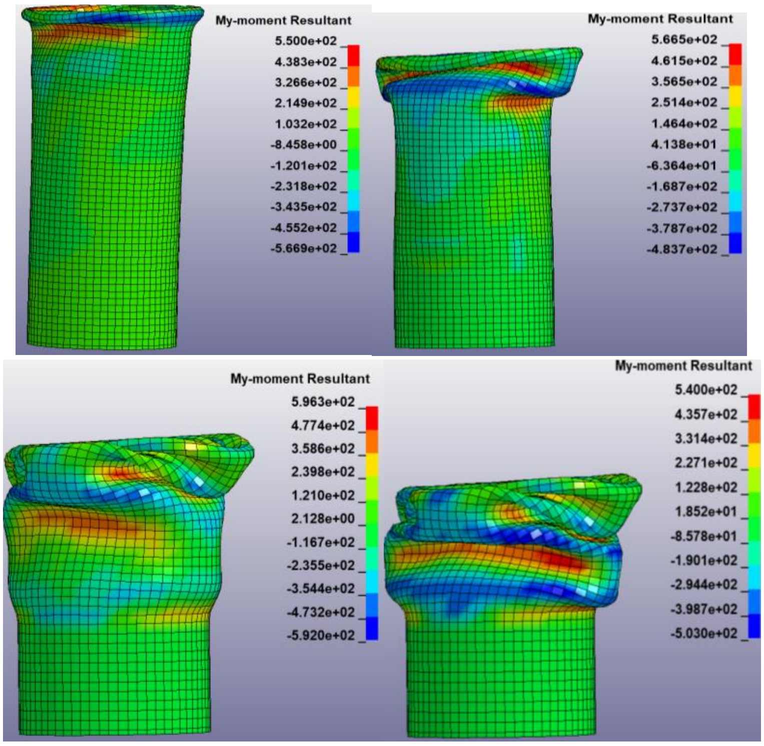

Figure 82 Local buckling and folds formulation of specimen 2

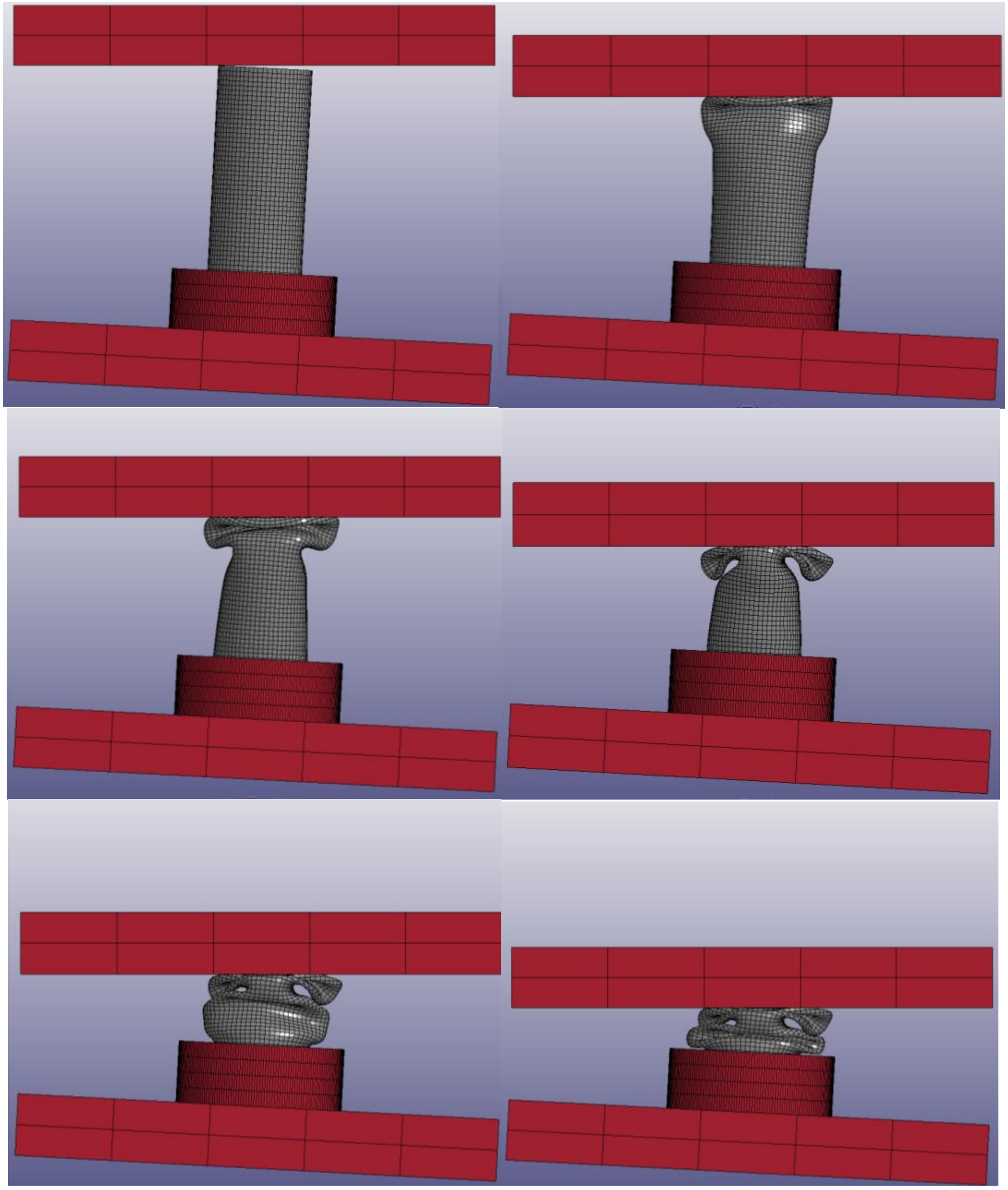

Figure 83 States of axial collapse from specimen 2 simulation

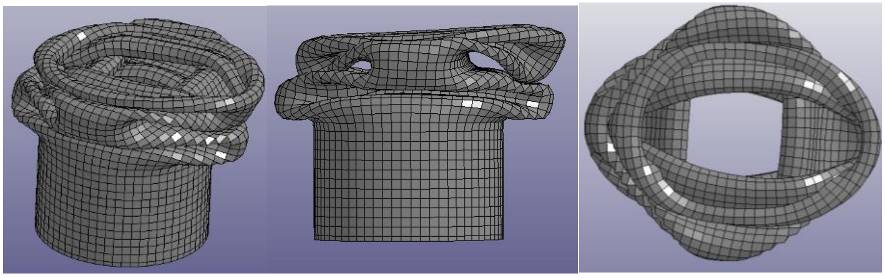

Figure 84 Fully collapsed aspect of specimen 2

4.3.3 Simulation of specimen 3 case study

The results regarding the numerical finite element simulation for specimen 3 case subjected to oblique loading of 6° angle are presented below in terms of load-displacement curve and main crashworthiness response parameters. Specifically, the numerical simulation revealed that specimen 3 deformed under a progressive and stable collapse mechanism formulating three 2-D diamond convolutions. The numerical results analysis showed more that the plastic collapse initiation occurred around 5 mm of shortening at about 50 kN, however the maximum crushing force lied to almost 89 kN at the final stages of collapse where the concentrated crushed structure mass revealed great resistance against further shortening as depicting by the significant load increase during the final moments of collapse beyond 56 mm shortening. Compared to specimen 1 and specimen 2 examined cases, both plastic collapse load and mean sustained load proved to be decreased as the oblique loading angle of 6° is currently greater which brings additionally higher bending loads facilitating the collapse initiation and its progress.

Further, the introduced bending loads react to a bending moment distribution of greater magnitude than specimen 2 case where loading angle was adjusted at 3°. However, current examined loading angle of 6° seems to be not high enough to react in a Euler-type buckling mode which is also avoided by the fixedly supported bottom tube end reducing its effective initial length about the 20 mm of the ringed base configuration height. Moreover, specimen 3 revealed lower energy absorbing levels compared to specimen 1 and specimen 2 as expected because of the greater angle of loading.

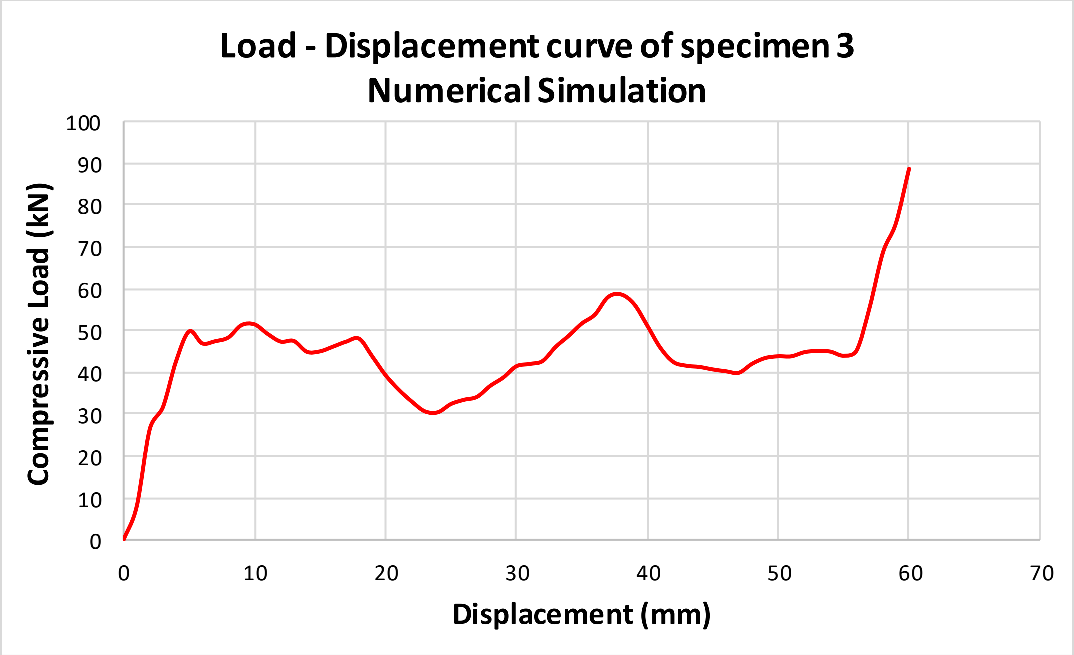

Figure 85 Numerical results for load-displacement curve of specimen 3

Numerical results – Specimen 3	
Peak Load (kN)	88.70
Mean Load (kN)	44.21
Absorbed Energy (kJ)	2.65
SEA (kJ/kg)	23.27
Load Uniformity (-)	0.50

Table 11 Numerical results for specimen 3 crashworthiness assessment

Taking further a look at the progressive collapse states of the following figures, a 2D-diamind failure mode is occurred like specimen 2 case, while Figure 86 highlights the bending moment circumferential distribution around the formulated convolutions. As observed, in the areas of external and internal fold sights, a non-uniform bending moment of opposite magnitude is distributed around the 2D-diamond folds which is considered to be responsible for current collapse mode causing the formulation of elliptical folds, while is also affected by the oblique loading angle as in the case of specimen 1 the examined tube was subjected to concertina axial collapse mode under axisymmetric convolutions.

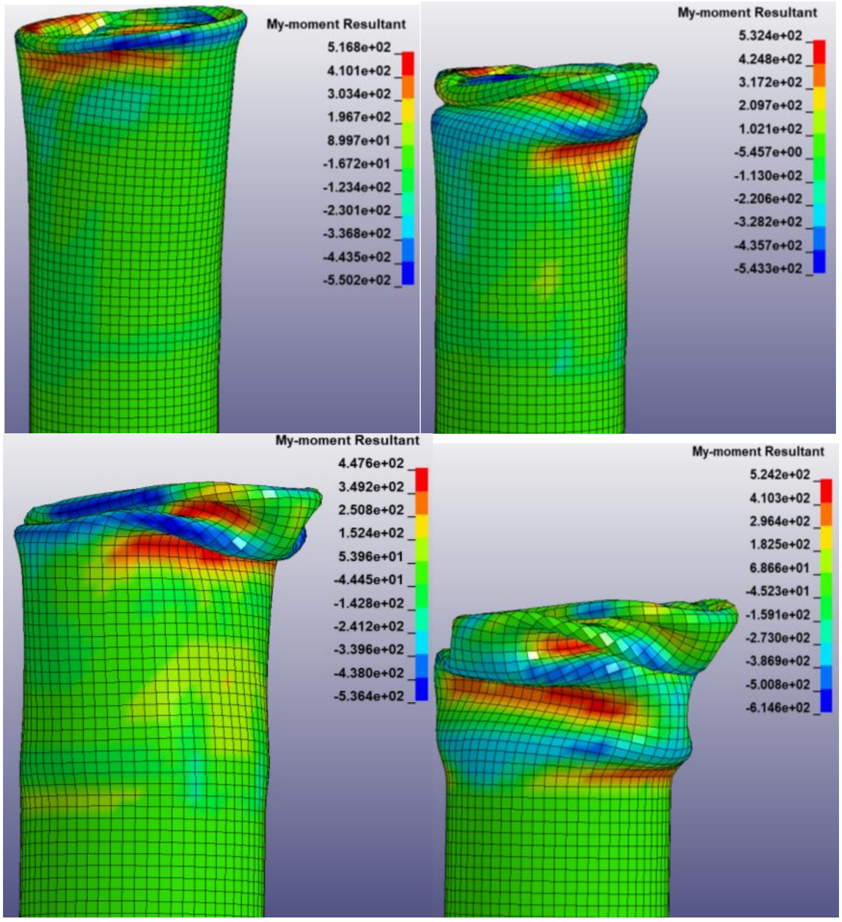

Figure 86 Local buckling and folds formulation of specimen 3

Finally, Figure 88 depicts the final views of the fully crushed structure showing that the bottom tube end remains undeformed due to its fixed support, while more the 2-D diamond folds can be observed focusing in the bottom view at the right.

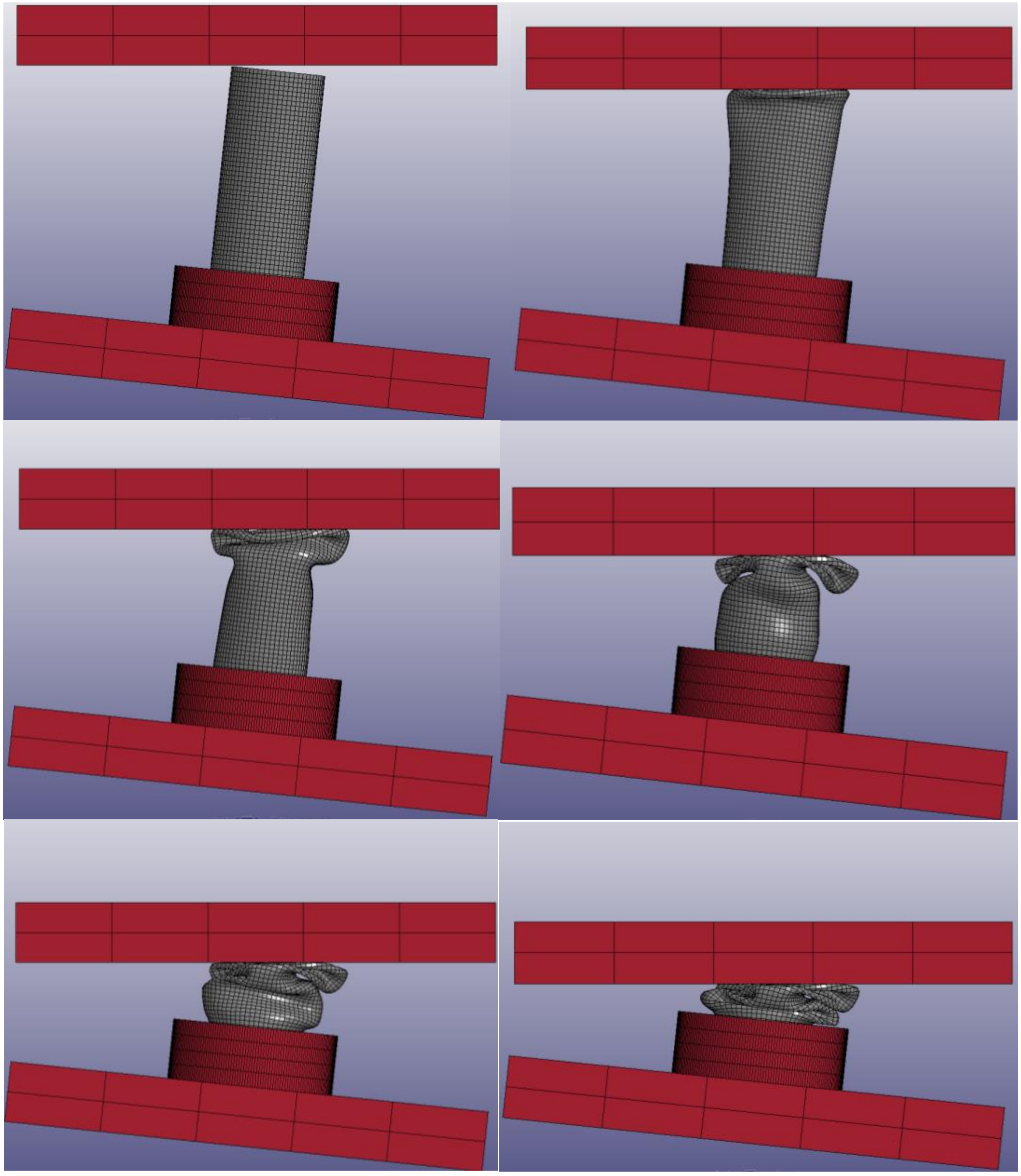

Figure 87 States of axial collapse from specimen 3 simulation

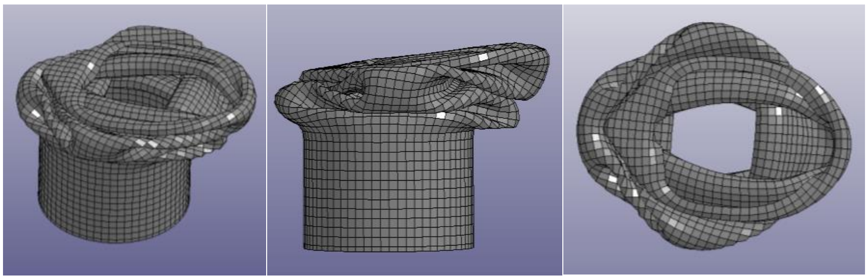

Figure 88 Fully collapsed aspect of specimen 3

4.3.4 Simulation of specimen 4 case study

The results regarding the numerical finite element simulation for specimen 4 subjected to oblique loading of 9° angle are presented in this sub-section in terms of load-displacement curve and main crashworthiness response parameters. Specifically, the numerical simulation revealed that specimen 4 deformed under a progressive and stable collapse mechanism formulating three 2-D diamond convolutions. In current examined case, the plastic collapse initiation began at 8 mm shortening under almost 48 kN, while during post buckling region of load-displacement curve the sustained load seems to be maintained around of mean load of 32.95 kN. However, at the final stages of oblique collapse beyond 60 mm of tube shortening, a significant increase in the applied loads lying up to 103 kN peak crushing force is occurred due to the higher material resistance against further deformation which is caused by the concentrated plastically deformed mass of crushed structure around the ringed configuration of base. Further, after the plastic collapse initiation, the applied loads show a progressive distribution with a slight decrease through the collapse because of the bending moment introduced by the oblique loading angle revealing so lower energy absorbing levels compared to previous examined cases.

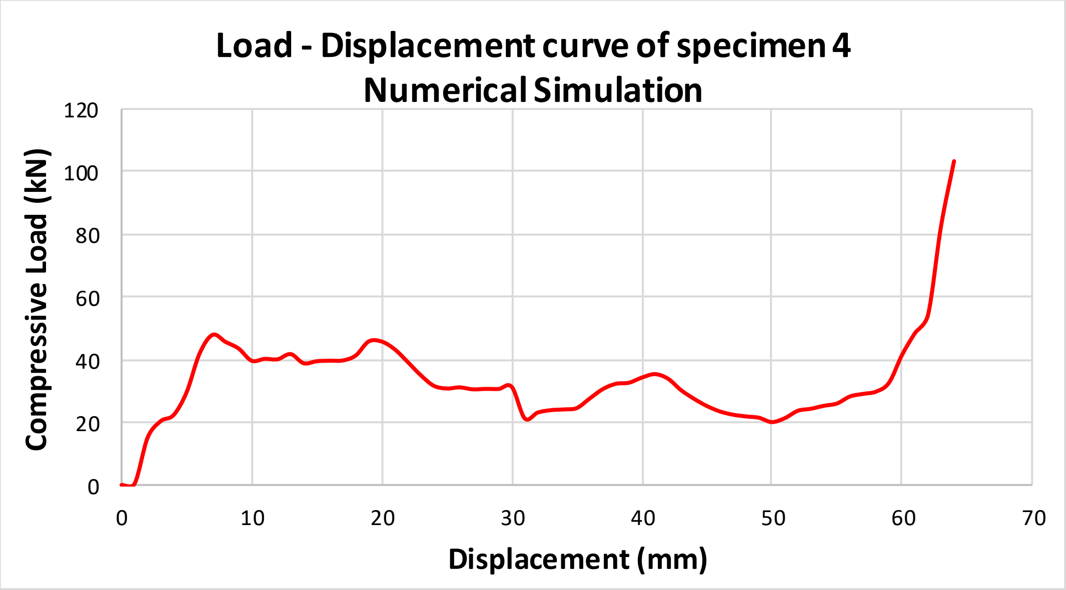

Figure 89 Numerical results for load-displacement curve of specimen 4

Numerical results – Specimen 4	
Peak Load (kN)	103.35
Mean Load (kN)	32.95
Absorbed Energy (kJ)	2.11
SEA (kJ/kg)	18.42
Load Uniformity (-)	0.32

Table 12 Numerical results for specimen 4 crashworthiness assessment

A more detailed look at the collapse states depicted in following figures shows a 2D-diamond collapse mode under a progressive formulation of elliptical convolutions caused by the circumferentially non-uniform bending moment distribution. In particular, opposite magnitudes of bending moment is occurred around external and internal folds areas, affected additionally by the increased loading angle. As depicted in the next figures, the folding formulation begins on the top tube end while the bottom one remains undeformed due to its fixed support. The 2D-diamond folds are formulated and pushed to the opposite sight of the crushed side of the tube reducing the area in which the crushing force is applied reacting in lower sustained load during the collapse.

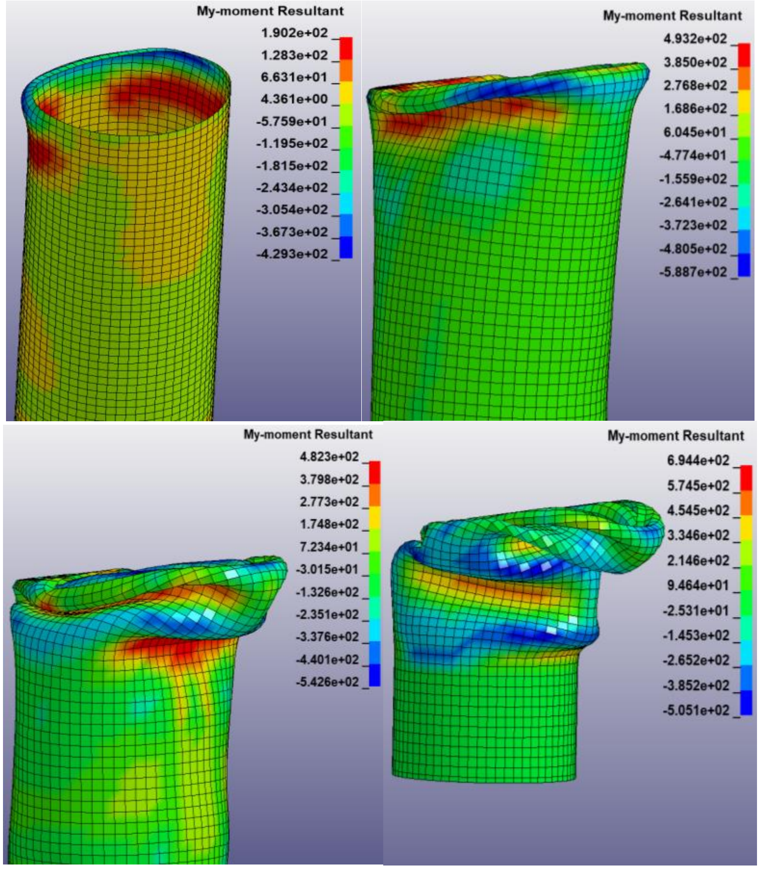

Figure 90 Local buckling and folds formulation of specimen 4

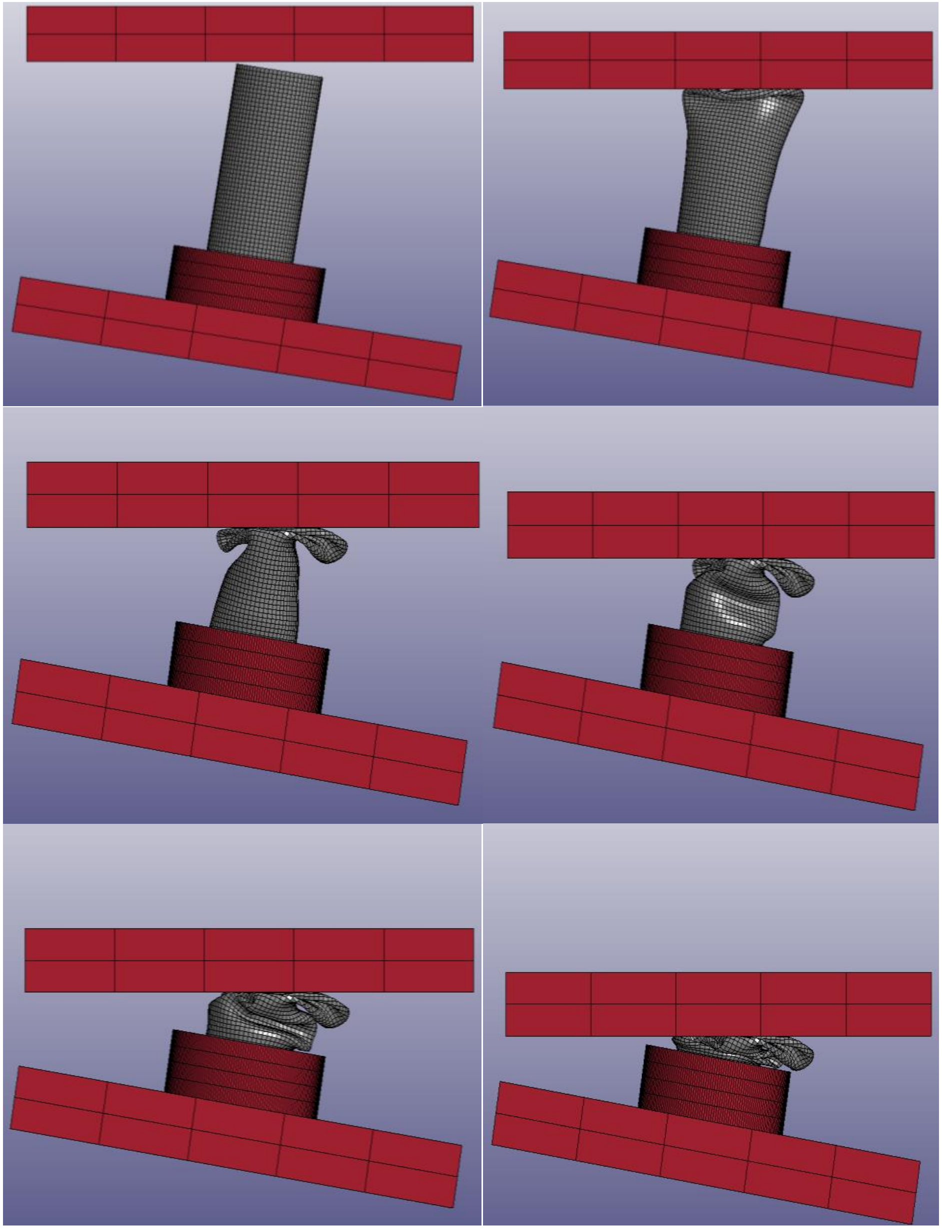

Figure 91 States of axial collapse from specimen 4 simulation

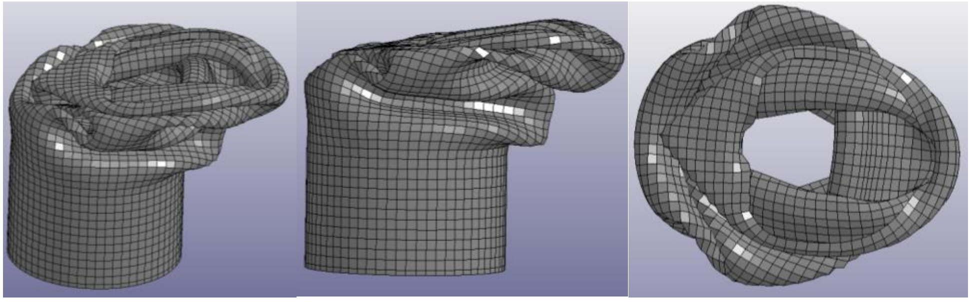

Figure 92 Fully collapsed aspect of specimen 4

4.3.5 Simulation of specimen 5 case study

The numerical results regarding the last conducted simulation of specimen 5 subjected to the greatest examined oblique loading angle of 11° are presented below in terms of load-displacement curve and main crashworthiness response metrics as provided by the produced numerical curve. In particular, the numerical simulation revealed that specimen 5 deformed under a progressive and stable collapse mechanism formulating three 2-D diamond convolutions as the local peaks in the post buckling region of load distribution curve. In this examined case, the plastic collapse initiation happened at a shortening about 8 mm under 45 kN, while the mean crushing load during collapse lied around 31 kN. This sustained load was initially observed 20% higher for the formulation of the two first folds, however after 25 mm of shortening the distributed load showed a slight decrease revealing finally the mean load value reported in Table 13. At the final stages of the collapse although, beyond 60 mm of tube shortening, the simulation revealed a sharp load increase up to 97 kN of peak crushing force due to the higher material resistance against further deformation which is caused by the concentrated plastically deformed mass of crushed structure around the ringed configuration of base. However, the occurred maximum load is lower than the previous case of specimen 4, as now the crushed structure mass has been bended laterally because of the greater loading angle.

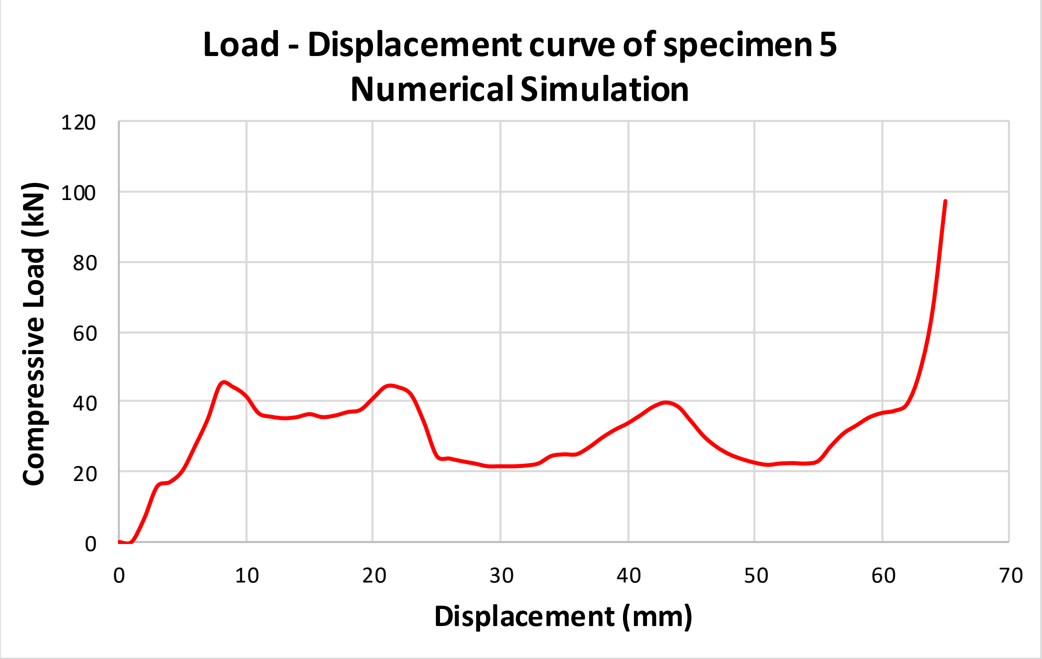

Figure 93 Numerical results for load-displacement curve of specimen 5

Numerical results – Specimen 5	
Peak Load (kN)	97.17
Mean Load (kN)	31.02
Absorbed Energy (kJ)	2.02
SEA (kJ/kg)	17.53
Load Uniformity (-)	0.32

Table 13 Numerical results for specimen 5 crashworthiness assessment

The examined structure of specimen 5 case collapsed initially by formulating 2D-diamond folds, while at the final stages the tube was bended around its bottom fixedly supported end. As the following figures depict, the circumferentially non-symmetric bending moment distribution is considered to be responsible for the elliptical convolutions formulation and the final tube bending. Finally, the energy absorbing levels regarding the current configuration revealed the lowest among all previous ones, affected by the greatest loading angle of 11o which introduced the highest observed bending loads.

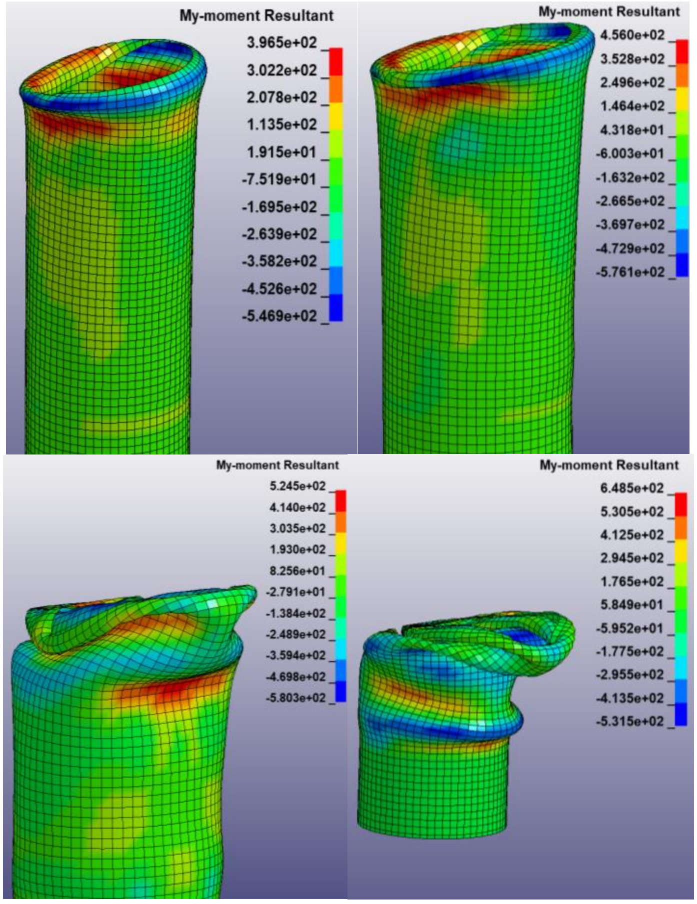

Figure 94 Local buckling and folds formulation of specimen 5

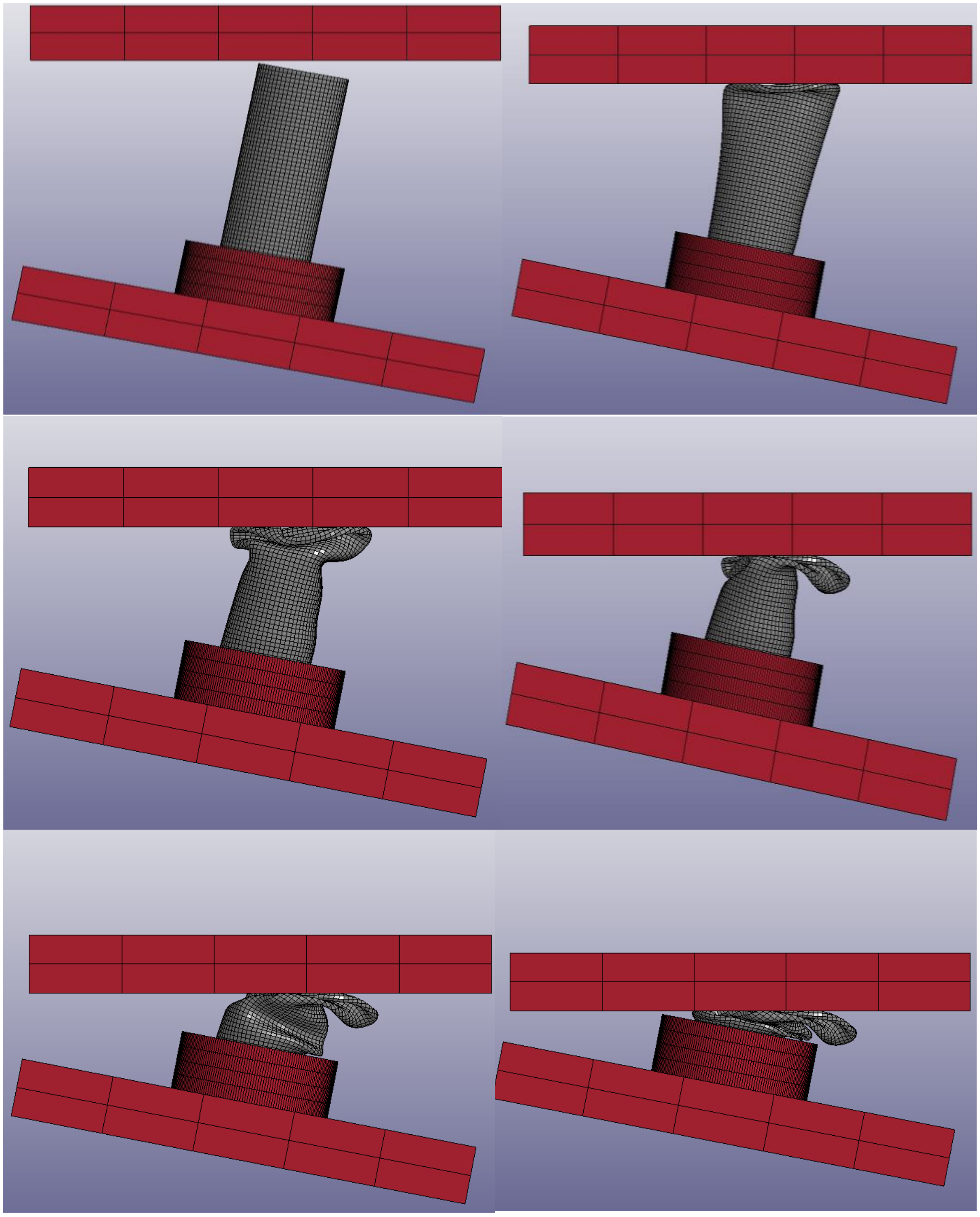

Figure 95 States of axial collapse from specimen 5 simulation

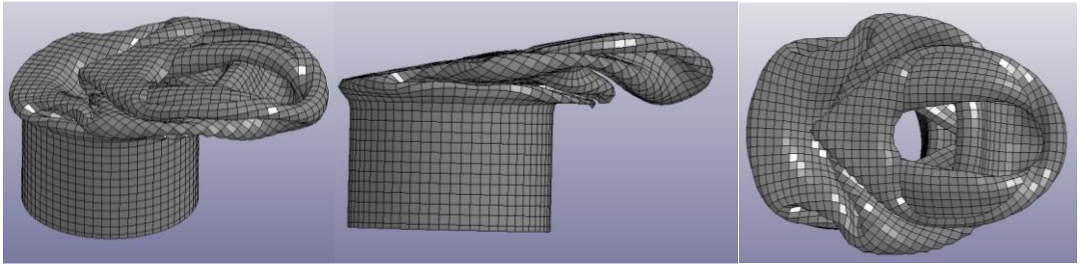

Figure 96 Fully collapsed aspect of specimen 5

4.4 Conclusions

By summarizing the provided results from the numerical simulations, critical conclusions can be extracted for the crashworthiness response of the examined loading cases by the provided analysis results from the load-displacement curve and the observation of the occurred collapse mode. Thus, regarding the occurred failure mechanism taking place according to the conducted simulations, specimen 1 case subjected to axial crushing revealed a concertina collapse type formulating axisymmetric convolutions and receiving exclusively compressive crushing loads revealing that way the greatest energy absorption capability. In contrast, specimen 2 – 5 cases which all were subjected to oblique crushing conditions under angles of 3^o to 11^o respectively, revealed also a progressive and stable type of collapse formulating 2D-diamond folds, with only the case of specimen 5 showing a light bending mode through the final stages of collapse, but not capable of enforcing any instability through the collapse like a Euler-type bucking mode would react to. The elliptical shape of 2D-diamond folds was attributed in all cases of obliquely collapsed specimens to the non-uniformity of the bending moment along the tubes cross-section, which revealed an opposite magnitude through the area of internal and external formulated convolution sides resulting in an elliptical shape for them.

Regarding the crashworthiness response metrics, Figure 97 shows that the plastic collapse initiation load reveals a progressive reduction from specimen 1 to specimen 5 as the loading angle gets higher, as current tendency is expected due to the additional bending loads which the loading angle introduces.

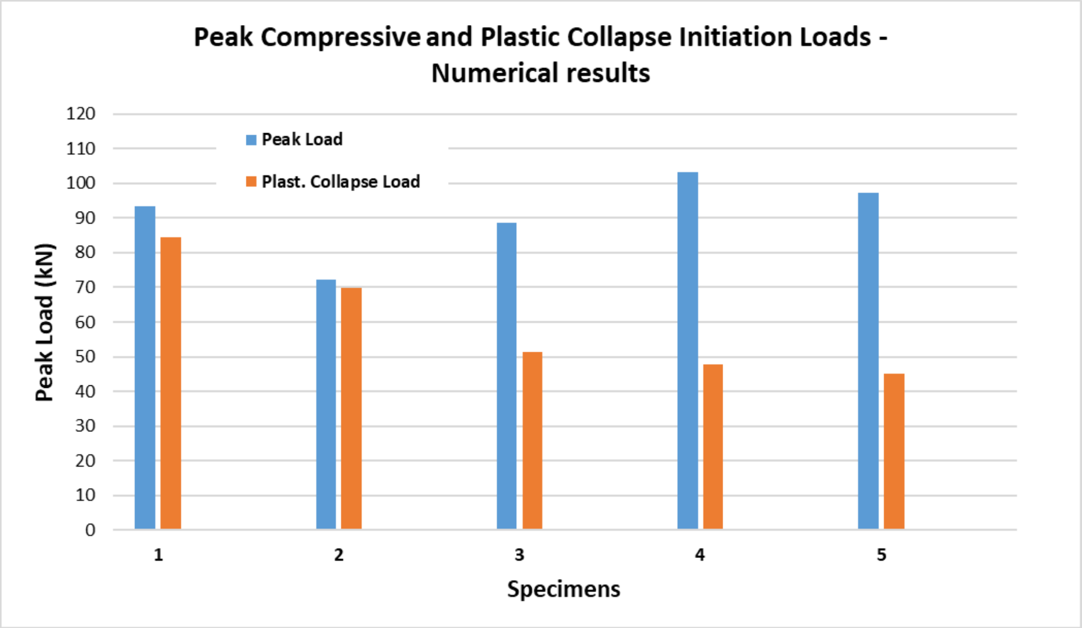

Figure 97 Numerical results for peak and plastic collapse initiation loads

In contrast, the peak crushing force shows an opposite variation with respect to the loading angle. More specific, as the angle of loading gets greater, the peak crushing load proves to be increased which in fact is attributed to the concentrated mass of the fully collapsed structure around the bottom ringed base configuration resulting in significantly higher resistance against further shortening. The above tendency can be observed to the final stages of collapse in the load-displacement curves as provided by the numerical simulations regarding the obliquely loading cases of specimens 2 – 5.

Following, as depicted by Figure 98, the mean crushing load shows also a decrease as the loading angle gets greater from specimen 1 to specimen 5. In particular, regarding specimens 4 and 5, the sustained load reveals a sharper decrease compared to a linear drop with respect to loading angle, as a light bending of the compressed structures occurred around the bottom tube zone because of the significant bending loads in the case of 9^o and 11^o angle respectively. More, the sustained load would decreased further if the examined maximum shortening of the examined tubes was slightly lower, as a sudden load increase would not be occurred at the final stages of collapse. All specimens, including the obliquely loading ones, revealed a stable load distribution in post-buckling region which showed a progressive light decrease in specimens 4 and 5 of the highest loading angles.

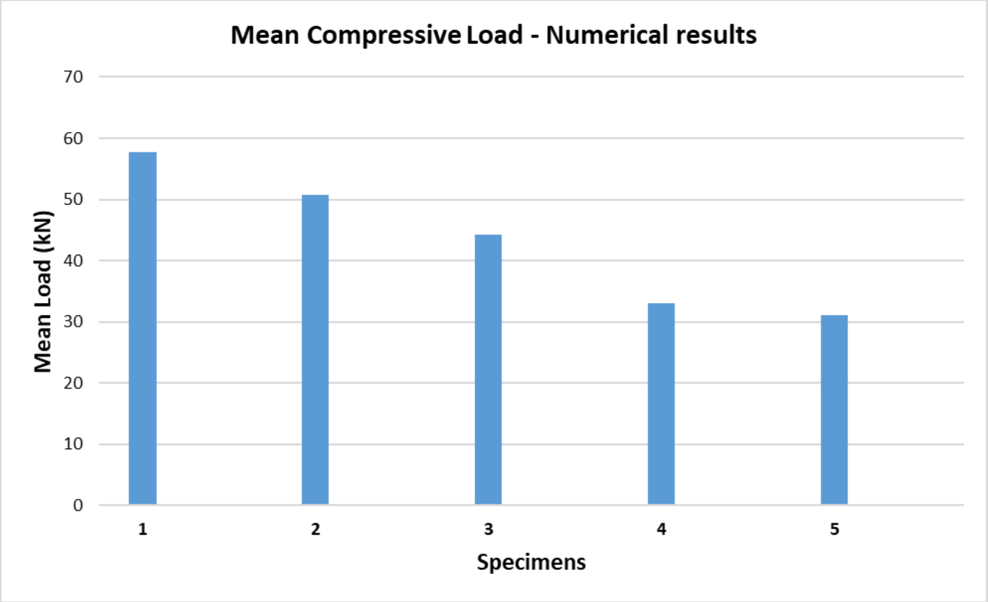

Figure 98 Numerical results for mean crushing load

The above can be confirmed looking at the following two figures which depict the variation of the absorbed energy and the specific one. Specifically, it is obvious that as the loading angle gets higher the energy absorption capability of the examined structure decrease because of the additional bending loads introduced by the oblique crushing. The variation of specific energy absorption is affected similarly by the tendency of mean crushing load, revealing a sharper decrease in the cases of 9° and 11° loading angles regarding specimens 4 and 5 respectively. Therefore, axial loading conditions are proved to be more beneficial regarding the energy absorption capacity of structures, revealing a more efficient energy dissipation behavior for the crushed tubes, while in the case of oblique crushing the increase of the loading angle affects negatively the crashworthiness structures efficiency.

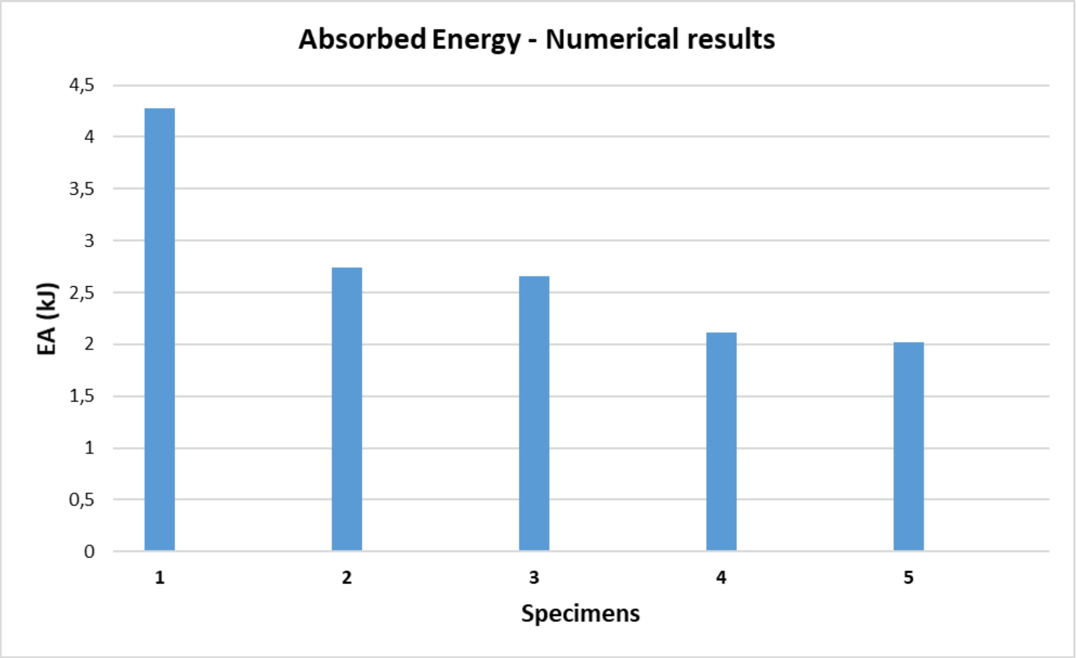

Figure 99 Numerical results for energy absorption

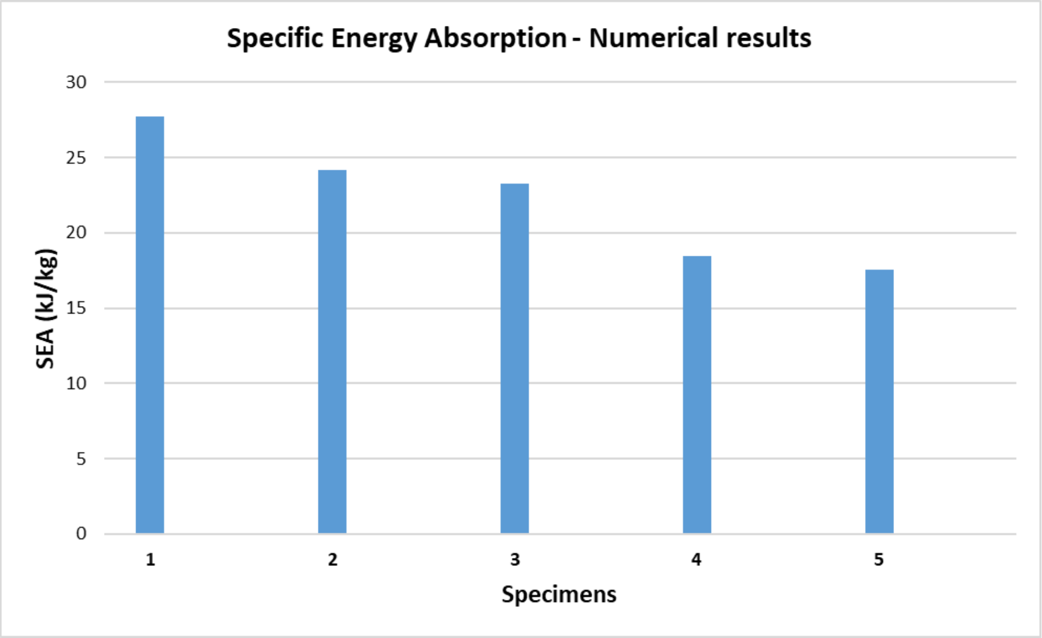

Figure 100 Numerical results for specific energy absorption

Similarly affected, the uniformity of the load distribution along the post-buckling region shows in general to decrease as the loading angle increases, with the two last examined cases revealing a significant decrease due to the extremely high peak crushing forces occurred at the final stages of collapse. Figure 101 depicts that specimen 2 revealed the greatest load uniformity factor as the sustained load was yet high enough due to the low angle of loading combined by a not significantly high peak crushing force which was occurred during the second fold formulation.

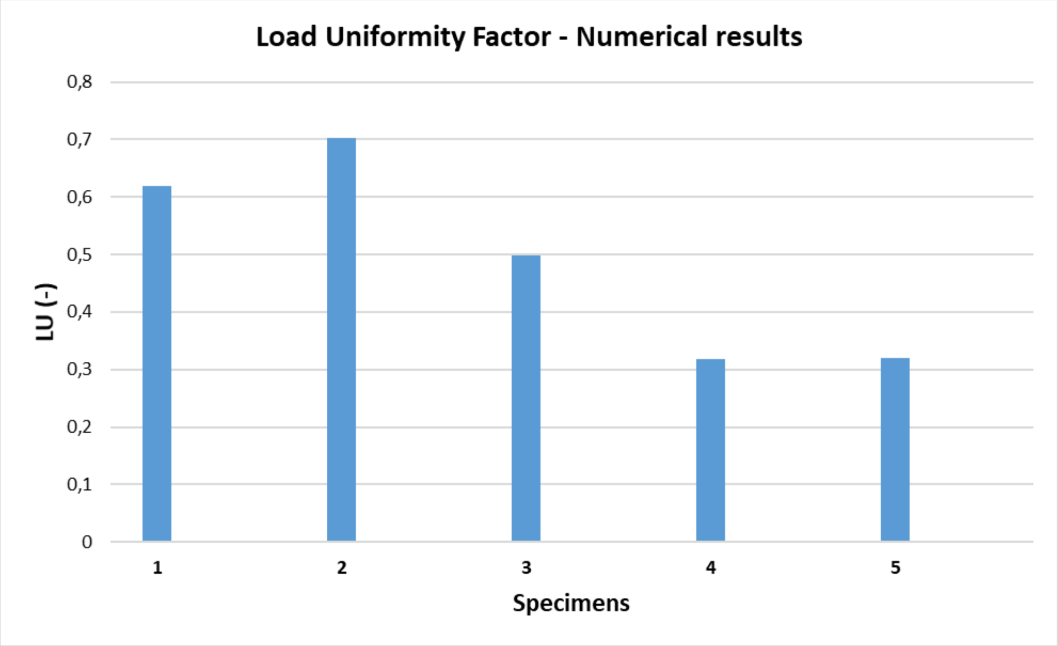

Figure 101 Numerical results for load uniformity

Last but not least, the following two figures summarize the revealed variation of the plastic collapse initiation load and the mean crushing one as the numerical results provided. A detailed look shows that beyond 6° loading angle the mean crushing load reveals a more significant decreasing affecting similarly the energy absorption capability of the crushed structure, as the additional introduced bending loads become more significant resulting in lower required loads for the collapse progress. In fact, as the loading angle gets even higher, the occurred bending loads could result in an unstable bending collapse mode which would react to a sudden and sharp drop in the energy absorption levels. More, as the plastic collapse initiation load also reveals a decrease with respect to loading angle, which could be beneficially utilized in crashworthiness design of structures as a light loading angle – not capable to bring any unstable phenomena during collapse – could react as a triggering configuration facilitating the collapse initiation, which in fact is already taken into account in crashworthiness design of structures by designing for example beveled tube edges for a angled loading in the first stages of the impact.

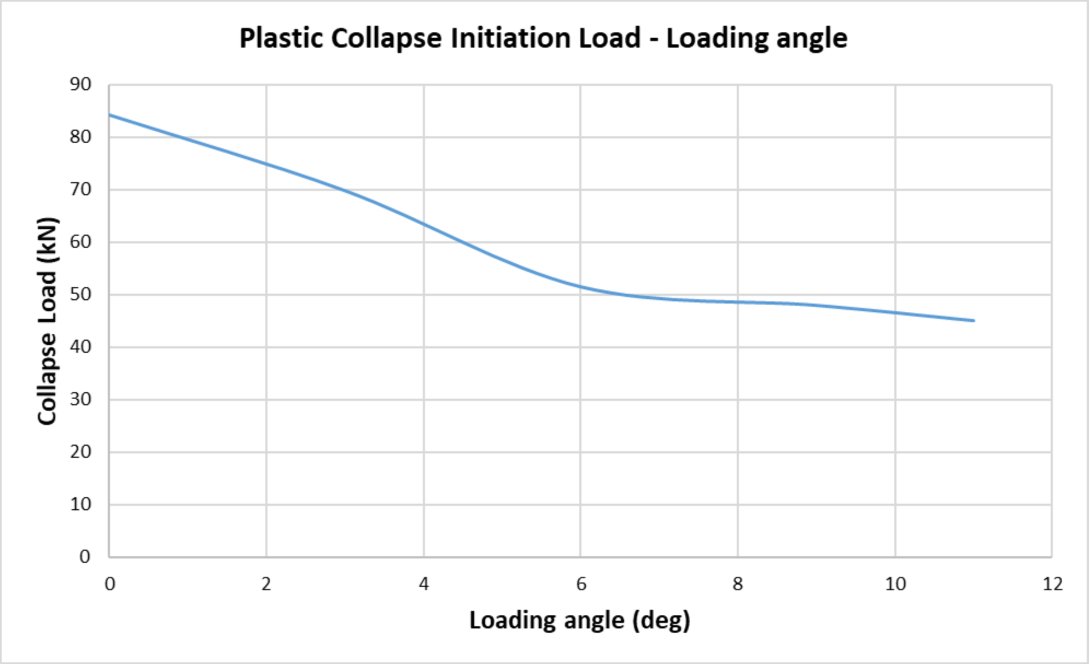

Figure 102 Numerical results for plastic collapse load variation via loading angle

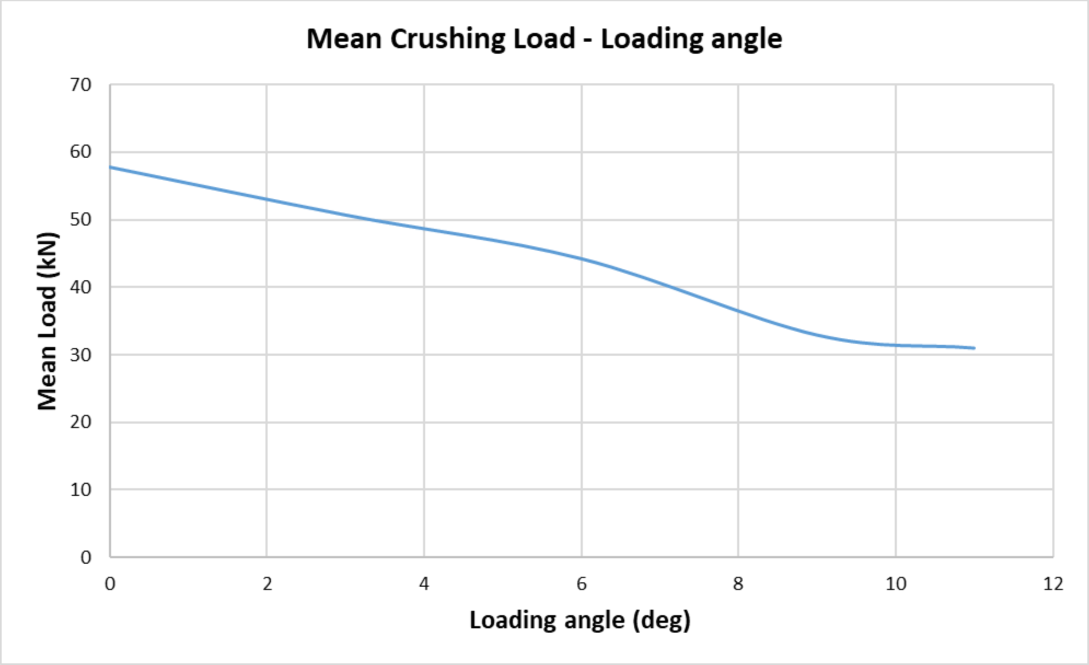

Figure 103 Numerical results for mean load variation via loading angle

5. Experimental vs. Numerical simulation results

5.1 Introduction

This chapter contains a comparison between the experimental and numerical results as the last ones provided by the simulations of created finite element models carried out in LS-Dyna software. In each examined case, the provided load-displacement curves and the revealed crashworthiness response metrics are presented and set into comparison, while further the final views of the crushed structure are also depicted in order to observe the predicted failure mechanism which was occurred.

The comparison between the experimental and numerical results aims to validate the developed finite element models behavior against the experimental data provided by the conducted tests in terms of both crashworthiness response metrics and predicted collapse mode, while further aims to evaluate the crashworthiness efficiency of each examined case and offers useful conclusions the consideration of which would improve the crashworthiness behavior of the designed structures.

5.2 Comparison of experimental and numerical results

In the following sections of current chapter, the experimental and numerical results are set into comparison in terms of the revealed load-displacement curve and the provided crashworthiness response parameters from the respective analysis combined with the final views of crushed structures as both experimental tests and numerical simulations revealed. In each examined case, the numerical results are compared against both conducted tests in order to evaluate their validity and assess the response behavior with the highest level of accuracy and reliance.

5.2.1 Specimen 1 case

At first, the examined case of axially compressed specimen 1 is presented below by depicting the provided experimental and numerical load-displacement curves in Figure 104 and the crashworthiness response parameters in Table 14 as the respective analyses revealed. A detailed look reveals that the finite element simulation predicts accurately the occurred concertina collapse mode compared to experimental test case of specimen 1b, as both of them showed axisymmetric formulated convolutions during plastic deformation in contrast to the experimental case of specimen 1a which revealed a 2D-diamond mode, agreeing although all study cases in a progressive and stable collapse. The difference however between the predicted concertina collapse mechanisms between the simulation and the first experimental case is that the first one predicts six in total axisymmetric folds compared to the specimen 1b experimental case which showed a five axisymmetric convolutions plastic deformation.

According to above, both experimental case 1b and numerical simulation revealed a slightly higher energy absorption capacity for axially loaded specimen 1 compared to experiment 1a, as the concertina collapse mode reveals greater energy dissipation levels compared to diamond one according to open literature observations. Further, both experiments and simulation revealed a sufficient agreement in load-displacement curve and in subsequence the revealed crashworthiness response metrics as depicted below.

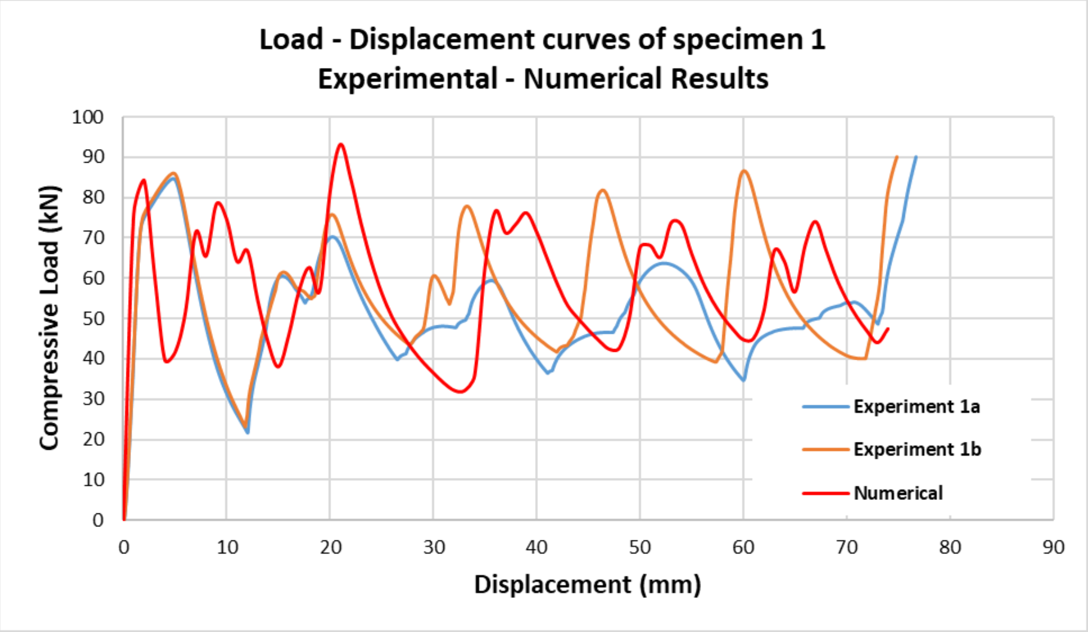

Figure 104 Experimental vs. numerical load-displacement curves for specimen 1

In particular, the numerical results proved to be slightly closer to the experimental ones of second case (experiment 1b) as both predicted exactly the same collapse mechanism and thus the load distribution during plastic deformation. The revealed deviations between the numerical and the experimental results lied about only 2% regarding both predicted energy absorbing levels and plastic collapse initiation load, while the peak crushing force showed a relative error of about 4% in the case of experiment 1b.

Therefore, the provided experimental results confirm the validity of the developed finite element model in case of axially collapsed specimen 1 case as the depicted relative errors in following table are assessed to reveal a sufficient agreement between them.

Specimen 1			
	Numerical Simulation	Experiment 1a	Experiment 1b
Peak Load (kN)	93.26	90.01	90.04
Plastic Collapse Load (kN)	84.34	84.61	85.98
Mean Load (kN)	57.73	52.11	56.03
Absorbed Energy (kJ)	4.27	4.00	4.19
SEA (kJ/kg)	27.74	26.25	27.23
Load Uniformity (-)	0.62	0.58	0.62
	Numerical – Experim. 1a error (%)	Numerical – Experim. 1b error (%)	
Peak Load	3.61	3.58	
Plastic Collapse Load	0.32	1.91	
Mean Load	10.8	3.05	
Absorbed Energy	6.85	1.88	
SEA	5.67	1.88	
Load Uniformity	6.93	0.52	

Table 14 Results in comparison between experiments and simulation for specimen 1

In fact, both simulation and experiments revealed that specimen 1 subjected to axial collapse showed the greater energy absorbing capability among every other examined case. More, due to no bending moment occurred because any oblique loading, the plastic collapse initiation load revealed also at its highest levels compared to examined cases of specimens 2 – 5 which collapsed under oblique loading.

Figure 105 Collapsed structures of specimen 1 (experimental 1a-1b vs. numerical simulation results from top to bottom)

5.2.2 Specimen 2 case

Following, the examined case of 3° obliquely compressed specimen 2 is described below by presenting the provided experimental and numerical load-displacement curves and the main crashworthiness response parameters as the experimental and numerical results analysis revealed them.

As depicted below, the numerical load-displacement curve followed the tendency of the experimental ones without however capturing accurately the peak crushing force as the experiments revealed a sharp load increase at the final stages of collapse due to the significant resistance of the concentrated fully crushed mass structure against further shortening. Instead, the required load for the plastic collapse initiation was predicted with more sufficiently by the numerical simulation considering the experimental case of 2a, while the numerical results revealed a sufficient agreement in the predicted energy absorption capability compared to both experiments as the deviations in mean crushing load and the absorbed energy lied around 4% and 5% in the cases of experiment 1a and 1b respectively. In fact, the load distribution during post-buckling region showed a highly accurate predicted behavior in terms of sustained load, without however capturing the applied loads through the final stages.

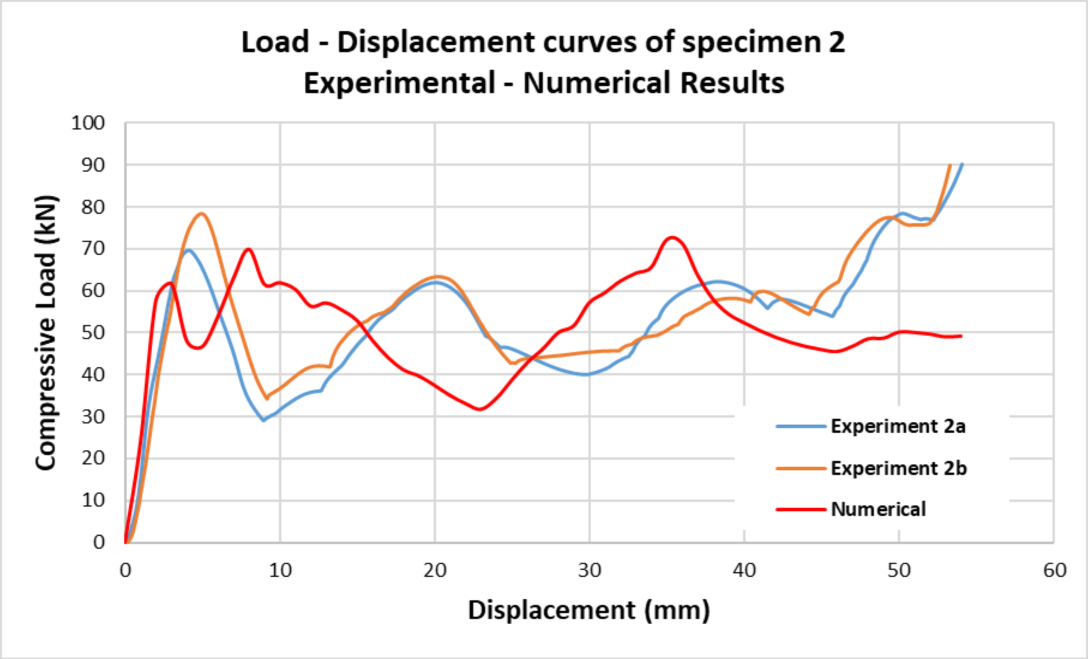

Figure 106 Experimental vs. numerical load-displacement curves for specimen 2

<table>
<tr><th colspan="4">Specimen 2</th></tr>
<tr><td></td><td>Numerical Simulation</td><td>Experiment 2a</td><td>Experiment 2b</td></tr>
<tr><td>Peak Load (kN)</td><td>72.15</td><td>90.06</td><td>90.04</td></tr>
<tr><td>Plastic Collapse Load (kN)</td><td>61.67</td><td>69.55</td><td>78.48</td></tr>
<tr><td>Mean Load (kN)</td><td>50.67</td><td>52.81</td><td>54.29</td></tr>
<tr><td>Absorbed Energy (kJ)</td><td>2.74</td><td>2.85</td><td>2.89</td></tr>
<tr><td>SEA (kJ/kg)</td><td>24.17</td><td>25.12</td><td>25.61</td></tr>
<tr><td>Load Uniformity (-)</td><td>0.70</td><td>0.59</td><td>0.60</td></tr>
<tr><td colspan="4"></td></tr>
<tr><td></td><td colspan="2">Numerical – Experim. 2a error (%)</td><td>Numerical – Experim. 2b error (%)</td></tr>
<tr><td>Peak Load</td><td colspan="2">19.89</td><td>19.86</td></tr>
<tr><td>Plastic Collapse Load</td><td colspan="2">11.34</td><td>21.42</td></tr>
<tr><td>Mean Load</td><td colspan="2">4.05</td><td>6.67</td></tr>
<tr><td>Absorbed Energy</td><td colspan="2">4.13</td><td>5.37</td></tr>
<tr><td>SEA</td><td colspan="2">3.79</td><td>5.62</td></tr>
<tr><td>Load Uniformity</td><td colspan="2">19.77</td><td>16.46</td></tr>
</table>

Table 15 Results in comparison between experiments and simulation for specimen 2

Further, the simulation of specimen 2 examined case revealed a lower plastic collapse initiation load compared to specimen 1 case, as the additionally introduced bending loads due to the oblique loading facilitated the collapse initiation. Moreover, although 3o oblique loading proved not enough to cause any unstable phenomena during collapse such as a Euler-type buckling mode, the revealed energy absorption lied to lower levels compared to axially collapsed specimen 1 as both diamond mode of collapse and the introduced bending loads due to oblique conditions reacted to. Finally, all study cases concluding both experiments and numerical simulation predicted a stable and progressive plastic collapse formulating a series of 2D-diamond convolutions the deformation of which was attributed to the circumferentially non-uniform bending moment distribution along the internal and external folds area.

Figure 107 Collapsed structures of specimen 2 (experimental 2a-2b vs. numerical simulation results from top to bottom)

5.2.3 Specimen 3 case

The comparison between numerical and experimental results regarding specimen 3 case subjected to 6^{o} oblique loading is presented following by depicting the load-displacement curves and the crashworthiness response characteristic parameters, while also the final views of fully crushed structure are presented as revealed by the experimental rests and the numerical simulation. More specifically, as the following figure depicts, the numerical load-displacement curve captures the experimental ones with sufficient agreement during the post-buckling region and the final stages of collapse too, as in the first case the sustained load is predicted with sufficient accuracy especially compared to experiment 3b, while also the peak crushing load is predicted under relative errors about 1.7% compared to both experiments.

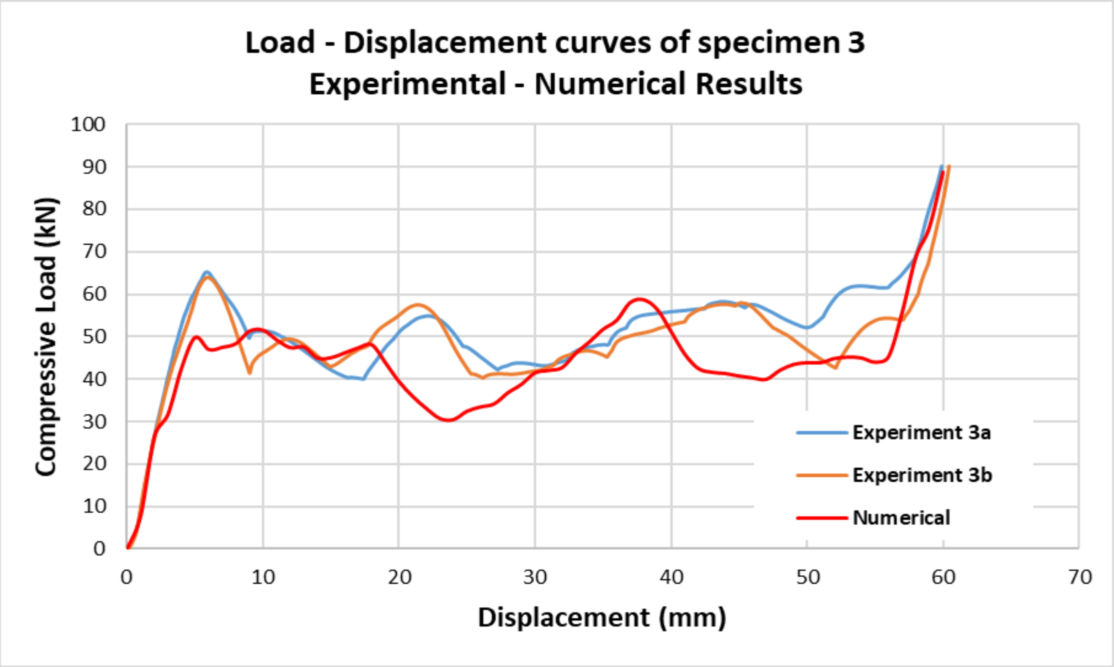

Figure 108 Experimental vs. numerical load-displacement curves for specimen 3

However, the collapse initiation load reveals a more significant deviation in contrast to the absorbed energy which is also shows a sufficient agreement between numerical and experimental results. More, the simulation captures the sharp significant load increase through the final stages of collapse caused by the highly concentrated crushed mass of the structure resisting against further shortening. In addition, both experiments and simulation confirmed a 2D-diamond stable and progressive collapse mechanism by formulating elliptical convolutions.

Finally, although both experiments and simulation similarly predicted the decrease of energy absorbing levels and the plastic collapse initiation load due to the increased loading angle which introduced further bending loads facilitating the start and the progression of the collapse, experimental results revealed a sharper drop in energy absorption capability and plastic collapse load than the numerical ones did, highlighting that the critical oblique loading angle of current examined cases was about 6^o represented by specimen 3 case, a tendency not captured by the numerical results as obviously as did by the experimental ones. In particular, a detailed look into the summarized numerical results reveal that both collapse load and absorbed energy show a continuous and constant decrease at higher loading angles without underlining any critical angle of loading as obviously as is observed via the experimental results in which a more significant decrease is observed.

Specimen 3			
	Numerical Simulation	Experiment 3a	Experiment 3b
Peak Load (kN)	88.70	90.22	90.19
Plastic Collapse Load (kN)	51.47	65.29	63.97
Mean Load (kN)	44.21	51.42	49.19
Absorbed Energy (kJ)	2.65	3.08	2.97
SEA (kJ/kg)	23.27	26.79	26.30
Load Uniformity (-)	0.50	0.57	0.55

	Numerical – Experim. 3a error (%)	Numerical – Experim. 3b error (%)
Peak Load	1.71	1.68
Plastic Collapse Load	21.16	19.54
Mean Load	14.01	10.11
Absorbed Energy	13.89	10.80
SEA	13.13	11.51
Load Uniformity	12.5	8.56

Table 16 Results in comparison between experiments and simulation for specimen 3

Figure 109 Collapsed structures of specimen 3 (experimental 3a-3b vs. numerical simulation results from top to bottom)

5.2.4 Specimen 4 case

Following, the numerical results are presented below in comparison to the experimental results regarding the load-displacement curved, the crashworthiness response parameters and the occurred collapse mechanism for the case of specimen 4 which is subjected to 9^o oblique loading angle. More specifically, the numerical results predict with sufficient accuracy the mean crushing load and in subsequence the amount of absorbed energy during collapse, as the load distribution captures the tendency provided from the experimental tests both qualitatively and quantitatively. However, experiments revealed a slight decrease in the load distribution during post-buckling region, a trend which seems to be predicted by the numerical results with although a more constant sustained load provided from the numerical simulation.

Further, both plastic collapse load and mean crushing force are predicted with sufficient accuracy by the developed finite element models with revealed deviations compared to experiments ling around 5.5 % and 3.9 % respectively. Therefore, the energy absorption capability of the examined tube under 9° oblique loading is sufficiently predicted with a relative error of 3.5 %, while the peak crushing force reveals a higher deviation. However, the occurred sharp load increase at the final stages of collapsed is properly predicted by the numerical load-displacement curve, as both simulation and experiments showed that tendency because of the great resistance caused by the crushed concentrated mass of the structure around the ringed bottom base.

In addition, both numerical and experimental results revealed that specimen 4 case showed the lowest energy absorption capacity and plastic collapse load between the previous presented examined cases. The above expected observation can be attributed to the higher loading angle which introduces the most significant bending loads which facilitate the collapse initiation and further the failure progress requiring lower mean sustained loads during post-buckling region in load-displacement curve. However, as the experimental results revealed, the loading angle effect seems to be stabilized for loading angles beyond 9° as will be suggested in next test case of 11° oblique angle of crushing, a tendency which is predicted by the numerical results which however can be observed by a more detailed look in the response metrics variance.

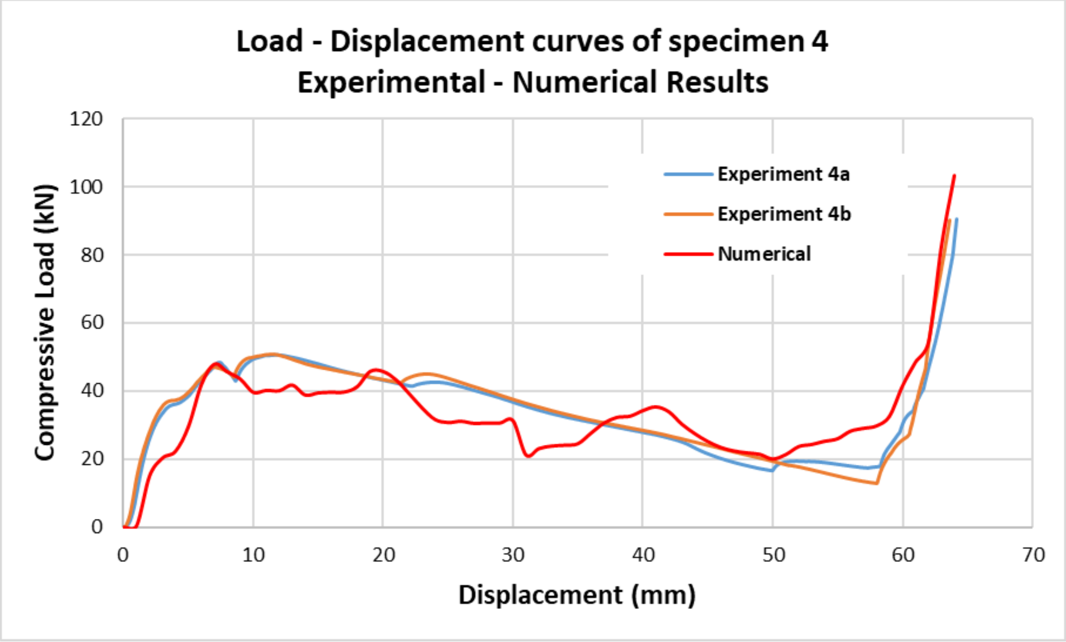

Figure 110 Experimental vs. numerical load-displacement curves for specimen 4

Specimen 4			
	Numerical Simulation	Experiment 4a	Experiment 4b
Peak Load (kN)	103.35	90.43	90.14
Plastic Collapse Load (kN)	47.92	50.55	50.73
Mean Load (kN)	32.95	33.99	34.27
Absorbed Energy (kJ)	2.11	2.18	2.18
SEA (kJ/kg)	18.42	19.01	19.08
Load Uniformity (-)	0.32	0.38	0.38

	Numerical – Experim. 4a error (%)	Numerical – Experim. 4b error (%)
Peak Load	14.28	14.65
Plastic Collapse Load	5.18	5.53
Mean Load	3.06	3.86
Absorbed Energy	3.31	3.26
SEA	3.14	3.49
Load Uniformity	15.18	16.45

Table 17 Results in comparison between experiments and simulation for specimen 4

Finally, both experiments and numerical simulation predicted similarly the occurred collapse mechanism which initially starting by formulating 2D-diamond elliptical folds, while at the final stages of shortening a local bending around the bottom crushed structure mass was observed reacting in a significant drop of energy absorption capability. The above tendency however can be observed more obviously by the depicted final views of specimen 4 crushed structure as revealed from the experiments, due to the fact that the simulation results followed that behavior being slightly lower affected.

Figure 111 Collapsed structures of specimen 4 (experimental 4a-4b vs. numerical simulation results from top to bottom)

5.2.5 Specimen 5 case

Lastly, in current final section of this chapter, the numerical and experimental results regarding the specimen 5 case are presented below in terms of the provided load-displacement curves and the revealed crashworthiness response metrics. In more specific, the numerical load-displacement curve predicts with sufficient accuracy the mean crushing load and the amount of absorbed energy during collapse revealing deviations about 5% and 6% respectively. Although experimental curve and numerical one show an agreement in sustained load during post-buckling region, the load distribution provided by the numerical results does not capture the progressive load reduction during collapse as shown by the experimental tests. However, both simulation and experiments depict a sudden significant load increase at the final stages of collapse which is caused by the increased resistance – provided by the fully crushed mass structure – against further shortening.

Moreover, the peak crushing force and the plastic collapse initiation load are also predicted with sufficient accuracy between experiments and simulation revealing relative errors below 7.5%, while both showed that specimen 5 case reacted to the lowest observed energy absorbing levels and collapse load compared to all previous cases. Thus, the effect of oblique loading angle was sufficiently predicted by both experimental and numerical results.

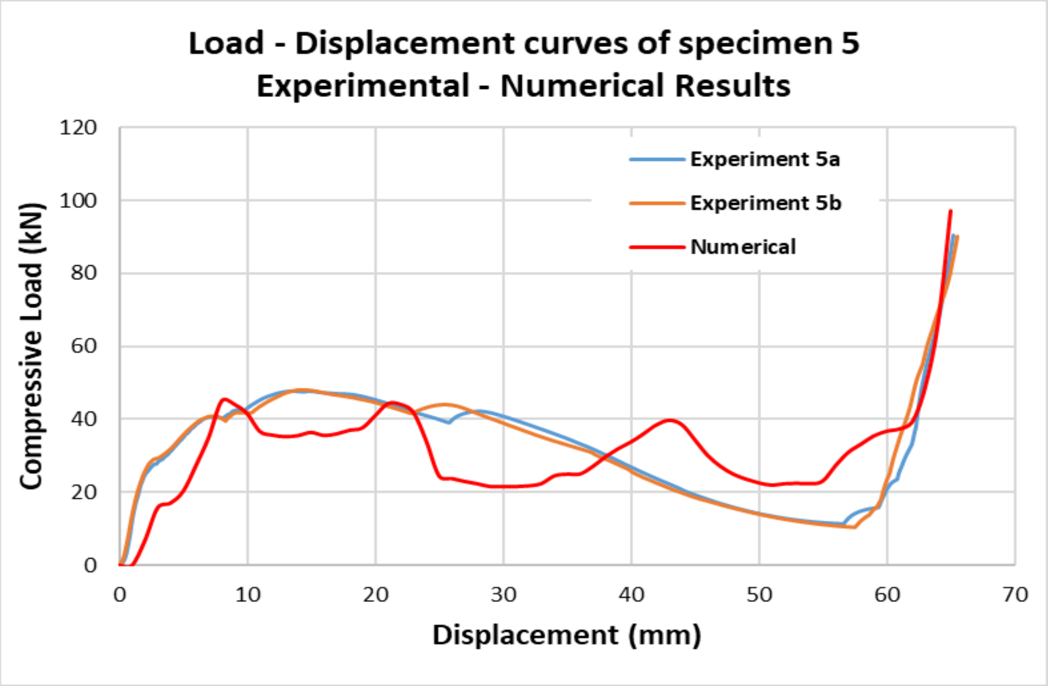

Figure 112 Experimental vs. numerical load-displacement curves for specimen 5

Finally, the collapse mechanism is confirmed by both experiments and simulation to initially formulate two elliptical 2D-diamond convolutions and continuously reveal a bending moment around tube bottom crushed mass which is considered to be responsible for the light load decrease of the sustained load as the experiments depict in the above load-displacement curves with this tendency however not be captured so well by the simulation results.

Specimen 5			
	Numerical Simulation	Experiment 5a	Experiment 5b
Peak Load (kN)	97.17	90.3	90.27
Plastic Collapse Load (kN)	45.00	47.94	48.07
Mean Load (kN)	31.02	32.40	32.81
Absorbed Energy (kJ)	2.02	2.11	2.15
SEA (kJ/kg)	17.53	19.08	18.67
Load Uniformity (-)	0.32	0.36	0.36

	Numerical – Experim. 5a error (%)	Numerical – Experim. 5b error (%)
Peak Load	7.61	7.64
Plastic Collapse Load	5.25	6.39
Mean Load	4.25	5.44
Absorbed Energy	4.54	6.25
SEA	4.96	6.09
Load Uniformity	11.02	12.15

Table 18 Results in comparison between experiments and simulation for specimen 5

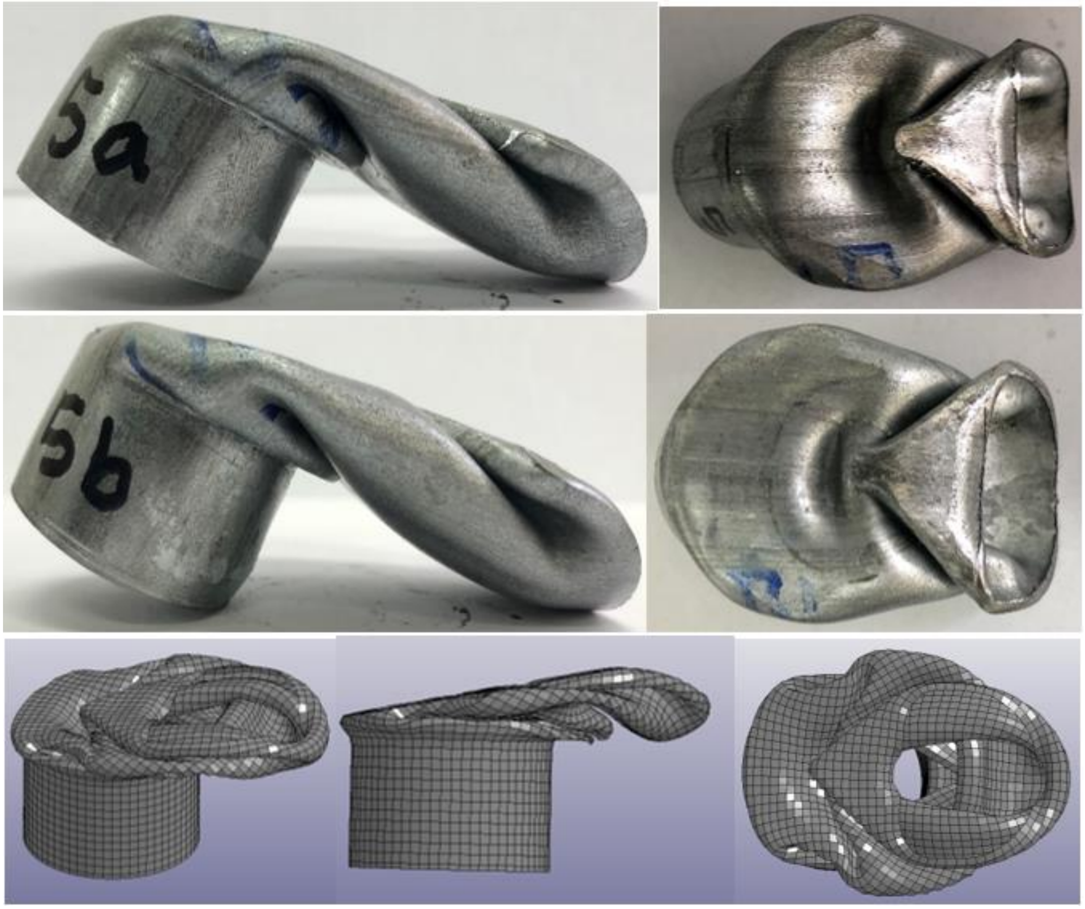

Figure 113 Collapsed structures of specimen 5 (experimental 5a-5b vs. numerical simulation results from top to bottom)

6. Summary, conclusions and recommendation for future work

6.1 Summary

The purpose of this study is to investigate the crashworthiness behavior of thin-walled steel tubes under both axial and oblique loading conditions in order to evaluate their response efficiency by assessing their energy absorption capability and observing the occurred collapse mechanism. Regarding the case of the examined oblique loading conditions, different loading angles varying from 3° to 11° were studied aiming to estimate their effect on the energy absorption capability of the crushed structures and the stability of collapse during plastic deformation in order to capture any critical loading angle beyond the which the dissipated energy reveals a significant drop due to local bending and buckling phenomena during collapse.

For the needs of current work, both experimental tests and numerical simulations were carried out in order to provide the load-displacement curve in each examined case and estimate the main crashworthiness response metrics such as the peak crushing force, the mean sustained load and the one required for the plastic collapse initiation, the absorbed energy and the specific one corrected to the structure mass and finally the uniformity of load distribution. Moreover, the occurred collapse mechanism was observed for each examined case capturing several states during plastic deformation in order to obtain its characteristics which affect the structure crashworthiness response and in subsequence its energy absorption capability.

Thus, regarding the experimental investigation, two experimental tests were carried out for each examined case in order to minimize the possible deviations which may occur due to data recording errors, varied material properties and unpredicted anisotropy, compression test variation etc. The examined specimens consisted of mild steel thin-walled tubes of 32.75 mm external diameter and 1.56 mm wall thickness, subjected to both axial and oblique loading conditions. In particular, specimen 1 case was examined against axial loading, while specimens 2 – 5 against oblique crushing with loading angle varied from 3° to 11° respectively. All experimental compression tests were conducted in quasi-static conditions applying a constant loading rate of 10 mm/min, while the oblique compression tests represented off-axis oblique loading conditions with the tube and bottom base being rotated to the proper angle and the upper plate moving downwards and applying the compressive loads vertically. Finally, in all examined configurations the bottom tube end was fixedly supported by about 20 mm in height as it was embedded in the ringed configuration of bottom base.

Regarding the conducted numerical simulations, at first a finite element model was created for each examined case in LS-Dyna software. During modelling procedure, the bodies geometry was initially designed and a finite element mesh was next generated. Upper plate and bottom base were modelled with 8-node solid elements which then were treated as undeformable and rigid bodies. In contrast, tubes were modelled via 4-node shell elements which have been proved quite efficient in crashworthiness modelling considering thin-walled structures. At next, tube and plates material properties were applied, while in the case of steel tube an experimental tension test was carried out in order to obtain its stress-strain curve and estimate its response behavior through plastic deformations. Following, the appropriate boundary conditions were applied at each interface in order to avoid any penetration between the tube surface and the plates, but also between tube folds too. Further, the embedded tube end into the ringed base was adjusted as fixedly supported by constraining the nodes of respective tube elements against any displacement or rotational degree of freedom. Finally, dynamic loading conditions were applied by adjusting a constant vertical loading velocity of 1 m/s to the upper plate. Both experimental and numerical investigation provided the load-displacement curve and the respective crashworthiness response metrics while also the occurred collapse mechanism was also observed.

6.2 Conclusions

By summarizing the provided results of experimental tests and finite elements simulations, all developed finite element models predicted accurately the occurred collapse mechanism of each examined case revealing that in the case of axially collapsed specimen 1 a concertina deformation mode was occurred formulating axisymmetric convolutions during plastic deformation. In contrast, the obliquely loaded specimens 2 – 5 showed a 2D-diamond collapse mode formulating elliptical folds, while specimens 4 and 5 revealed a local bending around the bottom crushed structure mass at the final stages of collapse. The numerical results depicted that the elliptical tube folds were formulated due to a non-uniform distribution of bending moment along the cross-section circumferential direction which was introduced by the angled loading conditions.

Furthermore, regarding the provided load-displacement curves, specimens 1 – 4 – 5 cases revealed a sufficient agreement between experiments and simulation in all sections of collapse, predicting both peak crushing load, mean sustained load and the absorbed energy with deviations lower of 5% in general. In contrast, specimens 2 and 3 revealed slightly higher deviation in peak load capturing however sufficiently the energy absorption capability as suggested by the experiments. Moreover, specimen 1 load distribution revealed a high variance during post-buckling region with several peaks and lows which represent the formulation of folds. In contrast, the obliquely loaded specimens 2 – 5 revealed a more constant sustained load, with specimens 4 and 5depicting a slight mean load decrease during collapse caused by the tube local bending around the bottom crushed structure mass. Additionally, the simulations captured the significant load increase at the final stages of collapse except the case of specimen 2. The above tendency occurred due to the high resistance against further shortening brought by the concentrated crushed structure mass around bottom tube end. For this reason, the peak crushing force of obliquely loaded specimens occurred at the final stages of collapse as it revealed significantly higher magnitude than the required one for the plastic collapse initiation. Concluding, both experimental and numerical results revealed that as the loading angle increases both plastic collapse initiation load and the energy absorption capability are decreased as higher loading angles introduce additional bending loads facilitating both the start and the progress of plastic collapse. In fact, the obliquely crushed specimens started to deform formulating 2D-diamond folds, while at higher loading angles of 9° and 11° local bending occurred at the final stages of collapse. Both above observations reacted to a decrease of energy absorption capacity with that trend becoming more significant at loading angles higher than 6° suggesting the last one as a critical oblique loading angle regarding the examined cases. Finally, low loading angles could be considered as beneficial in crashworthiness design of structures because they result to a decreased plastic collapse initiation load behaving that way as triggering configurations without however affecting much the structure energy absorption capacity.

6.3 Recommendation for future work

Some research fields which are recommended for future work are:

- Utilization of T-shell elements through the modelling approach of tube in order to assess its response against the plastic deformation during collapse

- Examination of different types of folds deformations and assessment of their impact on the revealed failure mechanism and in subsequence the crashworthiness response parameters

- Utilization of different material concept regarding the finite element modelling approach which would take into account the strain rate effect providing more reliable results regarding their behavior through plastic deformation under dynamic crushing conditions

- Examination of angled loading type of oblique crush in order to estimate revealed behavior, the crashworthiness metrics and the observed failure mechanism during collapse

7. Bibliography

[1] W.J. Hughes (2016). "*Crushing Behavior of Laminated Composite Structural Elements: Experiment and LS-DYNA Simulations*" Federal Aviation Administration, U.S. Department of Transportation, DOT / FAA / TC-15/25

[2] US Dept. of Transportation FAA (2009). Advisory Circular 20-107b. pp: 1-37

[3] F. Garattoni (2011). "*Crashworthiness and composite materials: development of an experimental test method for the energy absorption determination and implementation of the relative numerical model*" PhD thesis. University of Bologna

[4] H. Nikkhah, A. Baroutaji, A. Ghani Olabi (2019). "*Crashworthiness design and optimisation of windowed tubes under axial impact loading*" ELSEVIER

[5] F. Tarlochan, S. AiKhatib (2017). "*Energy absorption capabilities of complex thin walled structures*" 4th Internacional Conference of Mechanical Engineering Research. IOP Publishing

[6] W. Suzhen, Z. Gang, S. Guangyong, L. Qiang, L. Guangyao, L. Qing (2016). "*On design of milti-cell thin-walled structures for crashworthiness*" ELSEVIER. Internacional Journal of Impact Engineering

[7] The Aluminium Automotive Manual (2013). Applications-Car Body-Crash Management Systems ELSEVIER. Internacional Journal of Impact Engineering. European Aluminium Association

[8] A.Riccio, S.Saputo, A.Sellitto, A.Russo, F. Di Caprio, L.Di Palma (2019). "*An insight on the Crashworthiness Behavior of a Full-Scale Composite Fuselage Section at Different Impact Angles*" Aerospace MDPI

[9] G.L. Farley, R.M.Jones (1989). "*Energy-absorption capability of compsite tube and beams*" NASA Technical Publications. TM 101634. pp: 1-248

[10] C. Bisagni (2009). "*Experimental Investigation of the Collapse Modes and Energy Absorption Characteristics of Composite Tubes*" Internacional Journal of Crashworthiness. Vol.14. No.4. pp: 365-378

[11] A.G. Mamalis, D.E. Manolakos, M.B. Ioannidis, D.G. Chronopoulos, P.K. Kostazos (2009). "*On the crashworthiness of composite rectangular thin-*

walled tubes internally reinforced with aluminium or polymeric foams: Experimental and Numerical simulation" ELSEVIER. Composite Structures

[12] M. Ptak, P.Kaczynski, F.A.O. Fernandes, R.J. Alves de Sousa (2017). "*Assessing impact velocity and temperature effects on crashworthiness properties od cork material*" ELSEVIER. Internacional Journal of Impact Engineering

[13] P.Florent, Y.Wenyi, W.Cui'e (2007). "*Crushing modes of aluminium tubes under axial compression*" 5th Australian Congress on Applied Mechanics. Brisbane Australia

[14] E. Acar, M. Altin, M.A. Guler (2019). "*Evaluation of various multi-cell design conceptsfor crashworthiness design of thin-walled aluminium tubes*" ELSEVIER. Thin-walled Structures

[15] A.G. Mamalis, D.E. Manolakos, M.B. Ioannidis, D.P. Papapostolou (2004). "*Crashworthy characteristics of axially statically compressed thin-walled square CFRP composite tubes: experimental*" ELSEVIER. Composite Structures

[16] P. Shivdayal, R. V. Venkata, C. S. Guedes (2019). "*Crashworthiness analysis of polymer composites under axail and oblique impact loading*" International Journal of Mechanics and Science. Vol. 156. pp. 221-234

[17] H. R. Zarei (2019). "*Experimental and numerical crashworthiness investigation of hybrid composite aluminium tubes under dynamic axial and oblique loadings*" Intern. Journal of Automative Engineering. Vol. 5. No.3. pp. 1084-1093

[18] D. Fauzan, A. Shahrum, A. Ariffin, M. N. Zilkifli (2016). "*Finite element analysis and crashworthiness optimization of foam-filled double circular tubes under oblique loading*" Latin American Journal of Solids and Structures. Vol. 13. pp. 2176-2189

[19] H. S. Kim, T. Wierzbicki (2000). "*Numerical and analytical study on deep biaxial bending collapse of thin-walled beams*" Latin American Journal of Solids and Structures. Vol. 13. pp. 2176-2189

[20] D. C. Han, S. H. Park (1999). "*Collapse behavior of square thin-walled columns subjected to oblique loads*" Thin-walled strctures. Vol. 35 (3). pp. 167-184

[21] A. Reyes, M. Langseth, O. S. Hopperstad (2002). "*Crashworthiness of aluminum extrusions subjected to oblique loading: experiments and numerical analyses*" Intern. Journ. of Mech. Sciences. 44 (9). pp. 1965-1984

[22] Y. Crutzen, A. Inzaghi, M. Mogilevsky, C. Albertini (1996). "*Computer modelling of the energy absorption process in box-type structures under oblique impact*" Automotive Automation Limitied UK. pp. 1293-1298

[23] C. Qi, S. Yang, F. Donf (2012). "*Crushing analysis and multiobjective crashworthiness optimization of tapered square tubes under oblique impact loading*" Thin-walled Structures. 59. pp. 103-119

[24] J. Song (2013). "*Numerical simulation on windowed tubes subjected to oblique impact and a new method for the design of obliquely loaded tubes*" Intern. Journ. of Impact Engineering. 54. pp. 192-205

[25] J.M. Alexander (1960). "*An approxiamte analysis of the collapse of thin cylindrical shells under axial loading*" Imperial College of Science and Technology

[26] W. Abramowicz, N. Jones (1984). "*Dynamic axial crushing of circular tubes*" Intern. Journ. of Impact Engineering. Vol. 2. pp. 263-281

[27] T. Wierzbicki, S. U. Bhat, W. Abramowicz, D. Brodkin (1992). "*Alexander revised – A two folding elements model of progressive crushing of tubes*" Intern. Journ. od Solid Mechanics. Vol. 29 (2). pp. 3269-3288

[28] W.Johnson, P.D. Soden, S.T.S. Al-Hassani (1997). "*Inextensional collapse of thin-walled tubes under axial compression*" Journal of Strain Analysis. Vol. 12. No. 4

[29] A.G. Mamalis, D.E. Manolakos, G.A. Demosthenous, W.Johnson (1991). "*Axial Plastic Collapse of Thin Bi-Material Tubes as Energy Dissipating Systems*" Internacional Journal of Impact Engineering. Vol.11. No.2. pp: 185-196

[30] D. Kecman (1983). "*Bending collapseof rectangular and square section tubes*" Intern. Journ. of Mech. Sciences. 25 (9-10). pp. 623-636

[31] Livermore Software Technology Corporation (2007). "*LS-DYNA keyword user's manual*" Vol. I. Version 971